ACUTE BICEPS AND SUPRASPINATUS TENDON CHANGES ASSOCIATED WITH WHEELCHAIR PROPULSION

by

Jennifer L. Collinger

BS, University of Pittsburgh, 2003

Submitted to the Graduate Faculty of

Swanson School of Engineering in partial fulfillment

of the requirements for the degree of

Doctor of Philosophy

University of Pittsburgh

2009

UNIVERSITY OF PITTSBURGH

SWANSON SCHOOL OF ENGINEERING

This dissertation was presented

by

Jennifer L. Collinger

It was defended on

March 23, 2009

and approved by

Mark S. Redfern, PhD, Associate Dean for Research, Swanson School of Engineering

George D. Stetten, MD, PhD, Professor, Bioengineering

Dany Gagnon, PhD, PT, Faculty, School of Rehabilitation, University of Montreal

Dissertation Director: Michael L. Boninger, MD, Chair, Physical Medicine and Rehabilitation

ACUTE BICEPS AND SUPRASPINATUS TENDON CHANGES ASSOCIATED WITH WHEELCHAIR PROPULSION

Jennifer L. Collinger, PhD

University of Pittsburgh, 2009

Manual wheelchair uses rely on their upper limbs for mobility and activities of daily living. Unfortunately more than half of manual wheelchair users will experience shoulder pain, due in part to repetitive loading during wheelchair propulsion and transfers. While chronic upper extremity pathology has been well documented, no research has investigated acute rotator cuff changes that occur as a result of wheelchair propulsion. Ultrasound is a non-invasive, convenient method to examine soft tissue structures of the shoulder, but tendinosis is rated subjectively by the operator. Here we apply image analysis techniques to quantify tendon size, echogenicity, and greyscale texture. We have developed a standardized protocol, and custom reference marker, to maximize reliability of these measures. Further, content validity was established by relating greyscale-based quantitative ultrasound measures to known risk factors for shoulder pain and pathology including increased age, duration of wheelchair use, and body weight. Quantitative ultrasound measures also correlated to clinically graded tendinosis and discriminated between people with and without symptoms on physical examination. Sixty-seven manual wheelchair users underwent quantitative ultrasound examinations of the biceps and supraspinatus tendons before and after an intense wheelchair propulsion task. Biceps tendon greyscale texture post-propulsion was significantly impacted by clinically graded tendinopathy, duration of wheelchair use, resultant force, and stroke frequency when controlling for pre-propulsion ultrasound image texture. Subjects with tendinopathy or a longer duration of

wheelchair use tended to have a darker, less organized tendon microstructure following propulsion likely due to the presence of inflammatory factors or other fluid. In contrast, subjects who used a higher stroke frequency or resultant force showed a brighter, more aligned tendon fibrillar structure due to mechanical loading of the tendon. In a subsample of subjects, we found that increased shoulder forces and moments during propulsion correlated with more severe supraspinatus tendinopathy. These subjects also experienced a larger decrease in supraspinatus tendon width and greyscale variance following the intense propulsion task. Quantitative ultrasound measures describe tendon microstructure and are sensitive to risk factors for shoulder pain and pathology. This technique may help identify the best interventions to reduce an individual's risk of developing upper limb pathology.

TABLE OF CONTENTS

LIST OF TABLES

LIST OF FIGURES

ACKNOWLEDGEMENTS

The work described in this dissertation could not have been completed without the contributions and encouragement of many special people. First, I would like to thank my advisor, Dr. Boninger, who helped guide me through the ups and downs of research by supplying a fresh point of view to every situation. More importantly he has served as a mentor and role model for achieving professional and personal fulfillment. Thank you for all of the opportunities and advice you have given me over the last few years. All of my committee members have been instrumental in developing this project. Dr. Redfern sparked my interest in ergonomics and biomechanics and has been a constant source of guidance since early in my undergraduate career. Dr. Stetten's classes and direction gave me the tools I needed to incorporate imaging into my doctoral work. Dr. Gagnon has shown me a new level of enthusiasm for research and taught me more than I thought I'd ever know about statistics. Thank you to all of you. Also, although not officially part of my graduate committee, Dr. Cooper and Dr. Koontz have provided invaluable contributions to this project.

I am grateful for the support I have received over the years from everyone at HERL. Thank you to all of my fellow graduate students, in particular past and present Biolab members, who assisted with subject testing and were always willing to listen and provide a helping hand. Brad Impink deserves special thanks for helping me collect ALL of the data included in this dissertation, and serving as the go-to troubleshooter. Thanks to Paula and Christine for helping

me with publications, posters, and all things HERL-related. I am grateful for the IRB-related advice (and never-ending candy supply) Annmarie, Michelle, and Emily have provided me. Thank you to the shop staff for always helping out when last minute projects arose. Everyone at HERL has made this an enjoyable place to work everyday.

Finally, I'd like to thank my family and friends for their support and encouragement. My parents always believed I could do anything and have helped me keep going even when I was struggling. John, you have kept me motivated and have always believed in me. Thanks for always being there to support me. You always know how to make me smile and I am so grateful to have you in my life.

1.0 INTRODUCTION

1.1 MOTIVATION

Shoulder pain among manual wheelchair users has been well documented with prevalence estimates between 30 and 73% [1-4]. Unfortunately, shoulder pain can be debilitating for a manual wheelchair user whose independence requires upper limb integrity. Lundqvist et al. found that pain was the only factor correlated with lower quality of life scores [5]. Gerhart et al. reported that upper limb pain was a major reason for functional decline in individuals with SCI who required more physical assistance since their injury [6]. Many attribute the high prevalence of shoulder pain to "overuse syndrome" resulting from the repetitive loading that occurs during wheelchair propulsion [7-9]. Additionally, multiple studies have found that the prevalence of shoulder pain increases with the duration of wheelchair use [3,9-11].

Despite the well known impact and high prevalence of shoulder pain, little research has been published on its treatment or prevention. Many advocate conservative therapies since rotator cuff surgery is often ineffective in treating pain in individuals with SCI [7,12]. However, Subbarao et al. found that individuals with SCI and upper limb pain did not get relief from the majority of these treatments [8]. They believed that treatment ineffectiveness could be explained, in part, by the fact that primary contributing factors to upper limb pain, wheelchair propulsion and transfers, could not be avoided.

Clinical guidelines with specific recommendations have been published related to preserving upper limb function [13]. These guidelines are based on expert opinion, ergonomics literature, and correlational studies. The guidelines include specific recommendations related to manual wheelchair propulsion. However, the guidelines are not based on randomized controlled trials. Randomized control trials on primary prevention of shoulder injury could be very costly and may take years to show results. However, if we identify acute markers of injury that relate to long term risk and are sensitive to change, we could test interventions and gain insight into their effectiveness. This study is specifically targeted at finding ultrasound based acute markers of injury that relate to long term pathology as well as biomechanical variables. Future research could use these ultrasound measures to test interventions acutely and in a subject specific fashion.

1.2 MUSCULOSKELETAL SHOULDER PATHOLOGY FOLLOWING SCI

While there are many pathological conditions that produce shoulder pain in the SCI population, musculoskeletal causes, particularly injuries to the rotator cuff (often collectively referred to as *impingement syndrome*), are among the most common [7,14]. Bayley et al. found the most common pattern of pain at the shoulder consistent with chronic impingement syndrome was subacromial bursitis [7]. In individuals with pain, follow-up arthroscopy revealed that 65% had chronic rotator cuff tears. The authors attribute the high rate of shoulder problems to the abnormal stress distribution across the subacromial area during wheelchair propulsion and transfers. In a study by Gellman et al., the most common cause of shoulder pain was bicipital tendonitis [3]. Escobedo et al. used magnetic resonance imaging (MRI) to evaluate the shoulders

of thirty-seven individuals with paraplegia for partial or full-thickness rotator cuff tears [14]. Of the 26 individuals who were symptomatic, 73% showed evidence of rotator cuff tear. The presence and severity of the rotator cuff tear was reported to increase with age or duration of injury. In contrast, a study published from our lab found only one rotator cuff tear in MRIs of both shoulders of 28 individuals with SCI [15]. However, a number of other abnormalities were seen. These abnormalities included distal clavicular edema, acromioclavicular degenerative arthrosis, subacromial spur formation, and coracoacromial ligament thickening and were associated with body mass index. In addition to differences in recruitment criteria, the individuals in the study completed by Escobedo were older than the individuals in our study. The discrepancy between these two studies provides justification for intervening with younger individuals before chronic pathologies, such as rotator cuff tears, have a chance to develop. Additionally, many of these studies have suggested that subject weight, age, and injury duration can influence the presence of shoulder pathology.

1.3 SHOULDER BIOMECHANICS DURING MANUAL WHEELCHAIR PROPULSION

With a stroke cycle time of less than a second, manual wheelchair propulsion places repeated loads on the upper extremity a likely contributes to the development of upper limb pain and pathology. It would only take 16 minutes of wheelchair propulsion at this frequency to exceed the number of repetitions completed by a factory worker performing a highly repetitive task in an 8 hour day. Our laboratory found that, on average, manual wheelchair users actively propel their chair for approximately 45 minutes per day [16]. The shoulder joint, designed for mobility, not

load-bearing, is loaded during every stroke cycle [17,18]. Previous studies have reported that the posterior directed reaction force is the largest directional component of shoulder joint force and the extension moment is the largest shoulder moment experienced during the push phase of propulsion [18,19]. Posterior directed force and the extension moment are a direct result of the tangential force required to propel the wheelchair. Manual wheelchair users also experience abduction and internal rotation moments during propulsion. The shoulder remains internally rotated throughout the propulsion cycle, which leaves the shoulder at risk for impingement, especially when combined with an internal rotation moment [20] (Figure 1).

Increased posterior directed force is related to coracoacromial ligament edema – a risk factor for rotator cuff injury [21,22]. The same study found that internal rotation moment is associated with physical examination abnormalities. For this reason, we believe that posterior directed force and internal rotation moment will also be associated with acute markers of shoulder soft tissue pathology.

Fine-wire electromyography (EMG) has been used to describe muscle activity of the rotator cuff and other surrounding shoulder muscles, like the biceps, during wheelchair propulsion [23,24]. Others have used surface EMG to study the superficial muscles of the shoulder [25]. In a study of individuals with paraplegia, Mulroy et al. reported that the supraspinatus displayed the highest peak intensity of all shoulder muscles active during propulsion, reaching 67% of the maximum intensity during the early part of push phase, leaving it the most vulnerable to overuse [23]. The infraspinatus reached a maximum intensity of 44%. The supraspinatus and infraspinatus remained active as external rotators for approximately two-thirds of the push phase. The biceps reached a peak intensity of 38%. The biceps act as an elbow flexor to pull on the pushrim during the initial pushing phase [23,25]. Rotator cuff

muscles are also active during the recovery phase, leaving them susceptible to fatigue [23]. We chose to focus our ultrasound exam on the supraspinatus and the long head of the biceps tendon based on their dominant role during the push phase of wheelchair propulsion and because of their known susceptibility to injury. A recently published study reported that 100% of a sample of manual wheelchair users (n=49) showed some degree of supraspinatus tendinopathy upon ultrasound examination [26]. Almost 80% showed signs of biceps tendinopathy. Often biceps tendon inflammation and tenderness is indicative of rotator cuff pathology.

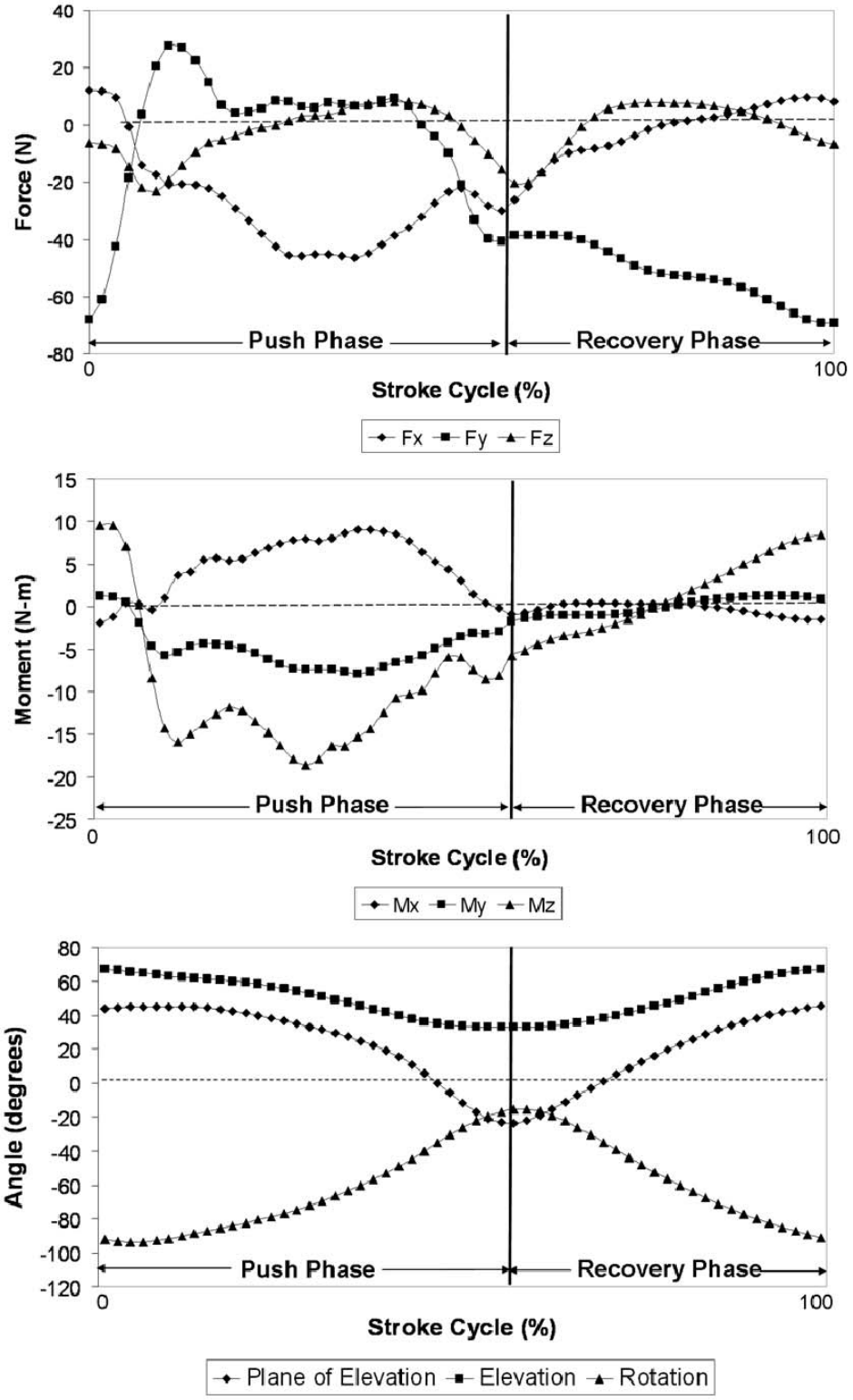

Figure 1. Representative shoulder forces, moments, and Euler angles during wheelchair propulsion at 0.9 m/s

1.4 ANATOMY OF THE BICEPS AND SUPRASPINATUS TENDONS

The long head of the biceps tendon originates from the supraglenoid tubercle of the scapula and passes through the intertubercular groove of the humerus [27]. The peak of the lesser tubercle serves as a bony landmark for localizing the proximal-distal ultrasound transducer location during examination. Near the elbow, the long head and short head of the biceps muscle unite and insert on the prominent radial tuberosiry of the proximal end of the radius. The biceps muscle acts to flex and supinate the forearm and to flex the arm at the shoulder. During wheelchair propulsion, the biceps acts both as an elbow flexor and shoulder flexor during different phases of propulsion.

The supraspinatus originates on the supraspinatus fossa of the scapula and passes beneath the acromion [27]. The supraspinatus muscle inserts on the greater tubercle of the humerus. Contraction of the supraspinatus muscle abducts the arm. Previously we reported that on average, the humerus is abducted 30-55 degrees throughout the entire propulsion cycle [28]. Between the supraspinatus tendon and the acromion lies the subacromial bursa which is often inflamed when a broader pathology, impingement syndrome, is diagnosed. The biceps and supraspinatus are not the only muscles that act to move the shoulder joint. In particular, the deltoid muscle overlays the humeral head and also contributes significantly to shoulder flexion and abduction.

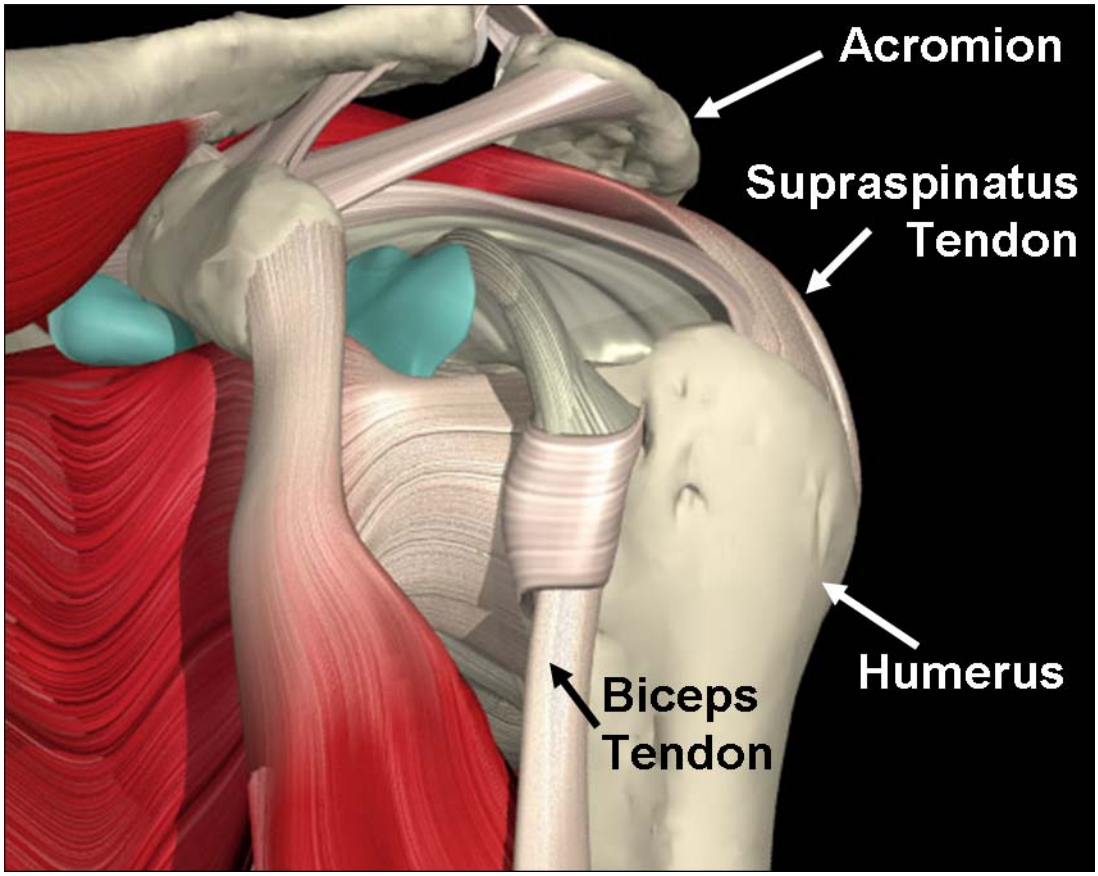

Figure 2. Anatomy of the biceps and supraspinatus tendons

Adapted From: Interactive Shoulder v1.0 © 2000 Primal Pictures Ltd.

1.5 MECHANISMS OF SHOULDER INJURY

Mechanisms of injury to the rotator cuff are often divided into intrinsic and extrinsic causes [23]. The most commonly cited intrinsic factor associated with rotator cuff disease is a degenerative change at the "critical zone" (the portion of the rotator cuff located 1cm medial to the insertion of supraspinatus on the greater tuberosity). Other intrinsic factors include overuse and aging. The most commonly cited extrinsic factor in rotator cuff pathology is mechanical impingement of the rotator cuff tendon by the overlying coracoacromial arch itself (*primary impingement*).

Impingement may result from any factor causing functional narrowing of the subacromial space (*secondary impingement*), such as glenohumeral or scapular instability [30,31]. The upward thrust of the humerus during weight-bearing activities, like wheelchair propulsion and transfers, can cause compression of the rotator cuff against the overlying acromion [18,32]. During wheelchair propulsion, there is an upward force generated at the shoulder which increases significantly when a person uses a faster traveling speed or ascends a ramp [18]. The humerus remains internally rotated throughout wheelchair propulsion, further increasing the risk for impingement [20]. Figure 1 illustrates shoulder forces, moments, and Euler angles for a single subject propelling at 0.9 m/s. Another extrinsic factor leading to secondary impingement and rotator cuff injury is instability of the glenohumeral joint [30,33]. This instability is thought to relate to a combination of attenuation of supporting structures of the glenohumeral joint, such as the glenoid labrum, and to muscle imbalance. Muscle imbalance, caused by overuse, can lead to abnormal biomechanics and thus injury. The most common disparity in strength associated with rotator cuff injury is an imbalance between the internal and external rotators of the shoulder [34]. Burnham demonstrated muscle imbalance in a group of wheelchair athletes and was able to correlate this imbalance to shoulder pain [35].

1.6 TENDON OVERUSE INJURIES

Excessive mechanical loading is considered to be a major cause of tendon overuse injuries, or tendinopathy. Tendon microinjuries occur from small repetitive strains that are below the failure level of the tendon. Tendon inflammation occurs after the microinjuries causing the production of PGE_2 and LTB_4 in response to mechanical loading. These inflammatory factors may

contribute to tendon degeneration [36]. The term "overuse" implies a repetitive stretching of the tendon which results in the inability of the tendon to withstand further tensile loading [36].

Tendons are surrounded by a synovial sheath, the paratendon, which is also susceptible to injury. The paratendon can be injured due to trauma or excessive loading. Inflammation, or peritendinitis, occurs in response to excessive loading and features edema and swelling. Inflammatory or metabolic changes often occur simultaneously within the paratendon and tendon substance [30]. Langberg et al. used microdialysis to show that acute exercise causes changes in tendon metabolism and increases the inflammatory reaction in the paratendon [37].

Some researchers have attempted to create animal models of tendinopathy. One research group has investigated overuse of the supraspinatus tendon in rats [38,39]. Anatomically, the rat animal model is similar to the human rotator cuff structure. The supraspinatus tendon must pass through an enclosed arch in the rat shoulder, similar to the coracoacromial arch found in humans. The study was designed to investigate the effect of extrinsic and intrinsic factors on developing tendinopathy. Four groups of rats were delineated: control, extrinsic compression, overuse, and combination of extrinsic compression and overuse. Extrinsic compression was created by placing an allograph around the acromion, which applied compression to the supraspinatus. Rats in the control and extrinsic compression groups participated in normal cage activity. Overuse was simulated by training the rats to run downhill on a treadmill 1 hr/day, 5 days/wk. Tendon cross-sectional area, maximum stress, and modulus were measured at 4, 8, and 16 weeks. Rats in the external compression only group showed no significant changes when compared to the control group. Rats in both overuse groups saw a significant increase in cross sectional area and decrease in maximum stress and modulus. Rats in the combination group saw the greatest changes when compared to controls. This leads us to believe that overuse alone can cause

tendinopathy. When combined with other intrinsic risk factors, such as a hooked acromion, the risk of tendinopathy increases. A new study by this group found that the long head of the biceps tendon increased in size, and showed decreased modulus values, in the presence of a rotator cuff tear [39]. They hypothesize that altered biomechanics increase the load on the biceps tendon. Clearly, musculoskeletal structures of the shoulder are interdependent and can be affected by injuries to surrounding structures.

1.7 ULTRASOUND

Ultrasound is a well established method for examining soft tissue structures of the shoulder including rotator cuff tendons and the long head of the biceps tendon [40-45]. Symptoms of pathology of the rotator cuff detected by ultrasound include a hypoechoic tendon appearance due to increased fluid or loss of a collagen fibrillar pattern [40-43] and hypertrophy of the long biceps tendon [44,45]. Fluid in the biceps tendon sheath, or a hypoechoic biceps tendon appearance may be evidential of a rotator cuff tear [41,43,44]. An enlarged biceps tendon is the result of chronic inflammation and impingement [45] and bicipital tenosynovitis [41].

Evaluation of musculoskeletal pathology is subjective and depends on the operator's interpretation of the scan. Our laboratory recently developed a grading scale for various signs of shoulder pathology [26], however the validity of the ratings is dependent on the experience of the ultrasonographer. In the current study, we aim to develop objective, quantitative descriptors of tendon health which will facilitate ultrasound-based research. To date, quantitative analysis of tendons on ultrasound has primarily been limited to measurements of tendon width or cross-sectional area [46]. However, researchers have applied first-order statistics and texture analysis

to other medical images to characterize micro-structure [47-49]. One study investigated the grey scale intensity (first-order statistics) and grey scale structure (blob analysis) of the supraspinatus and vastus lateralis muscles [48]. The authors used the calculated image features to conclude that the vastus lateralis muscle had more contractile components and was coarser than the supraspinatus muscle. Another research group has employed quantitative ultrasound techniques, including structural measurements and echogenicity, to discriminate between skeletal muscle in children with and without neuromuscular disease [50,51]. Specifically related to tendons, one study developed a technique to analyze echogenic tendon texture based on spatial frequencies present in a small windowed area of the tendon [52]. This technique proved to be successful in identifying focal and diffuse tendon abnormalities. Abnormal Achilles tendons exhibited a less organized collagen pattern than healthy Achilles tendons. Finally, a recently published study examined eight spatial frequency parameters on ultrasound that discriminated between subjects with and without Achilles tendinopathy with approximately 80% accuracy [53].

While ultrasound is widely used to evaluate chronic pathology, limited work has been done to investigate acute musculoskeletal changes. A few studies have used ultrasound to examine acute changes of the median nerve due to occupational activities [54,55]. Median nerve swelling was observed following repetitive task such as cutting or opening and closing a jar. Gender, body mass index, and a history of carpal tunnel syndrome influenced the amount of change measured after the task. Our laboratory used ultrasound to measure an increase in biceps tendon diameter and a decrease in mean echogenicity following participating in a wheelchair sporting event [56]. Some evidence suggests that exercise induces vascular hyperemia within a tendon [57,58]. Shalabi et al. reported an increase in tendon volume and intratendinous signal, using MRI rather than ultrasound, following eccentric and concentric loading of the Achilles

tendon [59]. In the current study, we will examine echogenic changes within the biceps and supraspinatus tendons using image analysis techniques such as first-order statistics and texture analysis.

Part of the reason quantitative ultrasound has not been pursued previously is that many factors can influence the image appearance from which the region of interest is defined. First, the ultrasound waves must be perpendicular to an interface to result in maximal reflection of the ultrasound wave back to the transducer. We will address this concern by developing a standardized scanning protocol for the biceps and supraspinatus tendon that aims to minimize the effects of anisotropy. We have also developed a reference marker to help keep the transducer location and orientation consistent between imaging sessions. Ultrasound beams are attenuated as they pass through tissue, such as skin and muscle, so differences in anthropometry may artificially impact tendon appearance on the resulting image [60]. Modern ultrasound machines have image processing that attempts to minimize this effect, but methods may be different between machines. We expect that general trends identified on one machine translate to images collected with another ultrasound machine, however the absolute values of the quantitative ultrasound measures may be different. Also, machine settings that can be adjusted by the user impact signal gain, image resolution, and the dynamic range of the ultrasound signal. In this study, we have kept the machine settings constant for all imaging sessions. However, for this reason, absolute quantitative ultrasound values cannot be directly compared between studies completed with different settings. In this study, we aim to determine if quantitative ultrasound is a reliable measure of tendinosis and if acute tendon changes occur after intense wheelchair propulsion. We hope that this work provides a platform for establishing reliable quantitative ultrasound examination techniques using any ultrasound system.

1.8 RESEARCH GOALS

The overall goal of this dissertation was to develop and identify reliable and valid quantitative ultrasound measures of tendon health that are sensitive to biomechanical loads experienced during manual wheelchair propulsion. A standardized subject positioning protocol, scanning technique, and a custom reference marker, were developed to obtain ultrasound images of the long head of the biceps tendon and supraspinatus tendon. Nine quantitative ultrasound measures based on first-order statistics and co-occurrence matrix features were derived from these images. Chapter 2 describes inter- and intra-rater reliability, along with measurement error for a variety of experimental protocols. Chapter 3 establishes the content validity and face validity of the quantitative ultrasound measures. In addition to describing the theoretical basis for choosing these features, the quantitative ultrasound measures are related to established clinical tests for shoulder pathology. Chapter 4 describes the effect of an intense overground propulsion task on the quantitative ultrasound measures of tendon health. Finally, Chapter 5 focuses on a subsample of subjects to relate shoulder kinetics during constant velocity propulsion to baseline quantitative ultrasound measures as well as to the amount of acute change experienced after the intense propulsion task.

2.0 RELIABILITY OF QUANTITATIVE ULTRASOUND MEASURES OF THE BICEPS AND SUPRASPINATUS TENDONS

2.1 INTRODUCTION

Ultrasound is a well-established, non-invasive method for acutely examining soft tissue structures of the shoulder including rotator cuff tendons and the long head of the biceps tendon. Traditionally, ultrasound imaging has been a valuable tool in clinical practice to visually evaluate the integrity of musculoskeletal structures (qualitative approach) and, when applicable, to confirm musculoskeletal diagnoses. It is only recently that quantitative ultrasound imaging, has became more prevalent in research applications [26,48,50,51,54,56,61,62]. Symptoms of pathology of the rotator cuff detected by ultrasound include hypoechoic tendon appearance due to increased fluid or a diffusely organized collagen fiber matrix [40,42,43] and hypertrophy of the long biceps tendon [44,45]. Biceps tendon inflammation often coexists with rotator cuff disease and may be a result of chronic inflammation and impingement [45] or bicipital tenosynovitis [41]. We believe that the knowledge of musculoskeletal pathology appearance on ultrasound can be applied quantitatively in a research setting to identify risk factors for chronic pathology.

In order to use ultrasound as a research tool, reliable quantitative measures of tendon appearance and health must be derived. Healthy tendons are known to have a well-organized,

uniform, hyperechoic pattern of collagen along the long-axis of the tendon. Conversely, tendons with pathology have a more disorganized, diffuse, or hypoechoic appearance on ultrasound. In essence, tendon health is evaluated clinically by visually examining the greyscale image texture of the tendon. To our knowledge, no studies have quantified tendon health using image processing. However, a few studies have applied image analysis techniques to ultrasound images of muscle. Quantitative image features, including first order statistics, differentiate between coarse muscle with more contractile elements and smoother muscle better than mean greyscale alone [48]. Others have used quantitative ultrasound to reliably discriminate between neuromuscular and non-neuromuscular diseases [50,51]. Another group has applied ultrasound to quantify changes in muscle size and composition following strength training [62]. These studies provide a basis for the application of quantitative ultrasound to understanding chronic musculoskeletal pathology development. Despite the growing interest for this well established technique in research settings, there have been very few attempts to establish the psychometric properties of quantitative ultrasound measures beyond structural measurements such as cross-sectional area [63-65]. None have evaluated the repeatability and standard error of measurement for a set of tendon image features under multiple testing conditions. This information is needed to develop effective measurement protocols to quantify acute or chronic tendon changes linked to cumulative trauma disorder of the upper limb.

Manual wheelchair users are an important group in which to study the development of musculoskeletal injuries and would also benefit from interventions designed to reduce risk exposure. Shoulder pain and pathology is highly prevalent among manual wheelchair users who depend on their upper limbs for independent mobility and many activities of daily living. Over time, the muscular demand and forces placed on the upper limbs during propulsion and transfers

augments the risk of developing secondary impairments affecting the integrity of the upper limb. While there are many cause of shoulder pain among individuals with paraplegia, musculoskeletal causes, particularly injuries to the rotator cuff, are the most common [7,14]. Precise quantification of shoulder tendon health could lead to a better understanding of the etiology of secondary musculoskeletal impairments, and consequently guide prevention and rehabilitation interventions in manual wheelchair users and others.

The main objective of this study was to quantify the reliability and measurement error of quantitative ultrasound outcomes of the long head of the biceps tendon and supraspinatus tendon among able-bodied subjects and long-term manual wheelchair users. The second objective of this study was to define a time-efficient, reliable, quantitative ultrasound measurement protocol that could be used in the future to quantify acute or chronic tendon changes. We chose 9 outcome measures to quantitatively describe the greyscale texture of tendons on ultrasound using image analysis techniques such as first-order statistics and co-occurrence matrix properties (Appendix A). We expected that inter-evaluator reliability would be lower than intra-evaluator reliability, as has been previously reported [63]. Overall, it was expected that a standardized protocol in which one examiner places a reference marker and records a single ultrasound image of the tendon would result in reliable (Φ>0.75) and precise (standard error of measurement <15%) quantitative ultrasound measurement outcomes. We expected that differences between subjects would be the largest source of variance, followed by the effect of repeated imaging sessions (preparations).

2.2 METHODS

2.2.1 Participants

Fifteen able-bodied individuals (12 male, 3 female; age=43.8±13.1 years; height=1.80±0.09 m; body mass=86.58±11.13 kg) and five manual wheelchair users (5 male; age=43.5±15.5 years; height=1.80±0.12 m; body mass=84.64±18.22 kg) volunteered to participate in this reliability study, which was approved by our local review board. All five manual wheelchair users had a spinal cord injury and were an average of 15.5±10.1 years post-injury. All twenty subjects were analyzed as a single group. All participants provided informed consent before entering the study. Subjects were eligible to participate if they were between 18 and 75 years old and if they were able to attend multiple ultrasound sessions. Participants were not screened for the presence of shoulder pain or pathology prior to participation.

2.2.2 Ultrasound Examination

Two examiners conducted ultrasound examinations of each participant. Both were trained in a specially developed quantitative ultrasound examination of the shoulder and had approximately 3 years of experience. Study investigators met frequently to review and refine this quantitative ultrasound examination protocol, which is described in detail below. All quantitative ultrasound examinations were conducted using a Phillips HD11 1.0.6 ultrasound machine with a 5-12 MHz 50 mm linear array transducer **(**Philips Medical Systems**,** Bothell, WA). The machine settings were kept identical throughout testing. Of note, image field depth was set to 4 cm and gain was set at 85 dB. All images were saved for later analysis.

Test: The examination of the non-dominant biceps tendon was performed with the subject sitting in an upright position with the upper arm in line with the trunk, the elbow flexed to 90º, the forearm supinated and the hand resting on the ipsilateral thigh with the wrist in a neutral position (Figure 3A). The proximal end of the transducer was positioned such that the apex of the lesser tuberosity of the humerus was at the edge of the ultrasound image field of view and oriented to obtain a longitudinal view of the widest part of the biceps tendon, while maximizing collagen fiber reflection. Care was taken to ensure that the biceps tendon ROI was perpendicular to the ultrasound beams to minimize anisotropy. The transducer location was traced on the skin and a steel "A-shaped" reference marker was taped to the skin at the distal end of area covered by the transducer. The crossbars of the reference marker (Figure 4) create an interference pattern which is visible in the ultrasound image (Figure 5) and is used to define the tendon region of interest (ROI) used during image analysis. Once this initial set-up was completed (preparation #1), two consecutive longitudinal ultrasound images (images #1 and #2) of the long head of the biceps were collected while avoiding exerting undue pressure with the ultrasound head. Once the images were taken, the markers were removed and the skin was cleaned to erase all marks.

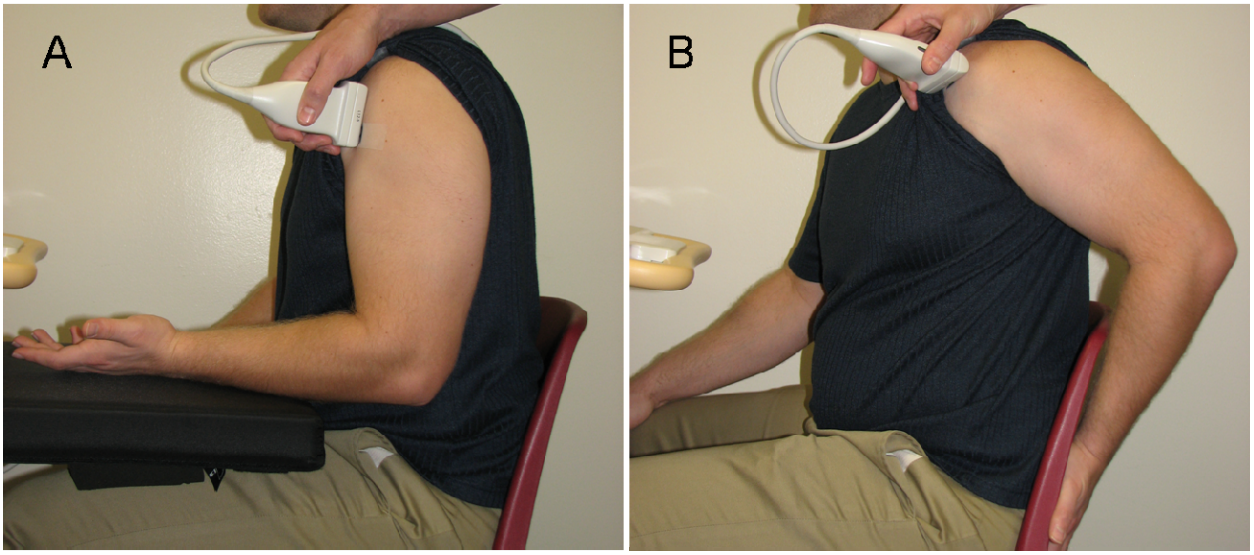

Figure 3. Subject positioning for imaging of the biceps (A) and supraspinatus (B) tendons

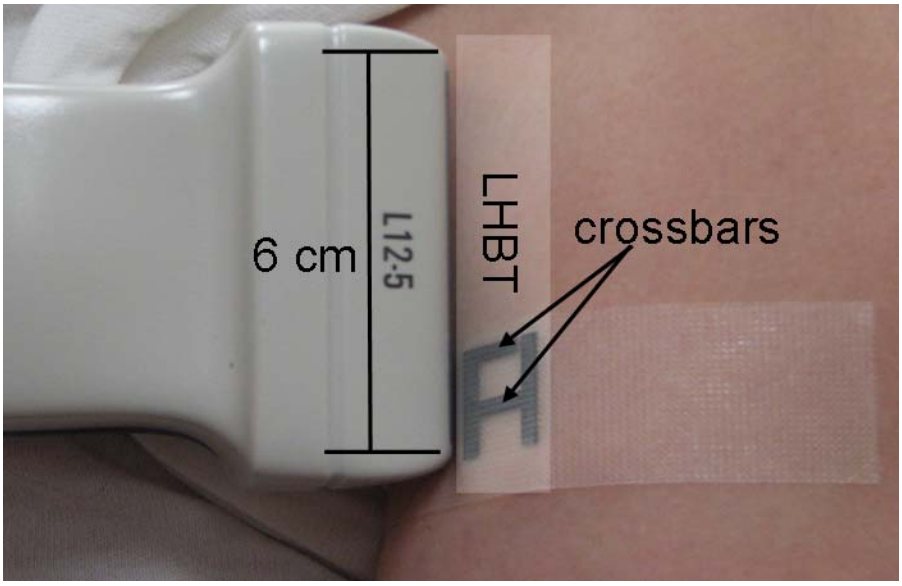

Figure 4. Transducer and reference marker position relative to the long head of the biceps tendon (LHBT) The crossbars create an interference pattern visible on the ultrasound image.

A similar protocol was followed for the supraspinatus tendon although the upper limb positioning was modified to optimize viewing. The subject placed his palm on his lower back, or wheelchair backrest, with the elbow pointing posteriorly (Figure 3B). The transducer was positioned to obtain a transverse image of the widest part of the supraspinatus tendon, with the rotator interval and cross-sectional view of the biceps tendon clearly in view. The probe was adjusted to maximize brightness within the tendon. A second reference marker was taped to the skin and two images were collected under preparation #1.

Retest: After a rest period of approximately 30 minutes, participants underwent a second quantitative ultrasound examination (preparation #2) during which two additional images (images #3 and #4) of the biceps and supraspinatus tendons were recorded. Care was taken to maintain the same standardized seated position, to keep the ultrasound machine settings constant, and to replicate the exact measurement protocol during the test and retest examinations.

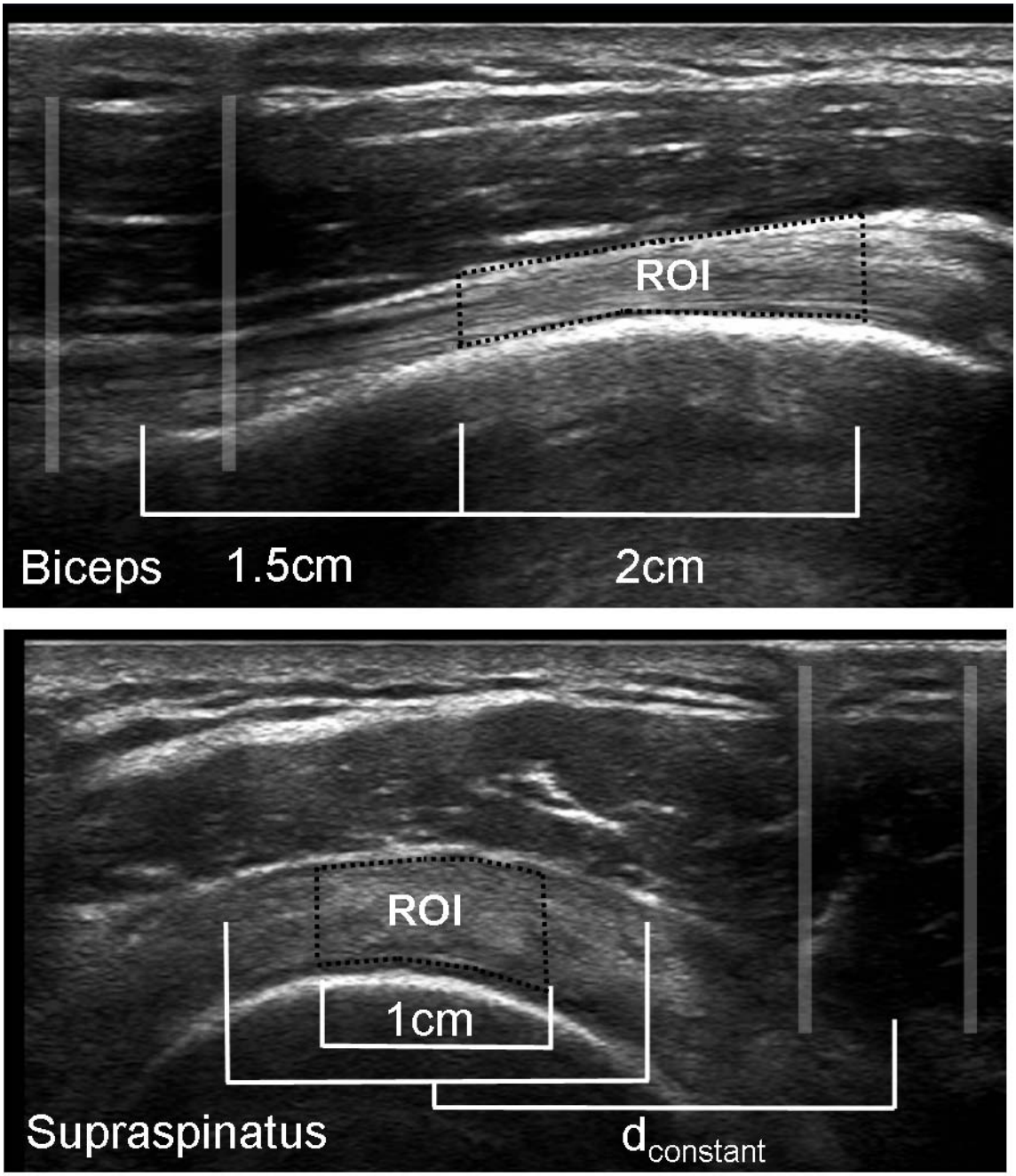

Figure 5. Marker interference pattern and region of interest for LHBT and supraspinatus tendons

$d_{constant}$ was defined for each subject as the distance from the midpoint of the interference pattern to the midpoint of the tendon for the first analyzed image.

2.2.3 Image Analysis

Each pixel in the ultrasound image represents a greyscale value ranging from 0 (black) to 255 (white). Collagen will reflect ultrasound beams back to the traducer and appear hyperechoic (closer to 255), while the beams pass through fluid which appears darker (closer to 0) on the resulting image. The ROI for each tendon was defined in relation to the center of the interference pattern created by the externally placed reference markers using a customized interactive Matlab function (The Mathworks, Natick, MA) as illustrated in Figure 5 (Appendix B). All images were processed in Matlab twice (readings #1 and #2) by an evaluator who was blinded to the preparation and image number during analysis. Overall, a total of eight scores were obtained for each outcome measure when combining the results from the test and retest sessions (2 preparations*2 images*2 readings). Features calculated for the tendon ROI include tendon width, echogenicity, variance, skewness, kurtosis, entropy, contrast, homogeneity, and energy. These image features have previously been used to assess image greyscale texture [66,67].

The upper and lower boundaries of the ROI were outlined manually and a 200 point cubic spline was fit to each border. The splined borders were each converted into 10 sub-sections and the minimum distance between corresponding sub-sections was computed and averaged to quantify tendon width within the ROI. Increased tendon width may be a result of chronic inflammation and may indicate the presence of rotator cuff pathology [39].

To determine echogenicity, the mean pixel greyscale was computed from all pixels within the ROI. A tendon can appear hypoechoic (darker) due to the presence of fluid, or if the collagen is not organized parallel to the long axis of the tendon as occurs with tendon degeneration. The greyscale values of all pixels within the ROI were represented as a greyscale

histogram from which first-order statistics were derived. The variance, skewness, kurtosis, and entropy describe the spread, symmetry, peakedness, and uniformity, respectively, of the greyscale histogram. While these image features have previously been used to describe ultrasound image texture, clinical interpretation of these features remains to be clarified. In general, a healthy tendon with highly aligned collagen fibers should have a striped appearance of alternating light and dark bands, while a tendon with degeneration would have a more uniform, darker appearance. Based on previous comparisons of muscle tissue [48], we would expect the greyscale histogram of a healthy tendon to be wider (increased variance), more symmetrical (less skewed), flatter (less kurtosis), and more heterogeneous (increased entropy).

Second-order statistics provide additional information about the texture of a ROI. This analysis considers the pixels of an image in pairs at a set distance (d) apart with a relative orientation angle (φ). For each histogram, a co-occurrence matrix of size (N_g x N_g), where N_g equals the total number of greyscale values in an image, can be defined. The co-occurrence matrix essentially describes the probability of a pixel pair with a defined spatial relationship (d, φ) having given greyscale level values (r,c) where r and c range from 0-255 (MATLAB 2008a). Using Matlab, texture coefficients (contrast, energy, and homogeneity) were derived from this co-occurrence matrix which describes the spatial dependence of the pixels in a ROI. Since a horizontal striped pattern within the ROI is expected due to the collagen organization within the tendon, the sum of texture values for φ =90° and d=1:5 was computed.

Contrast measures the intensity difference between a pixel and its neighbour over the entire image, and is equal to zero for a constant image and increases for a heterogeneous image. Energy is defined as the sum of squared elements along the diagonal of the co-occurrence matrix and is equal to 1 for a constant image and decreases with the presence of spatial greyscale

texture. Homogeneity measures how close the distribution of elements in the co-occurrence matrix is to a diagonal matrix. Homogeneity equals 1 for a diagonal co-occurrence matrix and gets closers to zero as the spatial texture increases. Therefore a healthy tendon would have higher contrast, lower energy, and lower homogeneity than a tendon with signs of degeneration.

2.2.4 Statistical Analysis

Generalizability theory is an extension of the intraclass correlation coefficient (ICC) and provides additional information about sources of variance and the effect of the experimental design [68]. Based on the analysis of variance, the generalizability theory is divided into two parts: the generalizability study (G-study) and the dependability study (D-study). The G-study allows one to determine the magnitude of the variances attributed to specified sources of variance. The D-study relies on information generated from the G-study to determine the reliability of specific pre-determined testing protocol designs.

First, we analyzed data from both evaluators to determine overall, inter-evaluator, inter-preparation, and inter-image reliability, measured as the dependability coefficient. Subject (S), Evaluator (E), Preparation (P), Image (I), and all possible combinations of these four facets were included as possible sources of variance. The dependability coefficient (Φ) is the ratio between the inter-subject variance and the sum of the inter-subject variance and all possible sources of error [69]. Like the ICC, the dependability coefficient ranges between 0 (null reliability) and 1 (perfect reliability). General interpretation guidelines suggest that a $\Phi<0.50$ represents poor reliability, and a Φ between 0.50 and 0.75 indicates moderate reliability, while values greater than 0.75 signify good reliability [70].

Since inter-evaluator reliability was fairly low (Table 1), data from a single evaluator (Evaluator #1) was used for the remainder of the analysis. Using the G-study, variance due to the subject (S), to the systematic errors related to subject's preparation (P), image (I) and reading (R), and to random errors associated with the interactions between these different sources of variance (listed in Tables 2 and 3) was calculated. The residual error is the interaction between all sources of error (SPIR). In an ideal experiment with no measurement error, 100% of the variance would be explained by the variance between subjects. A well-designed experiment will have a low percentage of variation attributed to the other potential sources of error. A random design, which allows all facets to contribute to the total error variance, was selected to estimate the test-retest reliability of quantitative ultrasound measures for various hypothetical testing protocols.

Absolute standard error of measurement (SEM), estimated in the units of the quantitative ultrasound measures, represents the square root of the absolute error variance. Theoretically, the SEM assumes that a subject will obtain an observed score within one SEM of their hypothetical true score about 68% of the time and within two SEMs of their hypothetical true score 95% of the time when data are normally distributed (within-subject standard deviation). Normalized SEM (SEM_{norm}), expressed as a unitless percentage, was calculated as (SEM/overall mean) * 100 to facilitate clinical interpretation. The overall mean reflects the mean of all measurements obtained at the test (n=4) and retest (n=4) sessions for a given outcome measure for all participants. These measures provide an estimation of the amount of uncertainty of an observed measurement in reference to a hypothetical true score, assuming that all testing conditions remain stable. Absolute and normalized SEM are presented along with the dependability coefficient for multiple hypothetical experimental protocols. The analysis of variance and

generalizability analysis were completed with GENOVA statistical software, version 2.2 (JE Crick/National Board of Medical Examiner, Philadelphia, PA).

2.3 RESULTS

2.3.1 Inter-rater Reliability

Mean quantitative ultrasound results for both evaluators are presented in Table 1. Sources of variance were calculated using quantitative ultrasound measures computed from two evaluators who each captured two images in each of two preparations. Overall reliability for a study design employing a single evaluator capturing a single image during one preparation (E=1; P=1; I=1) is described, computed from a random D-study model which allows all sources of variance to contribute to measurement error. Three systematic facets of error were analyzed to determine inter-evaluator, inter-preparation, and inter-image reliability. In each case, the facet of interest contributed to measurement error, while the other facets were fixed in the mixed D-study model. Inter-evaluator reliability was the lowest for all quantitative ultrasound measures for both tendons. While good ($\Phi>0.75$) inter-evaluator reliability was achieved for tendon width, most measures showed moderate ($0.5<\Phi<0.75$; n=4) or poor ($\Phi<0.5$; n=12) inter-evaluator reliability. The inter-preparation dependability coefficient, Φ, describes reliability between the test and re-test sessions, while inter-image Φ isolates reliability of quantitative ultrasound measures computed from two images captured during a single preparation. Inter-preparation reliability was generally lower than inter-image reliability. Inter-preparation Φ ranged from 0.528-0.908 for the 18 quantitative ultrasound measures, while inter-image Φ ranged from 0.463-0.962.

Inter-preparation and inter-image reliability was moderate or good (Φ>0.5) for all ultrasound measures for both tendons, except supraspinatus kurtosis (Φ=0.463). No systematic differences in Φ were noted between the biceps and supraspinatus tendons. Tendon width was consistently the most reliable quantitative ultrasound measure.

Table 1. Quantitative ultrasound measures computed by two evaluators

Ultrasound Outcome Measures	Tendon	Evaluator #1 Mean (SD)	Evaluator #2 Mean (SD)	Overall Φ*	Inter-evaluator Φ†	Inter-preparation Φ‡	Inter-image Φ§
Width	Biceps	4.02 (0.86)	4.03 (0.89)	.804	.819	.872	.941
	Supraspinatus	4.87 (0.78)	4.78 (0.92)	.804	.814	.908	.962
Echogenicity	Biceps	114.33 (18.85)	103.84 (17.66)	.396	.397	.686	.836
	Supraspinatus	105.97 (18.08)	111.04 (23.12)	.605	.659	.771	.829
Variance	Biceps	2052.4 (669.7)	2064.8 (713.6)	.310	.330	.660	.806
	Supraspinatus	1306.4 (359.1)	1536.7 (575.8)	.368	.402	.631	.728
Skewness	Biceps	0.56 (0.32)	0.82 (0.34)	.261	.355	.569	.677
	Supraspinatus	0.17 (0.33)	0.12 (0.36)	.339	.360	.551	.678
Kurtosis	Biceps	3.66 (0.97)	4.03 (1.27)	.385	.453	.664	.684
	Supraspinatus	3.66 (0.47)	3.47 (0.52)	.252	.259	.535	.463
Entropy	Biceps	7.11 (0.27)	7.06 (0.35)	.312	.312	.636	.768
	Supraspinatus	6.88 (0.22)	6.99 (0.26)	.335	.376	.528	.669
Contrast	Biceps	6.02 (1.72)	5.86 (2.08)	.328	.348	.625	.707
	Supraspinatus	4.08 (0.92)	4.35 (1.17)	.504	.589	.666	.700
Energy	Biceps	0.58 (0.24)	0.68 (0.29)	.270	.297	.752	.826
	Supraspinatus	0.71 (0.22)	0.65 (0.21)	.506	.518	.649	.629
Homogeneity	Biceps	3.46 (0.21)	3.54 (0.24)	.360	.400	.698	.825
	Supraspinatus	3.65 (0.18)	3.61 (0.20)	.581	.655	.723	.736

Mean (SD) quantitative ultrasound outcome measures computed for each evaluator.

*Overall reliability for a study design with E=1,P=1,I=1 computed with a random D-study model that includes all possible sources of variation

† Inter-evaluator reliability computed with a mixed D-study design with fixed facets (P and I)

‡ Inter-preparation reliability computed with a mixed D-study model with fixed facets (E and I)

§ Inter-image reliability computed with a mixed D-study model with fixed facets (E and P)

2.3.2 Intra-rater Reliability

The magnitude of variance components for each facet and their interactions based on biceps tendon outcome measures obtained by Evaluator #1 are presented in Table 2. Variance components for the supraspinatus tendon are presented in Table 3. The largest source of variance was attributed to the subjects (S) for both tendons. Variance between subjects ranged

from 46.2-90.6% of the total variance for the biceps tendon and between 47.7% and 92.1% for the supraspinatus tendon. The systematic error variance associated with the preparation (P) and image (I) was less than 1.79% and 1.28% respectively for all ultrasound measures. The error variance associated with the number of readings performed (R) was negligible (<0.001%). The other facets significantly contributing to error variances were the subject-preparation (SP) interaction and subject-preparation-image (SPI) interaction. The SPI interaction was the second largest contributor to total variance, ranging from 1.89% for biceps tendon width to 38.76% for supraspinatus kurtosis. For the biceps tendon, the SP interaction explained 3.73-20.9% of the variance. Similarly, the SP interaction accounted for 0.44-20.92% of the total variance. All other two- and three-way interactions combined contributed to less than 3.85% of the total variance for each quantitative ultrasound outcome measure. Finally, the residual error (SPIR interaction) represented less than 1.206 % of the total variance for the biceps tendon and less than 10.99% for the supraspinatus tendon.

The test-retest dependability coefficient (Φ), standard error of measurement (SEM) for a 90% confidence interval, and normalized SEM_{norm} are summarized in Table 4. For each tendon, three experimental scenarios are presented. The first (P=1; I=1; R=1) describes a situation in which a single image is captured during a single preparation and is read only one time. Essentially, this compares a single measurement value to a hypothetical true value. Imaging of the biceps tendon with this experimental design would yield good ($\Phi>0.75$) reliability for tendon width (0.906) and homogeneity (0.764), moderate ($0.5<\Phi<0.75$) reliability for echogenicity (0.742), variance (0.614), skewness (0.533) entropy (0.616), contrast (0.646), and energy (0.709), and poor ($\Phi<0.5$) reliability for kurtosis (0.462). SEM_{norm} ranged from 2.28% (entropy) to 47.3% (skewness) for the biceps tendon. For the supraspinatus tendon, the dependability

coefficients confirmed good (Φ>0.75) reliability for tendon width (0.921) and echogenicity (0.754), moderate (0.50<Φ<0.75) reliability for skewness (0.579), contrast (0.589), energy (0.618), and homogeneity (0.657), and poor (Φ<0.50) reliability for variance (0.474), kurtosis (0.477), and entropy (0.484). SEM_{norm} fluctuated between 0.484% (entropy) and 163% (skewness). For both tendons, SEM_{norm} for skewness was twice as large as the second largest SEM_{norm}.

Table 2. Variance components of quantitative ultrasound measures of the biceps tendon

Variance Components	Quantitative Ultrasound Outcome Measures of the Biceps Tendon								
	Width	**Mean**	**Variance**	**Skewness**	**Kurtosis**	**Entropy**	**Contrast**	**Energy**	**Homogeneity**
S	90.61	74.24	61.44	53.31	46.23	61.57	64.56	70.90	76.37
P	0.00	1.79	0.00	0.00	0.00	0.00	0.39	0.49	0.99
I	0.00	0.76	0.00	0.82	0.00	0.00	0.00	0.00	0.00
R	0.00	0.00	0.00	0.00	0.00	0.00	0.00	0.00	0.00
SP	6.19	11.05	20.93	3.73	16.28	19.02	16.90	6.35	7.44
SI	0.00	0.16	1.03	0.00	0.00	2.48	0.00	0.00	0.00
SR	0.12	0.03	0.00	0.00	0.00	0.31	0.23	0.45	0.20
PI	0.37	0.00	0.00	0.00	0.00	0.00	1.82	0.00	0.00
PR	0.00	0.00	0.00	0.00	0.01	0.00	0.00	0.00	0.00
IR	0.01	0.00	0.00	0.00	0.00	0.00	0.00	0.00	0.00
SPI	2.03	11.83	16.04	41.34	37.20	15.56	14.68	20.77	14.18
SPR	0.28	0.03	0.24	0.47	0.12	0.00	0.17	0.00	0.00
SIR	0.04	0.01	0.00	0.00	0.05	0.00	0.00	0.00	0.00
PIR	0.00	0.01	0.00	0.08	0.00	0.05	0.06	0.09	0.09
SPIR	0.35	0.10	0.32	0.27	0.13	1.01	1.21	0.95	0.72
Total Variance									
Relative (%)	100.00	100.00	100.00	100.00	100.00	100.00	100.00	100.00	100.00
Absolute	0.78	436.96	599414.45	0.15	1.46	0.10	3.81	0.08	0.05

Magnitude of variance components, expressed as a percentage (%) of the total variance (100%), of quantitative outcome measures of the biceps tendon obtained by Evaluator #1. Variance was attributed to the subject (S), preparation (P), image (I), reading (R), or an interaction of these facets.

D-study measurement error estimates are presented for two additional experimental designs. The first (P=1; I=1; R=2) shows only a marginal improvement in reliability if an additional reading is performed. The second scenario (P=1; I=2; R=1) illustrates the effect of using the average outcome measure value from two images taken under a single preparation. Slightly larger improvements in reliability are observed using this experimental design.

Table 3. Variance components of quantitative ultrasound measures of the supraspinatus tendon

Variance Components	Quantitative Ultrasound Outcome Measures of the Supraspinatus Tendon								
	Width	**Mean**	**Variance**	**Skewness**	**Kurtosis**	**Entropy**	**Contrast**	**Energy**	**Homogeneity**
S	92.12	75.40	61.44	57.91	47.71	48.37	58.88	61.76	65.65
P	0.00	0.00	0.00	0.37	0.00	0.00	0.00	0.00	0.00
I	0.00	0.00	0.00	1.28	0.00	0.00	0.00	0.00	0.00
R	0.00	0.00	0.00	0.00	0.00	0.00	0.00	0.00	0.00
SP	4.10	0.44	20.92	7.25	2.26	1.75	0.00	1.56	0.00
SI	0.77	0.00	1.03	0.00	0.00	0.00	0.00	0.00	0.00
SR	0.25	0.00	0.00	0.00	0.28	0.25	0.00	0.04	0.00
PI	0.00	0.00	0.00	0.00	0.00	0.00	0.00	0.00	0.00
PR	0.05	0.00	0.000	0.00	0.00	0.00	0.00	0.00	0.00
IR	0.00	0.00	0.00	0.00	0.00	0.00	0.00	0.00	0.00
SPI	1.89	21.62	16.04	26.33	38.76	37.42	35.03	33.56	29.39
SPR	0.15	1.37	0.24	1.66	0.00	0.00	3.57	0.00	2.81
SIR	0.00	0.00	0.00	0.73	0.00	0.00	0.00	0.00	0.00
PIR	0.00	0.07	0.00	0.94	0.00	2.39	0.38	0.42	0.09
SPIR	0.67	1.10	0.32	3.53	10.99	9.82	2.14	2.65	2.05
Total Variance									
Relative (%)	100.00	100.00	100.00	100.00	100.00	100.00	100.00	100.00	100.00
Absolute	0.62	405.21	204828.59	0.16	0.37	0.08	1.28	0.07	0.04

Magnitude of variance components, expressed as a percentage (%) of the total variance (100%), of quantitative outcome measures of the supraspinatus tendon obtained by Evaluator #1. Variance was attributed to the subject (S), preparation (P), image (I), reading (R), or an interaction of these facets.

Table 4. Measurement error estimations for multiple study designs

		D-study measurement error estimations for multiple study designs					
		Biceps Tendon			**Supraspinatus Tendon**		
		P =1 I =1 R =1	P =1 I =1 R =2	P= 1 I= 2 R= 1	P =1 I =1 R =1	P =1 I =1 R =2	P= 1 I= 2 R= 1
Width	Φ	0.906	0.910	0.919	0.921	0.926	0.937
	SEM	0.271	0.265	0.250	0.221	0.213	0.196
	SEM_{norm} (%)	6.727	6.582	6.206	4.547	4.384	4.038
Echogenicity	Φ	0.742	0.743	0.793	0.754	0.764	0.851
	SEM	10.610	10.591	9.190	9.985	9.723	7.316
	SEM_{norm} (%)	9.288	9.272	8.046	9.405	9.158	6.891
Variance	Φ	0.614	0.616	0.673	0.474	0.482	0.632
	SEM	480.747	478.994	423.072	328.352	322.874	237.531
	SEM_{norm} (%)	23.442	23.357	20.630	25.382	24.958	18.361
Skewness	Φ	0.533	0.535	0.677	0.579	0.600	0.693
	SEM	0.265	0.264	0.196	0.260	0.250	0.203
	SEM_{norm} (%)	47.302	47.097	34.917	163.133	156.348	127.432
Kurtosis	Φ	0.462	0.463	0.568	0.477	0.506	0.635
	SEM	0.887	0.886	0.716	0.443	0.418	0.320
	SEM_{norm} (%)	24.214	24.180	19.559	12.035	11.368	8.714
Entropy	Φ	0.616	0.620	0.681	0.484	0.516	0.643
	SEM	0.196	0.194	0.170	0.198	0.185	0.142
	SEM_{norm} (%)	2.756	2.731	2.389	0.484	0.516	0.643
Contrast	Φ	0.646	0.651	0.708	0.589	0.607	0.725
	SEM	1.162	1.148	1.006	0.725	0.698	0.534
	SEM_{norm} (%)	19.260	19.033	16.674	17.655	16.988	13.015
Energy	Φ	0.709	0.714	0.796	0.618	0.627	0.756
	SEM	0.150	0.148	0.118	0.162	0.159	0.117
	SEM_{norm} (%)	25.884	25.551	20.470	22.973	22.500	16.582
Homogeneity	Φ	0.764	0.768	0.826	0.657	0.673	0.779
	SEM	0.113	0.112	0.094	0.124	0.119	0.091
	SEM_{norm} (%)	3.272	3.237	2.704	3.392	3.267	2.495

Dependability coefficient (Φ), standard error of measurement (SEM) calculated for various D-study designs using a single value (design: P=1; I=1; R=1) or a mean value (all other designs) obtained by Evaluator #1.

P= preparation: number of time markers were affixed to skin and upper limb positioned
I= image: number of ultrasound images recorded
R= reading: number of readings completed for each ultrasound image recorded

2.4 DISCUSSION

The objective of this study was to quantify the sources of variance, reliability, and measurement error of quantitative ultrasound outcomes of the biceps and supraspinatus tendons. Furthermore, this study also aimed to translate these results into recommendations for the development of a

time-efficient and reliable quantitative ultrasound measurement protocol. This study represents the first investigation into the psychometric properties of quantitative ultrasound measures in the biceps and supraspinatus tendon.

2.4.1 Inter-evaluator Reliability

As expected, inter-evaluator reliability was generally low, which is in agreement with previous studies that suggest that ultrasound is an operator-dependent modality. Brushoj et al. reported significant differences in Achilles tendon width and thickness measurements between observers, although cross-sectional area was statistically similar [63]. No explanation of observer experience is provided. In the current study, biceps and supraspinatus tendon width measurements showed good dependability (Φ>0.75), between evaluators who had approximately the same level of experience and followed a standardized protocol. However, other quantitative ultrasound measures exhibited only poor or moderate dependability. Ying et al. reported 68% and 81% reproducibility between 5 observers, based on the intra-class correlation coefficient, in the sonographic measurement of Achilles tendon thickness and cross-sectional area respectively [65]. The authors suggest that the high inter-observer reliability they observed was due to a standardized scanning protocol. Inter-preparation and inter-image reliability reported in the current study are higher than inter-evaluator reliability that has been previously reported. Ideally, research or clinical applications that seek to identify musculoskeletal changes should ensure that a single examiner performs all ultrasound scans.

Since evaluator error can easily be eliminated, it is desirable to quantify reliability assuming that only one evaluator conducted the ultrasound examinations. Using data from both evaluators, we also examined inter-preparation and inter-image dependability. The significance

of these two types of reliability can be illustrated by imagining a protocol designed to examine acute changes within a tendon in response to some type of intervention, or physical activity. Inter-preparation Φ describes the reliability of the baseline measurement on any given day. We have developed an external reference marker and standardized positioning protocol, which essentially allows the preparation to be kept constant. Therefore post-intervention ultrasound images taken on the same day with the same external marker placement could be considered part of the same preparation. For this scenario, reliability is more closely represented by the inter-image Φ presented in Table 1. The development of a reference marker and standardized positioning protocol improves reliability and will give increased power to detect acute changes occurring within a tendon. All quantitative ultrasound measures exhibited moderate or good inter-preparation dependability (Φ >0.5) and 17 of the 18 ultrasound measures a similar level of inter-image dependability. It should be noted that the estimate of reliability presented in this study are more conservative than other measures of reliability, including ICC. Inter-evaluator Φ describes variability between two evaluators taking a single image during a single preparation, as opposed to comparing averaged data from all images and preparations. Similarly inter-preparation and inter-image reliability are computed for one evaluator, taking a single image during one preparation. The variance and measurement error is estimated using data from two evaluators capturing two images during each of two preparations.

Although not a focus of this study, Table 1 also illustrates differences between the biceps and supraspinatus tendons. The supraspinatus tendon was wider than biceps tendon, while no clear difference in echogenicity was observed. In general, lower variance, skewness, kurtosis, entropy, and contrast values were computed for the supraspinatus tendon than for the biceps tendon. These differences in quantitative ultrasound measures should not be interpreted as

structural differences between the tendons. Instead, the differences are likely due to the imaging protocol used in this study. The biceps tendon was imaged along the longitudinal axis, which optimized imaging of the horizontal collagen pattern within the tendon. Conversely, the supraspinatus tendon was imaged in the transverse direction to provide the most uniform measurement of tendon width and provide a fairly flat section to define our ROI while avoiding anisotropy. In the longitudinal direction, the supraspinatus tendon has a triangular appearance making it difficult to calculate tendon width consistently for all subjects and images. Also, it is not possible to orient the transducer perpendicular to the entire tendon in this view, resulting in anisotropy. No studies have reported all of the quantitative ultrasound measures presented in this study, but our results for tendon width are in agreement with previous results. Wallny et al. measured a mean biceps tendon diameter of 3.5 mm in asymptomatic shoulders, and 5.5 mm in symptomatic shoulders [44]. In this study, we measured a mean biceps tendon diameter of 4.0 mm. O'Connor et al. reported supraspinatus tendon width to be 4.88 mm which is close to the values reported by both evaluators (4.87 mm and 4.78 mm) in this study [64].

2.4.2 Sources of Measurement Error

Since inter-evaluator reliability was poor when compared to inter-preparation and inter-image reliability, we focused on a single evaluator to quantify other sources of variance including Subjects, Preparation, Image, and Reading. As hypothesized, the largest source of variance was always attributable to differences among participants (S) with a percentage of total variance representing up to 92.12% of the total variance. This represents the proportion of variance without error and may consequently explain the moderate and good dependability coefficients (Φ>0.50) found in the D-study for the majority of outcomes. The systematic effect of the

reading (R) was almost null and confirmed that negligible systematic changes in quantitative ultrasound measures exist across readings. The effect of the preparation (P) and image (I) was generally low which confirms that only a small systematic increase or decrease occurred across preparations and across images recorded. However, the error variance components associated with the interaction between the subject and preparation (SP), and to a greater extent the interaction between the subject, preparation and image (SPI), were the highest. The SP interaction suggests that the marker placement and upper limb positioning may have varied between the test and retest session differently between subjects. The SPI interaction highlights that the placement, orientation angle or pressure exerted over the ultrasound head in an effort to record the best image possible may have been different between the two sessions.

Since random error interactions resulting from reference marker placement and upper extremity positioning (P) are the largest, capturing multiple images with the ultrasound transducer in the same location, and the upper limb in the identical position (P fixed) would improve the reliability of quantitative ultrasound measures. Pre- and post-activity images captured with the reference marker remaining in place would reduce the error due to preparation. Another way to reduce this error would be to capture images under multiple preparations (P) and compute an average quantitative ultrasound measurement value. However, repeated preparations may not be practical in the context of an experiment examining acute changes. If a musculoskeletal structure is changing in response to activity, rapidly repeated measurements are required and therefore two positionings cannot be performed without compromising the validity of the measurements. All other interactions were negligible (<3.57%). The residual error (SPIR interaction) reflects unknown or random sources of error. Therefore it is difficult to suggest experimental design improvements based on this interaction. SPIR interaction was very low for

the biceps tendon (<1.21%) and less than 11% for all ultrasound measures describing the supraspinatus tendon. Error may be less systematic during imaging of the supraspinatus tendon and more difficult to control for with modifications to experimental design.

2.4.3 Effect of Study Design

For all study designs presented in Table 4, greyscale variance, skewness, and kurtosis demonstrated the lowest reliability while tendon width and echogenicity were the most repeatable. This discrepancy can be explained by the sensitivity of ultrasound to probe orientation, as well as how the different quantitative ultrasound measures are calculated. While the differences among subjects contributed to most of the variability, differences between images were likely operator-dependent and due to slight changes in probe orientation or tilt or the amount of force applied to the transducer. Tendon width and echogenicity are calculated as mean values using information from the entire ROI. Small changes in one area of the tendon may be balanced out by opposing changes in a different region. Ultrasound measures calculated as averages would be less sensitive to these types of changes. However, first order statistics (variance, skewness, kurtosis, and entropy) quantify changes in the shape of the greyscale histogram. Small changes in the greyscale echotexture that may be obscured by averaging could affect the greyscale distribution. In order to isolate the horizontal striped pattern of a healthy tendon, pixel pairs were only examined in the vertical direction. Focusing on a single axis, may have lessened the effect of small micro-texture changes due to probe orientation. Additionally, image features values were averaged over a distance ranging from 1-5 pixels which may also have reduced the operator-dependent error.

The values of SEM_{norm} listed in Table 4 provide a guideline for interpreting changes within a single subject as real or due to measurement error. SEM_{norm} (for P=1;I=1;R=1) essentially describes how close any single measurement is to a hypothetical true score. Minimum detectable change (MDC) is linearly related to SEM and can be calculated as 1.65 * √2 * SEM where 1.65 represents the two-sided tabled *z* value for the 90% confidence interval and √2 accounts for the variance of the measurements to be compared that were recorded at two distinct points in time. Therefore within a single individual, observed changes greater than the MDC can be considered significantly different. This may be useful in clinical applications tracking a single patient's progress or to stratify research subjects into groups based on who experienced significant change. MDC may be too conservative when examining difference between groups or multiple measurements within the group. Due to the limited application of ultrasound to study acute musculoskeletal changes, it is difficult to know if these quantitative ultrasound measures are sensitive enough to detect tendon changes in response to an intervention. Research needs to investigate the responsiveness of tendons to physical activity. One study used MRI to compare Achilles tendon volume and echogenicity before and after an eccentric loading task [59]. They observed a significant ($p<.001$) 12% increase in tendon volume and a 31% increase in echogenicity (intratendinous signal). Using the biceps as an example, the most conservative MDC estimate (P=1;I=1;R=1) within an individual would be 15.7% for tendon width and 21.6% for tendon echogenicity. Although MRI and ultrasound are different imaging techniques, the similarity between observed change (on MRI) and MDC (for ultrasound) provides justification to pursue quantitative ultrasound as a method to identify acute musculoskeletal responses.

Reliability of two hypothetical experimental situations in which either two images are captured, or two readings of a single image are performed, and averaged is presented in Table 4. Performing a second reading does not provide a meaningful improvement in reliability. Capturing a second image provides a marginal increase in the reliability coefficient and reduction in SEM. Therefore, when making comparisons within a single individual, capturing more than one image at each time point may provide a quantitative ultrasound measure value closer to a hypothetical true score. We believe that we limited error by using an external reference marker which was developed in lieu of a reliably identifiable bony landmark in the same plane as the tendon. If a protocol involves repeated measurements, we recommend using a reference marker that remains in place as described in this study. This would reduce the source of variation due to preparation between ultrasound images captured before and after an intervention. The amount of error within each image remains the same as presented in Table 4 (P=1;I=1;R=1), but the error due to the subject-preparation (SP) interaction has been reduced. Therefore the MDC would be less for two images captured under the same preparation than between two images captured at different times with a different preparation. It should be noted that variance due to the SP interaction also involves subject positioning. Taking care to use a strict positioning protocol could further reduce the error due to preparation.

Ultrasound reliability studies have been primarily limited to tendon width or cross-sectional area. Brushoj et al. reported within observer limits of agreement for Achilles tendon cross sectional area to be ±1.25mm (19%) [63]. Achilles tendon diameter in the sagittal (thickness) and frontal (width) planes, calculated as the mean of two measurements, demonstrated within observer agreement of 0.6mm (13%) and 2.09mm (12%) respectively. In our study, observed measurement error was slightly lower for these outcomes. The SEM for

tendon width was 6.7% for the biceps and 4.5% for the supraspinatus. O'Connor et al. reported an 8% coefficient of variation in supraspinatus short axis thickness between visits [64]. This translated to a 90% confidence interval of ±23% for supraspinatus thickness as measured by an experienced examiner, which is larger than was observed in the current study. Nielsen et al. reported first-order greyscale statistics of the supraspinatus muscle on two different days in 8 subjects [67]. Although specific values are not presented, the authors note that no statistically significant differences were found between the two different days for any of the first-order greyscale statistics. Due to the lack of detail, it is difficult to make direct comparison to the current study. Ultrasound reliability is dependent not only on the evaluator, but also on the properties of the machine itself. It is likely that the ultrasound machines used in these studies have different resolution, probe frequency, and internal image processing algorithms which could explain some of the variability in reported repeatability. This alludes to the notion that repeatability results describe context-specific reliability and can only serve as guidelines to other researchers. Exact values of SEM and MDC depend on the evaluator, the ultrasound machine, and the subject. Consistency can be enhanced by following a standardized scanning procedure that specifies subject positioning, probe location and orientation, and machine settings. Differences in ultrasound machines become less significant when making within-individual comparisons.

2.4.4 Limitations

The results of the current study are specifically based on a relatively small sample of subjects (N=20). As with any reliability study, these results should be interpreted with caution when applied to other groups. Five manual wheelchair users, along with 15 able-bodied subjects, were

studied because of future applications to studying injury development and prevention in wheelchair users. Subjects were not screened for shoulder pain or injury prior to participation as future studies will include individuals with both healthy and degenerated tendons. Varying levels of tendon health were informally observed among the subjects in this study. Healthy tendons often have better-defined borders and the collagen pattern is more easily visualized. Therefore, a reliability study of individuals with healthy tendons may result in inflated reliability estimates that would not translate to tendons with tendinopathy which may be more difficult to image. Additionally, we need to ensure that anisotropy is not affecting the quantitative ultrasound measures. Future studies should relate quantitative ultrasound measures to clinical pathology to establish the validity of these image features.

2.5 CONCLUSIONS

Quantitative ultrasound is a promising tool for quantitatively evaluating tendon appearance. Although the measured reliability for most outcomes was lower than we hypothesized ($\Phi>0.75$), we are encouraged that most quantitative ultrasound measures exhibit at least moderate ($\Phi>0.50$) reliability when images are captured by a single evaluator. The largest contributors to variance, in this case preparation (P), need special attention when designing an experimental protocol that minimizes measurement error. To this end, we have developed an external reference marker and a subject positioning protocol to reduce the error due to multiple preparations. Additionally, due to the inherent measurement error associated with this operator-dependent technology, normalized standard error of measurement (SEM_{norm}) should serve as a guideline for interpreting results within an individual. Intra-rater reliability was greater than inter-rater reliability and

therefore it is recommended that a single examiner perform all ultrasound examinations, particularly if multiple exams are being performed for each individual. First-order statistics seems to be more susceptible to error than tendon width and echogenicity and therefore extra caution should be used when interpreting these parameters. Research is needed to further examine quantitative ultrasound variability within individuals, and also to quantify the expected acute change magnitude. We believe that an appropriately designed protocol will allow quantitative ultrasound to illustrate acute tendon changes and lead to the development of interventions to reduce risk factors for musculoskeletal injury.

3.0 VALIDATION OF GREYSCALE-BASED QUANTITATIVE ULTRASOUND: RELATIONSHIP TO ESTABLISHED CLINICAL MEASURES OF SHOULDER PATHOLOGY

3.1 BACKGROUND

Ultrasound enables dynamic real-time evaluation of musculoskeletal structures and has been widely applied to evaluate shoulder integrity [45,71]. Tendinopathy on ultrasound has been qualitatively described as an enlargement of the tendon and a disruption of the normal fibrillar pattern [46]. Often the diagnosis of tendinopathy is subjective and based on the experience of the examiner. We have recently described a grading scale of musculoskeletal shoulder pathology that includes a rating of tendon health ranging from normal to varying degrees of tendinopathy or tears [26]. While this scale allows researchers to quantify various pathologies at the shoulder, the validity of the ratings is still dependent on the operator's perception of the scan. Using image analysis and a unique localization method, we aim to derive objective, quantitative descriptors of tendon health which will facilitate ultrasound-based research.

Few attempts have been made to relate quantitative measures of tendon appearance to clinically documented pain or pathology. Subjects with chronic tendinopathy have been shown to have larger cross sectional areas (CSA) compared to an asymptomatic control group [46]. An MRI study of chronic Achilles tendinopathy found that increased intratendinous signal correlated

to severity of pain and functional impairment [72]. Quantitative analysis of tendon appearance has primarily been limited to these two simple measures (CSA and mean echogenicity) which do not quantify the fibrillar pattern that becomes more disorganized with tendon degeneration. One recent study explored the spatial frequency content of Achilles tendon ultrasound images [53]. Using eight spatial frequency parameters, the authors were able to discriminate between subjects with and without tendinopathy with approximately 80% accuracy. Based on this evidence, further investigation of the greyscale pattern within the tendon on ultrasound seems warranted.

We will investigate 9 greyscale-based quantitative ultrasound (QUS) measures of biceps and supraspinatus tendon appearance including tendon width and mean echogenicity. The reliability of these QUS measures when using standardized protocol and reference marker has been established (Chapter 2), but the content validity of these measures has not been determined. First-order statistics (variance, skewness, kurtosis, and entropy) will be calculated to describe the global greyscale distribution within a region of interest. Co-occurrence matrix derived measures (contrast, energy, and homogeneity) will quantify the greyscale distribution in the expected direction of the fibrillar pattern within the tendon [66,67]. Healthy tendons with a strong directional pattern should exhibit increased contrast and lower energy and homogeneity. While there is no gold standard for measuring tendinopathy, we will investigate the content validity of the QUS descriptors of tendon appearance by describing their relationship to established clinical evaluations of pain and pathology.

QUS measures may facilitate a new line of research to identify risk factors for and to prevent musculoskeletal injuries. One group that could benefit from this type of research is manual wheelchair users. It is well-established that the majority of manual wheelchair users develop shoulder pain or pathology over time due to repetitive loading of the upper limb and that

this can have a negative impact on independence and quality of life [5,8,21]. Since shoulder pain and pathology is more common with increasing age and duration of wheelchair use, it is important to intervene as early as possible [29]. Fortunately, research in the area of wheelchair biomechanics has shown that interventions related to wheelchair setup or propulsion biomechanics can reduce cadence and the amount of force required to push a wheelchair [73]. Evaluating the acute musculoskeletal response to varying propulsion conditions using ultrasound may allow for earlier identification of interventions that reduce the risk of injury.

The primary aim of this study is to establish the content validity of greyscale-based QUS measures by describing their relationship to established measures of pain and pathology including questionnaires, physical examinations, and clinical ultrasound examination findings in manual wheelchair users [26,74]. We expect that tendinosis will present as an enlarged tendon with a less organized fibrillar pattern as has been previously described. Quantitatively, this will translate to increased width, skewness, kurtosis, energy and homogeneity and to decreased echogenicity, variance, entropy, and contrast. Further discussion of the theoretical basis for selecting the proposed QUS measures will be presented to establish their face validity.

3.2 METHODS

3.2.1 Subjects

Study participants were recruited through a research registry, local rehabilitation clinics, as well as at the 2007 and 2008 National Veterans Wheelchairs Games. Twenty-two individuals participated in this study at the Human Engineering Research Laboratories. All testing

equipment was transported to the National Veterans Wheelchair Games, where an additional 48 subjects were tested. Subjects were eligible if they used a manual wheelchair as their primary means of mobility, were 18-65 years of age, and were at least one year post in-patient rehabilitation. Subjects were excluded if they had a progressive or degenerative disability, a history of cardiopulmonary disease, or traumatic upper extremity injury to both the non-dominant wrist and shoulder. All subjects provided informed consent prior to participation in this study which was approved by our local Institutional Review Board.

3.2.2 Questionnaires

Basic demographic information including age, height, weight, diagnosis, and date of diagnosis/wheelchair prescription was collected using self-report questionnaires. The Wheelchair User's Shoulder Pain Index (WUSPI) was used to quantify shoulder pain during activities of daily living. The WUSPI score is calculated by summing the pain score (0-10 on a visual analog scale) for each of 15 activities and corrected based on individual activity level [1]. Subjects were also asked to report whether they had experienced shoulder pain in the last month and whether it was specific to overhead activities or occurred during wheelchair propulsion.

3.2.3 Physical Examination

A trained physician conducted a physical examination focused on signs of shoulder injury. Specifically, subjects were tested for pain or discomfort during 11 clinical tests and each was scored as: 0 = symptom/sign absent, 1 = equivocal finding, 2 = symptom/sign present. The clinical tests have been previous described [26] and included bicipital tendon/groove tenderness,

supraspinatus tendon/greater tuberosity tenderness, resisted external rotation, resisted internal rotation, acromioclavicular (AC) joint tenderness, supraspinatus test, painful arc test, Neer's sign, Hawkin's sign, O'Brien's sign for AC joint pathology, and O'Brien's sign for labrum pathology.

3.2.4 Clinical Ultrasound Examination

All participants underwent a clinical ultrasound examination by a trained physiatrist (Boninger or Fullerton) who assigned a numerical score for each of seven ultrasound signs. The total Ultrasound Shoulder Pathology Rating Scale (USPRS) score was calculated as the sum of the 7 individual examination scores and ranged from 0 to a possible maximum of 23. The USPRS has been previously described in detail [26]. Two new static examinations have been added including joint effusion scored as 0 (absent) or 1 (present) and bursal thickening scored as 0 (normal) or 1 (>2mm thick). Briefly, bicipital and supraspinatus tendinopathy were each scored on a scale from 0-6 where:

0=normal,

1=mild tendinosis,

2=severe tendinosis,

3=intrasubstance abnormality,

4=partial-thickness tendon tear,

5=focal full-thickness tendon tear, and

6=massive full-thickness tear.

Greater tuberosity cortical surface was graded as: 0=smooth hyperechoic surface, 1=mild, 2=moderate, 3=marked cortical irregularity. Finally, dynamic evaluation of supraspinatus and

subscapularis impingement resulted in a score ranging from 0-3 for each tendon where 0 = no impingement, 1= mild impingement, 2=moderate impingement, and 3 = marked impingement.

3.2.5 Quantitative Ultrasound Examination

A single examiner (Collinger) conducted a quantitative ultrasound examination of the biceps and supraspinatus tendons of the non-dominant shoulder using a Phillips HD11 1.0.6 ultrasound machine with a 5-12 MHz 50 mm linear array transducer (Phillips Medical Systems, Bothell, WA). The subject remained seated in his own wheelchair in a standardized posture (Chapter 2). A longitudinal image of the long head of the biceps tendon was obtained and a steel reference marker was taped to the skin, which produced an interference pattern in the ultrasound image. This reference marker has been shown to improve the reliability of QUS measures of tendon appearance (Chapter 2). A 2 cm wide region of interest (ROI) was defined 1.5 cm from the center of the interference pattern. A transverse view of the widest part of the supraspinatus tendon, with the rotator interval clearly in view, was saved for later analysis. An interference pattern from a second steel marker provided a landmark on the image to define a 1 cm wide ROI within the supraspinatus tendon. A longitudinal view of the biceps tendon was collected to optimize the viewing of the fibrillar pattern. For the supraspinatus tendon, however, a transverse view was chosen to minimize anisotropy that occurs in the longitudinal view allowing for more reliable imaging.

Saved ultrasound images were post-processed using Matlab (The Mathworks, Natick, MA). A detailed description of the greyscale-based QUS measures has been previously presented (Chapter 2). Tendon width was defined as the average distance between the top and bottom border within the ROI. Mean echogenicity, variance, skewness, kurtosis, and entropy

were computed from a histogram that describes the greyscale distribution, or echotexture, within an ROI. Contrast, energy (smoothness), and homogeneity describe echotexture by comparing pixel pairs in the vertical direction since a horizontally oriented collagen fiber pattern exists within the tendons. A healthy tendon would be expected to have increased contrast, and decreased energy and homogeneity due to the striated reflection of the highly aligned collagen. Figure 6 illustrates the collagen fiber pattern in a healthy tendon (A) and for someone with severe tendinosis (B).

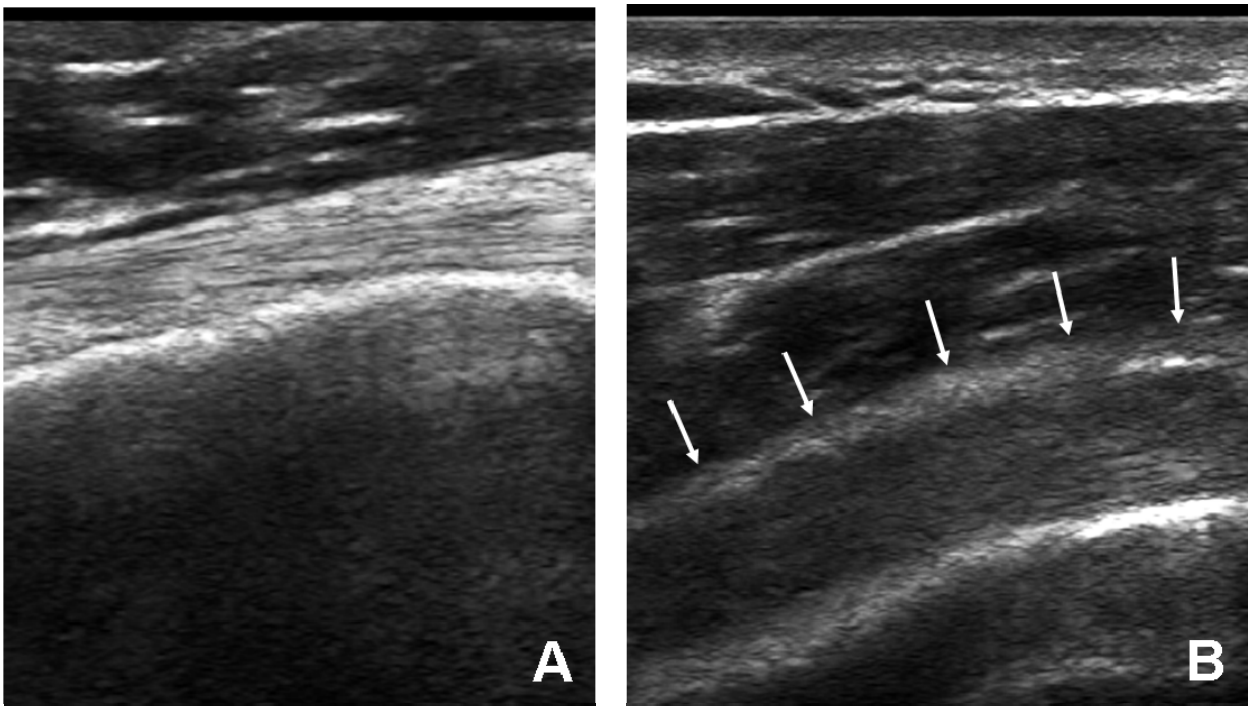

Figure 6. Ultrasound of a healthy biceps tendon (A) and one with severe tendinosis (B)

3.2.6 Statistical Analysis

Descriptive analysis of all data was performed first including mean and standard deviation for continuous variables (demographics and QUS variables) and frequency for discrete variables (pain, physical examination, clinical ultrasound scores). Content validity was determined by

computing correlations between QUS variables, demographics, and clinical ultrasound tendon grades. Non-parametric (Spearman's) correlations were used for tests involving clinical ultrasound scores. Since fewer clinical ultrasound scores were observed for the biceps tendon, an ANCOVA was used to compare QUS variables between subjects with healthy tendons, those with mild tendinosis, and those with severe tendinosis. Significant differences ($p=.019$) in tendon depth below the skin were noted between these groups. A larger distance between the skin and tendon could make it more difficult to obtain a clear image of the tendon and therefore tendon depth was entered as a covariate. T-test comparisons of QUS descriptors of tendon appearance were made between subjects with and without pain and between subjects with and without symptoms upon physical examination. All statistical analysis was performed using SPSS (SPSS, Inc., Chicago, IL).

3.3 RESULTS

3.3.1 Subjects and Questionnaires

Seventy subjects were recruited for this study and data from 67 manual wheelchair users is presented. Two subjects were withdrawn because they did not return for testing after providing informed consent. One subject's data was excluded because of poor image quality. Another subject had a completely ruptured biceps tendon so ultrasound examinations were only performed for the supraspinatus tendon. One subject had poor image quality for the supraspinatus, and therefore data was only analyzed for the biceps tendons. On average, subjects

were 45.2 ± 11.0 years old, weighed 82.6 ± 19.9 kg, were 1.77 ± 0.09 m tall, and had been using a wheelchair for 13.8 ± 11.2 years.

The prevalence of shoulder pain, physical examination symptoms, and clinical ultrasound examination findings has been previously described for 49 manual wheelchair users with spinal cord injury [40]. Although only 5 subjects participated in both studies, we found a similar incidence of shoulder pain and pathology. A brief summary of findings among the current group is provided.

The average WUSPI score was 11.8±26.5, however the data was highly skewed as 30 subjects had WUSPI score of 0. Another thirty-one subjects had a score of 25 or less. One subject scored 40.9, while the remaining five participants had a WUSPI score greater than 82.

33 subjects (49.3%) reported experiencing shoulder pain within the last month. Specifically, 17 subjects (25.4%) reported pain during overhead activities, while 15 (22.4%) experienced shoulder pain during wheelchair propulsion.

3.3.2 Physical Examination

35 (52.2%) participants exhibited at least one sign of pain/discomfort for the non-dominant shoulder during the physical examination. 10-15% of subjects showed symptoms during the supraspinatus test, resisted external rotation, the painful arc test, Neer's sign, and O'Brien's sign for labrum pathology. 20-25% of subjects exhibited pain during tests for biceps tenderness, supraspinatus tenderness, acromioclavicular (AC) joint tenderness, Hawkin's sign, and O'Brien's sign for AC joint pathology. Only 6% of subjects experienced pain during resisted internal rotation.

3.3.3 Clinical Ultrasound Examination

All but 1 participant showed some sign of shoulder pathology during the clinical ultrasound examination. Recorded total USPRS scores ranged from 0 to 16 points with a mean score of 6.3 ± 3.6. Most subjects had a normal biceps tendon appearance (39%) or presented with mild tendinosis (47%) while only 12% of subjects exhibited a normal supraspinatus tendon appearance. The majority of subjects either presented with mild supraspinatus tendinosis (29%) or a partial tear (28%).

61.2% of participants showed signs of supraspinatus impingement ranging from mild (40.3%), to moderate (19.4%), to marked (1.5%). 29.9% of subjects exhibited subscapularis impingement classified as either mild (25.4%) or moderate (4.5%). The majority of subjects (85.0%) showed some degree of cortical irregularity. 41.8% presented with mild irregularity, while 31.3% had moderate irregularity, and 11.9% showed marked cortical irregularity or pitting. 23.9% of subjects presented with bursal fluid or thickening and 11.9% showed signs of joint effusion of the long head of the biceps tendon sheath.

3.3.4 Quantitative Ultrasound

Mean quantitative ultrasound (QUS) values derived from the biceps and supraspinatus tendon ROI are presented in Table 5.

Table 5. Quantitative ultrasound measures of the biceps and supraspinatus tendons

QUS Measure	Biceps Tendon	Supraspinatus Tendon
	Mean (SD)	Mean (SD)
Width (mm)	5.01 (1.16)	5.32 (1.00)
Echogenicity	108.96 (24.11)	98.18 (29.26)
Variance	1729.38 (745.28)	1221.26 (692.93)
Skewness	0.54 (0.47)	0.27 (0.42)
Kurtosis	3.91 (0.96)	3.81 (0.85)
Entropy	6.98 (0.36)	6.72 (0.49)
Contrast	5.08 (2.07)	3.73 (1.80)
Energy	0.69 (0.32)	0.95 (0.62)
Homogeneity	3.59 (0.27)	3.78 (0.35)

SD= standard deviation
Note: No statistical comparisons were made between tendons.

3.3.5 Quantitative Ultrasound and Demographics

Significant correlations were observed between demographic variables and QUS descriptors of biceps and supraspinatus tendon appearance. Increased age, duration of wheelchair use, and body weight correlated with a darker, more homogenous tendon appearance, consistent with tendinopathy. Specifically, older individuals tend to have a darker biceps tendon appearance ($p = 0.044$, $r = -0.249$) and decreased greyscale variance ($p=0.011$, $r=-0.312$), entropy ($p=0.041$, $r=-0.253$), and contrast ($p=0.007$, $r=-0.331$). Biceps tendon homogeneity increased with age ($p=0.017$, $r=0.292$). For the supraspinatus tendon, duration of wheelchair use was correlated with decreased mean echogenicity ($p=0.014$, $r=-0.300$), variance ($p=0.049$, $r=-0.248$), and contrast ($p=0.001$, $r=-0.393$), and increased skewness ($p=0.003$, $r=0.364$) and homogeneity ($p=0.003$, $r=0.372$). Heavier individuals tended to have a larger biceps tendon ($p=0.010$, $r=0.320$) and a darker supraspinatus tendon ($p=0.004$, $r=-0.357$). They also exhibited less contrast ($p=0.009$, $r=-0.324$; $p=0.001$, $r=-0.393$) and increased homogeneity ($p=0.014$, $r=0.304$; $p=0.003$, $r=0.372$) for the biceps and supraspinatus tendons respectively. Increased body weight

also correlated with less entropy of the biceps tendon ($p=0.047$, $r=-0.249$) and less greyscale variance in the supraspinatus tendon ($p=0.049$, $r=-0.248$). Overall, these relationships suggest that the biceps tendon degenerates with age, while the supraspinatus tendon appears to be more affected by the years of wheelchair use. Increased body weight correlated with some indicators of tendon degeneration, while subject height did not impact tendon health. Quantitative ultrasound features did not discriminate between people with and without shoulder pain as reported by the WUSPI and other questionnaires.

3.3.6 Quantitative Ultrasound and Physical Examination

In general, QUS measures of the biceps tendon were not significantly different between those who experienced pain upon physical exam, and those who did not. The only exception was that those who had pain during the painful arc examination ($n=9$) had significantly lower homogeneity and energy in the biceps tendon. However, QUS descriptors of supraspinatus tendon health were significantly different between those with and without pain during tests for biceps tenderness and AC joint tenderness. In both cases, subjects with positive physical examination findings had significantly lower tendon echogenicity, variance, entropy, and contrast and significantly higher kurtosis, energy, and homogeneity (Figure 7).

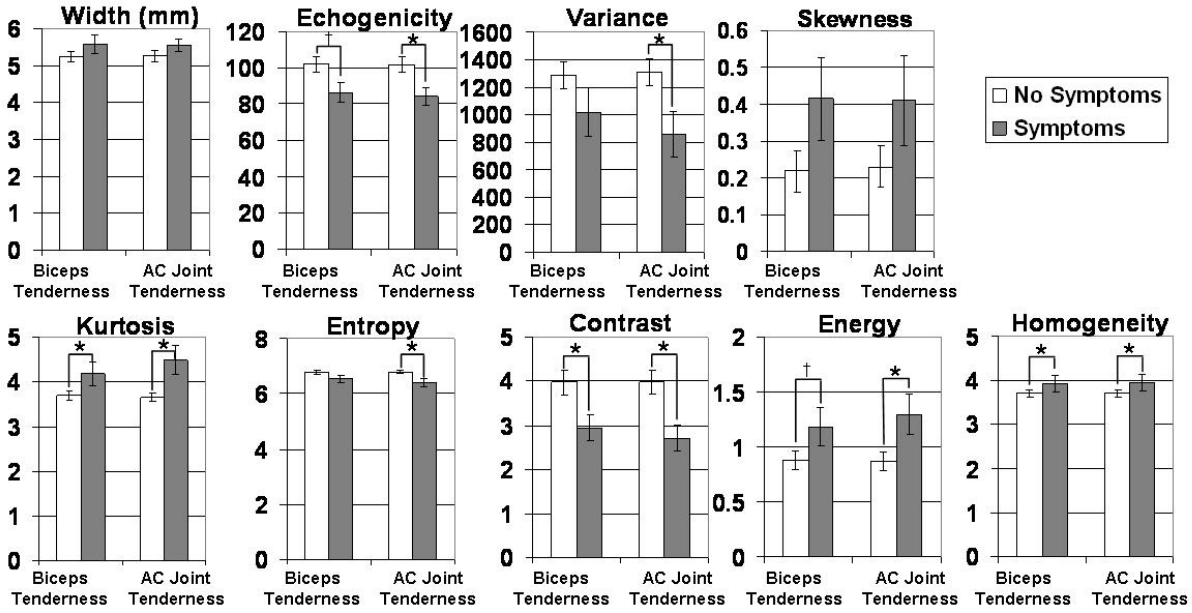

Figure 7. Quantitative ultrasound measures of the supraspinatus tendon for subjects with and without symptoms of biceps tendon tenderness and AC joint tenderness on physical examination

* indicates significant difference ($p < 0.05$) between subjects with and without symptoms
† indicates trend ($0.05 \leq p < 0.10$) towards difference between subjects with and without symptoms

3.3.7 Quantitative Ultrasound and Clinical Ultrasound Examination (USPRS)

An ANOVA was applied to test for differences in QUS measures of biceps tendon appearance between subjects with different tendon grades upon clinical ultrasound examination. For the biceps tendon, three groups were compared: Biceps Grade = 0; Biceps Grade = 1; Biceps Grade = 2 or 3. ANOVA revealed that subjects with more pathology, or a higher biceps tendon grade, were older ($p=0.011$) and weighed more ($p=0.011$) than subjects with healthy tendons. When controlling for tendon depth below the skin, subjects with more tendon pathology upon clinical ultrasound examination showed the following tendon characteristics upon QUS analysis: larger tendon width ($p<0.001$), darker echogenicity ($p=0.005$), less greyscale variance ($p=0.017$), increased skewness ($p=0.004$), increased kurtosis ($p=0.011$), less entropy ($p=0.057$), less contrast

(p=0.012), increased energy (p=0.006), and greater homogeneity (p=0.004). Significant post-hoc differences are indicated on Figure 8.

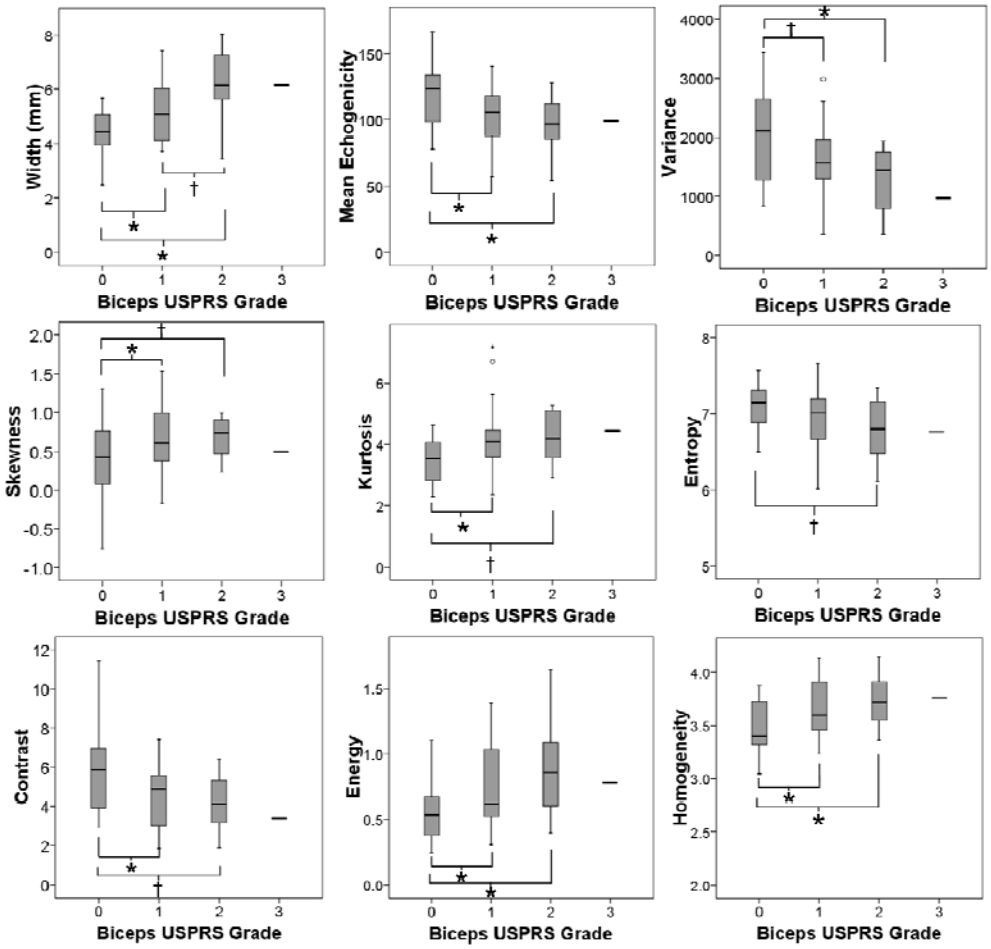

Figure 8. Quantitative ultrasound measures vs. clinical biceps tendon grade

Box-plots show the median and quartiles of raw quantitative ultrasound descriptors of biceps tendon appearance vs. biceps grade from the clinical ultrasound examination. Only 1 subject had a biceps grade of 3, and his data is represented as a single line for reference only. This subject's data was combined with the Biceps Grade = 2 group for statistical analyses. Post-hoc significant differences, when controlling for tendon depth below the skin, are noted as * ($p < 0.05$) or † ($0.05 \leq p < 0.10$).

Increased supraspinatus tendon pathology upon clinical ultrasound examination correlated with a larger supraspinatus tendon width (p=0.010, ρ=0.317), darker tendon echogenicity (p=0.013, ρ=-0.304), and greater homogeneity (p=0.029, ρ=0.269). Other relationships trended towards being significant, including increased greyscale skewness

(p=0.062, ρ=0.231) and energy (p=0.064, ρ=0.229) and decreased contrast (p=0.064, ρ=-0.230). As an example, a scatterplot of individual and mean values of tendon width for each USPRS supraspinatus tendon grade is shown in Figure 9.

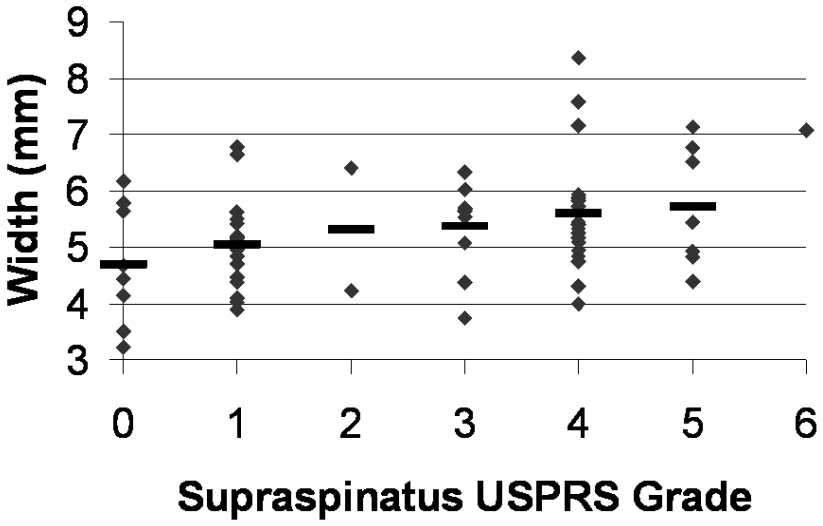

Figure 9. Supraspinatus tendon width increases with more severe tendinopathy

Mean values are denoted with a bold dash '-'. Only 1 subject had a supraspinatus grade of 6 so that subject's data is represented as a single dot.

Total USPRS, a measure of overall shoulder health, was significantly correlated to many QUS descriptors of biceps and supraspinatus tendon appearance. Spearman's correlation coefficients are presented in Table 6.

Figure 10 summarizes the relationship between increasing tendinopathy graded using the USPRS and greyscale-based QUS. Specific relationships, supported by statistical tests, have been described above.

Table 6. Correlations between quantitative ultrasound (QUS) measures and the ultrasound shoulder pathology rating scale (USPRS) score

QUS measure	Biceps Tendon QUS and Total USPRS score		Supraspinatus Tendon QUS and Total USPRS score	
	p-value	Spearman's rho	p-value	Spearman's rho
Width	.034	.261	.012	.307
Echogenicity	.098	-.206	.005	-.339
Variance	.069	-.225	.176	-.168
Skewness	.423	.100	.083	.215
Kurtosis	.188	.164	.986	.002
Entropy	.035	-.260	.120	-.193
Contrast	.037	-.258	.029	-.270
Energy	.023	.279	.040	.254
Homogeneity	.024	.278	.012	.307

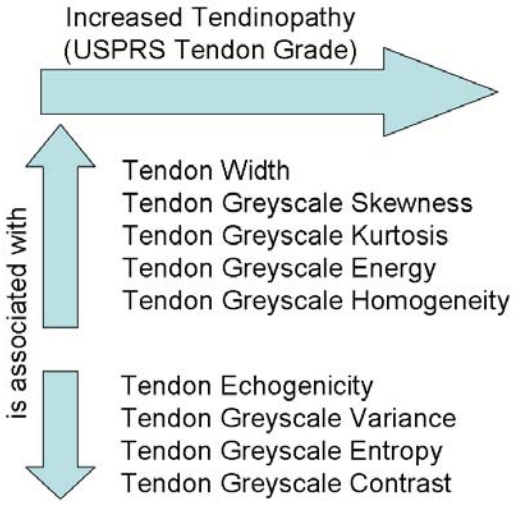

Figure 10. Summary of relationships between increasing tendinopathy and greyscale-based quantitative ultrasound

3.4 DISCUSSION

This study is unique in that it is the first to describe the relationship between greyscale-based quantitative measures of tendon appearance and clinical measures of shoulder pain and pathology. Using standardized positioning and a specially designed reference marker, we have established a reliable quantitative ultrasound (QUS) examination protocol (Chapter 2). Here we have established the content validity of these QUS measures by confirming their relationship with demographic risk factors for shoulder pathology and established clinical examinations of shoulder integrity in a sample of manual wheelchair users.

In agreement with our hypothesis, as tendinosis became more severe, tendons appeared larger, less echogenic, and showed less greyscale variance, entropy, and contrast. Compared to a normal tendon, more severe tendinosis also presented as increased greyscale skewness, kurtosis, energy, and homogeneity. All of these changes indicate a more diffuse collagen fiber organization as has been described clinically as a sign of tendon degeneration. Total USPRS score is a measure of overall shoulder integrity, specifically as it relates to risk factors of rotator cuff disease [26]. Higher USPRS scores correlated with tendinopathy of the biceps and supraspinatus tendon measured using greyscale-based QUS. Clinically, the grading of tendinosis is subjective so there is no gold standard for comparison; however the USPRS is the first scale to quantitatively describe shoulder pathology. We are encouraged that even with this relatively small sample size, greyscale-based QUS features change with tendon degeneration.

We have confirmed that increased age, duration of wheelchair use, and body mass are risk factors for greater shoulder pathology. Older individuals tended to have a more degenerated biceps tendon appearance, while duration of wheelchair use was more correlated to QUS descriptors of supraspinatus tendon appearance. Heavier individuals tended to have a tendon

appearance consistent with degeneration of both their biceps and supraspinatus tendons. Since heavier individuals likely experience more loading during propulsion and thus may develop more pathology [21], controlling for subject weight directly could obscure the relationship between clinical and QUS measures. Instead, we controlled for the distance from the skin to the top of the biceps tendon since ultrasound waves are attenuated as they pass through this tissue.

Physical examination findings, specifically biceps tenderness and AC tenderness, were accompanied by changes in QUS measures of supraspinatus tendon appearance. The direction of these changes was consistent with our hypothesis that persons with shoulder pain or pathology would have a larger tendon with a less organized collagen fiber structure. Contrary to our hypothesis, self-reported shoulder pain was not predictive of tendon health as described by QUS. This may indicate that some of the pathology identified in this study was still in the early stages of development and was asymptomatic [26]. Intervening before the development of pain is critical to preserving long term function of the upper limb.

Using clinical measures of shoulder pain and pathology including physical examinations and ultrasound-based grading scales, we have established the face validity of objective, QUS measures. It is also important to establish content validity by understanding the theoretical basis for the selection of these features. Tendinopathy results in tendon enlargement with reduced echogenicity and a loss of the normal fibrillar collagen pattern [75]. All of the greyscale-derived measures were chosen to quantify the presence or loss of a normal fibrillar pattern. A histogram describes the distribution of greyscale values, ranging from 0 (black) – 255 (white), within a region of interest. The mean value of this histogram, echogenicity, is often reduced with tendon degeneration because of a loss of the bright well-organized collagen structure, or because of increased fluid within the tendon.

Other first order statistics, including variance, skewness, kurtosis, and entropy, can be derived from the greyscale histogram. A healthy tendon would have a heterogeneous appearance because of alternating light and dark striations with a wide range of greyscale values, whereas a tendon with pathology would have a more homogeneous appearance since it is lacking the bright collagen pattern (Figure 6). Tendon degeneration translates to reduced greyscale variance and entropy, and increased skewness and kurtosis as observed in this study. To our knowledge, no one has applied first-order greyscale statistics to describe tendon appearance but researchers have employed these techniques to differentiate between muscles with varying amounts of contractile components [48] and between muscle appearance of subjects with and without neuromuscular disease [51,76].

Co-occurrence derived measures provide additional information about image greyscale texture in a specific orientation [47,66]. Contrast, energy, and homogeneity were computed in the vertical direction, perpendicular to the expected direction of collagen fiber alignment for a healthy tendon. Contrast quantifies the difference in greyscale level between adjacent pixels and is equal to 0 for an image with a constant greyscale, and increases for an image with sharp greyscale variations. Energy is equal to 1 for a constant image and decreases with non-uniformity. Homogeneity is equal to 1 for a completely uniform image and decreases when structural variations are present. Differences in image texture have been exploited to improve medical imaging segmentation [47], to develop iris recognition systems [77], and to differentiate between benign and malignant breast tumors using ultrasound [49]. To our knowledge, co-occurrence derived measures have not been used to quantify tendinosis, however theoretically a healthy tendon with a strong fibrillar organization should exhibit higher contrast and lower energy and homogeneity as was observed in this study. This is supported by Bashford et al. who

applied 2-D Fourier analysis to quantify the loss of collagen fiber organization in subjects with tendinosis [53]. A combination of eight spatial frequency parameters discriminated between a group with Achilles tendinopathy and a control group.

This study was limited because the degree of tendon pathology was not evenly distributed when scored using the USPRS. Specifically, no partial or full thickness tears of the biceps tendon were observed and only two subjects were graded as having severe supraspinatus tendinosis. However, we were still able to measure significant correlations between QUS measures of tendon health, demographic variables (age, weight, duration of wheelchair use) and clinical measures of pathology using ultrasound and physical examination techniques. The combined results from the biceps and supraspinatus tendons provide strong evidence that greyscale-based QUS measures are a valid, reliable way to measure tendinosis. Previously, tendinosis has only been judged subjectively, even when quantitative scores are assigned [40]. The combination of clinical grading scales and objective quantitative measures will enhance research related to musculoskeletal pathology and injury prevention.

Ultrasound is known to be an operator-dependent modality and for that reason, a single investigator collected all of the images in this study. The reliability of these QUS measures has been shown to be acceptable particularly when using a standardized protocol and reference marker as described in the current study (Chapter 2). One limitation of this protocol is that capturing a single image will only identify global tendinopathy and may miss partial tears or other localized abnormalities. However, for research purposes, it is important to capture the same area anatomically while minimizing the effects of anisotropy in each subject to derive reliable and objective measures of tendon appearance. We believe that subjects with more severe pathology will experience larger changes in these QUS measures globally throughout the

tendon when subjected to upper limb loading. This remains to be tested. Future work will need to establish which QUS measures are sensitive to change in order to identify risk factors and test interventions to reduce the risk of developing upper limb pathology.

3.5 CONCLUSION

In this work we have established the face and content validity of greyscale-based QUS measures. These measures correlate with known risk factors of shoulder pain and pathology including increased age, duration of wheelchair use, or body weight. Quantitative ultrasound descriptors of tendon appearance also correlated with clinically graded shoulder pathology (USPRS) and differentiated between subjects with and without pain upon physical examination. We believe that QUS provides a unique opportunity to evaluate risk factors for the development of shoulder pathology and the effectiveness of interventions to reduce this risk. In particular, manual wheelchair users have a high risk for developing shoulder pain and pathology that can negatively impact their quality of life. Fortunately, numerous interventions related to wheelchair setup and propulsion biomechanics can be tested to reduce this risk and to preserve independent mobility.

4.0 EFFECT OF AN INTENSE WHEELCHAIR PROPULSION TASK ON QUANTITATIVE ULTRASOUND OF SHOULDER TENDONS

4.1 INTRODUCTION

Shoulder pain and pathology is widely prevalent among manual wheelchair users who depend on their upper limbs for independent mobility. While there are many pathological conditions that produce shoulder pain in the SCI population, musculoskeletal causes, particularly injuries to the rotator cuff, are the most common [7,14]. Tendon overuse injuries, or tendinopathy, can be caused by intrinsic or extrinsic factors, or a combination of the two. Excessive mechanical loading of the upper limb, particularly during manual wheelchair propulsion and transfers, is a considered to be a major cause [13]. The repetitive nature of wheelchair propulsion leads to the development of chronic pathology in the absence of a traumatic injury to the upper limb. Repetitive strains of a tendon that are below the failure level induce microinjuries. These microinjuries stimulate the release of inflammatory factors, PGE_2 and $LTB_{4,}$ which are produced in response to mechanical loading and may contribute to tendon degeneration [36]. Using microdialysis, Langberg et al. showed that acute exercise induces changes in tendon metabolism and increases the inflammatory reaction in the paratenon [37].

Clinical practice guidelines have been published regarding preservation of the upper limb following spinal cord injury [13]. Based on evidence from expert opinion, ergonomics literature,

and correlational studies, the guidelines recommend propelling with a long, smooth stroke to minimize peak loading and the number of strokes taken. More evidence is needed regarding the effectiveness of interventions designed to optimize propulsion biomechanics and reduce the risk of repetitive strain injury. We propose a technique to identify acute markers of musculoskeletal injury that relate to long term risk. Ultrasound is a relatively inexpensive, dynamic imaging modality that may provide such an opportunity. Linking these acute markers to modifiable risk factors, such as propulsion biomechanics, may facilitate early intervention which is highly important for preserving the independence of manual wheelchair users.

Greyscale-based quantitative ultrasound (QUS) has recently been shown to be an objective, reliable way to describe tendon appearance (Chapter 2). Additionally, these QUS measures correlate to clinical measures of shoulder pathology in manual wheelchair users including physical examination maneuvers and clinical grading scales of tendinosis (Chapter 3). While chronic pathology is now quantifiable, a limited number of studies have investigated acute tendon changes in vivo. Significant increases in Achilles tendon volume and intratendinous signal were measured using magnetic resonance imaging following concentric and eccentric loading [59]. Evidence also suggests that vascular hyperemia occurs within a tendon following exercise [57,58]. Previously our laboratory used ultrasound to measure an increase in biceps tendon diameter and a decrease in mean echogenicity following participation in a wheelchair sporting event [56]. We believe that greyscale-based QUS measures will be sensitive to acute musculoskeletal changes and may provide additional information about the etiology of repetitive strain injuries.

We hypothesized that tendon microstructure would be altered following an intense propulsion task and that this would translate to significant changes in greyscale-based QUS

measures of tendon appearance. Based on an expected influx of fluid, which appears as black on ultrasound, we expected an increase in tendon width, variance, entropy, and contrast, and a decrease in echogenicity, energy, and homogeneity. Additionally, we expected that subjects with tendinosis or other risk factors for pathology including increased body weight, age, or duration of wheelchair use, would experience larger changes in quantitative ultrasound values. Finally, we expected subjects who used a faster stroke frequency or larger resultant force during the propulsion task to experience larger changes in tendon appearance.

4.2 METHODS

4.2.1 Subjects

Twenty-two individuals who were recruited through a research registry and local rehabilitation clinics participated in this study at the Human Engineering Research Laboratories. An additional 48 subjects participated at the 2007 and 2008 National Veterans Wheelchair games. Inclusion criteria for this study were: (1) use of a manual wheelchair as primary means of mobility, (2) between 18 and 65 years of age, and (3) at least one year post in-patient rehabilitation. Exclusion criteria for this study were: (1) a progressive or degenerative disability, (2) a history of cardiopulmonary disease, or (3) a traumatic upper extremity injury to both the non-dominant wrist and shoulder. Informed consent was obtained from all subjects prior to participation in this study which was approved by our local Institutional Review Board.

4.2.2 Demographics and Tendinopathy

Basic demographic information was self-reported by all subjects including age, weight, and years of wheelchair use. A trained physiatrist performed a clinical ultrasound examination of each subject's non-dominant shoulder. Numerical scores were assigned for bicipital and supraspinatus tendinopathy which are rated on a scale from 0-6: 0=normal, 1= mild tendinosis, 2= severe tendinosis, 3= intrasubstance abnormality, 4= partial thickness tendon tear, 5= focal full-thickness tendon tear, and 6= massive full thickness tear [26].

4.2.3 Wheelchair Propulsion Task

All subjects participated in a propulsion task that incorporated stops, starts, and turning. The 15-minute propulsion task included three 4-minute trials separated by 90 seconds of rest. Figure 11 shows the layout of the propulsion course. Participants were instructed to perform as many laps as possible during each 4 minute period. During each complete lap, participants made a left and right turn and were instructed to brake to a complete stop after each half lap. A SmartWheel (Three Rivers Holdings, LLC, Mesa, AZ) recorded the three-dimensional forces and moments applied to the pushrim on the non-dominant side during the first lap of each trial. Data analysis was performed to identify the straight-away regions (segments 1, 2, 3, and 4 in Figure 11). This analysis identified regions where the subject propelled at a constant velocity. Stroke frequency and maximum resultant force were computed from all strokes in these regions and averaged.

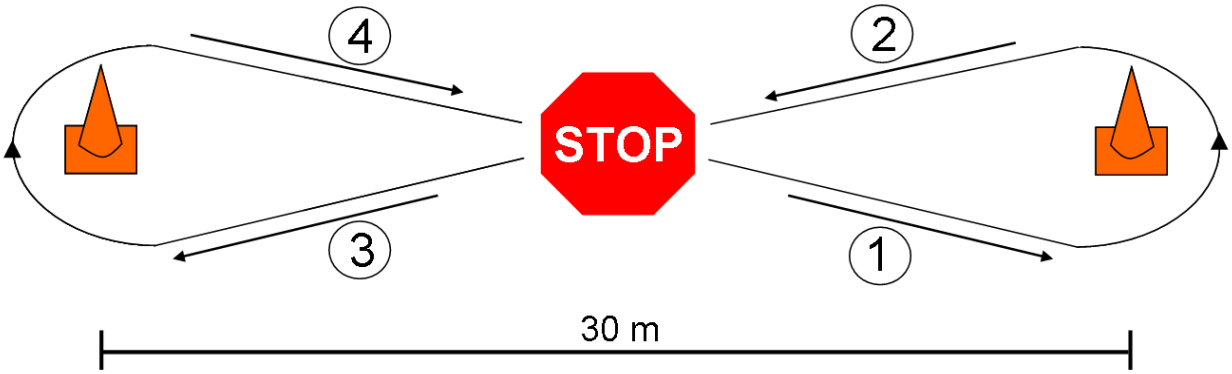

Figure 11. Schematic of overground propulsion course

Subjects made left and right turns around cones placed 30 m apart, braking to a complete stop at the center of the course after each half lap. Biomechanical data were computed from the 4 labeled straight-away sections of the course.

4.2.4 Quantitative Ultrasound Examination

A quantitative ultrasound examination was performed before and after a manual wheelchair propulsion task using a Phillips HD11 1.0.6 ultrasound machine with a 5-12 MHz 50 mm linear array transducer (Phillips Medical Systems, Bothell, WA). This protocol has been previously described in detail (Chapter 2). Images of the long head of the biceps tendon and supraspinatus tendon on the non-dominant side were captured before the propulsion task, immediately following the task (0 minutes post-propulsion), and every 5 minutes thereafter for a total of 30 minutes post-propulsion. During the baseline ultrasound examination (pre-propulsion) external reference markers were taped to the skin. The marker creates an interference pattern that is visible in the ultrasound image of the tendon and improves the reliability of quantitative ultrasound measures computed from multiple images (Chapter 2). Both reference markers remained in place during the propulsion task and during the post-propulsion imaging sessions. A region of interest within the tendon was defined in each image using the interference pattern created by the external marker. Seven greyscale-based quantitative ultrasound descriptors of

tendon appearance were computed from the region of interest including tendon width, mean echogenicity, greyscale variance, entropy, contrast, energy, and homogeneity. These features were chosen because they exhibit good reliability for the biceps and supraspinatus tendon (Chapter 2) and also correlate with severity of tendinosis (Chapter 3).

The QUS ultrasound measures chosen in this study describe the greyscale texture within the tendon. A healthy tendon has an anisotropic appearance, with alternating bands of light and dark pixels, due to the highly organized structure of collagen along the long axis of the tendon. Mean echogenicity, variance, and entropy consider all the pixels in a region of interest and describe the overall greyscale distribution. A healthy tendon would have increased echogenicity, variance, and entropy. Contrast, energy, and homogeneity describe variation among nearby pixels in the direction perpendicular to the collagen striations. A highly aligned collagen pattern translates to higher contrast and lower energy and homogeneity.

4.2.5 Statistics

Repeated-measures ANOVAs were performed to test the main-effect of time (baseline, 0, 5, 10, 15, 20, 25, and 30 minutes post-propulsion) on each quantitative ultrasound descriptor of the biceps and supraspinatus tendons. When appropriate, post-hoc analyses were performed to determined if the baseline quantitative ultrasound measures were significantly different from any of the post-propulsion ultrasound measures. Based on previously reported risk factors for shoulder pain and pathology, subject weight, age, years of wheelchair use, USPRS score for biceps and supraspinatus tendon pathology, stroke frequency, and resultant force were identified as possible predictors of tendon appearance following an intense propulsion task [23,26,73]. Stroke frequency and resultant force were computed from SmartWheel data collected during the

second 4-minute propulsion period to avoid the learning effect that may occur during the first trial and fatigue that may occur by the third trial. Repeated measures linear regression was performed to determine which independent variables predict quantitative descriptors of tendon appearance after the intense propulsion task. Additionally, quantitative ultrasound features computed at baseline were included as covariates in the regression models. All statistical analysis was performed using SPSS 15.0 (SPSS, Inc., Chicago, IL).

4.3 RESULTS

Ultrasound images were collected before and after the overground propulsion task in 66 manual wheelchair users. The remaining subjects were either withdrawn for not completing all portions of the study (n=2), or excluded because of poor image quality (n=2). On average, subjects were 45.2 ± 11.1 years old, weighed 82.8 ± 20.0 kg, were 1.77 ± 0.09 m tall, and had been using a wheelchair for 13.8 ± 11.3 years.

4.3.1 Main-effect of Time on Quantitative Ultrasound Measures

Mean values of the quantitative ultrasound measures of the biceps tendon and supraspinatus tendon at baseline and 0, 15, and 30 minutes post-propulsion are presented in Table 7. These time points are representative of the post-propulsion tendon appearance. Repeated-measures ANOVA with no covariates, in general, revealed that time did not significantly impact quantitative ultrasound descriptors of tendon appearance. A few exceptions were noted. Mean echogenicity of the biceps tendon differed significantly with time ($p=0.016$), but baseline was

not significantly different than any of the post-propulsion measures. Echogenicity at 0 minutes post-propulsion was significantly less than echogenicity at 5 (p=0.004) and 10 (p=0.021) minutes post-propulsion, although the mean difference was less than 6 greyscale units. Greyscale variance of the biceps tendon differed significantly with time (p=0.021), and post-hoc analysis showed that pre-propulsion tendon variance was marginally less (p=0.097) than the variance computed 15 minutes post-propulsion. Biceps tendon homogeneity was significantly influenced by time (p=0.04), but baseline was not significantly different from the post-propulsion measurements. Homogeneity at 0 minutes post-propulsion was greater (p=0.015) than biceps tendon homogeneity at 15 minutes post-propulsion. The main effect of time was also significant (p=0.021) for supraspinatus tendon greyscale energy, however no post-hoc differences were noted.

Table 7. Quantitative ultrasound (QUS) values for the biceps and supraspinatus tendons at baseline and post-propulsion

QUS Measure	Tendon	Baseline*	Time Post-Propulsion		
			0 min	15 min	30 min
Width (mm)	Biceps	5.01 (1.16)	5.00 (1.12)	4.96 (1.17)	4.99 (1.13)
	Supraspinatus	5.32 (1.00)	5.20 (0.85)	5.20 (0.93)	5.24 (0.91)
Echogenicity	Biceps†	108.75 (24.2)	106.53 (25.0)	110.54 (25.1)	111.70 (22.6)
	Supraspinatus	98.18 (29.3)	97.01 (31.1)	98.62 (28.6)	99.40 (28.0)
Variance	Biceps†	1723.9 (743.2)	1738.3 (741.5)	1876.7 (741.5)	1899.6 (746.4)
	Supraspinatus	1221.3 (692.9)	1217.0 (734.6)	1265.3 (768.4)	1263.1 (638.9)
Entropy	Biceps	6.98 (0.36)	6.97 (0.35)	7.02 (0.37)	7.05 (0.37)
	Supraspinatus	6.72 (0.49)	6.71 (0.53)	6.73 (0.50)	6.77 (0.45)
Contrast	Biceps	5.07 (2.06)	4.81 (1.91)	5.14 (2.17)	5.23 (1.84)
	Supraspinatus	3.73 (1.80)	3.63 (1.77)	3.75 (1.71)	3.77 (1.60)
Energy	Biceps	0.69 (0.33)	0.72 (0.31)	0.68 (0.33)	0.66 (0.31)
	Supraspinatus†	0.95 (0.62)	0.97 (0.65)	0.92 (0.62)	0.84 (0.43)
Homogeneity	Biceps†	3.59 (0.27)	3.63 (0.27)	3.59 (0.29)	3.57 (0.25)
	Supraspinatus	3.77 (0.35)	3.79 (0.36)	3.75 (0.33)	3.74 (0.31)

*Baseline QUS previously presented (n=67) (Chapter 3); one subject from the previous study did not complete the propulsion task and was excluded from the current analysis

†indicates significant main effect of time; only biceps tendon variance at 15 minute post-propulsion was significantly different from baseline

4.3.2 Prediction of Post-propulsion Ultrasound

Age, body weight, duration of wheelchair use, and large propulsion forces are all risk factors for pathology. However, since some of these variables were correlated to each other, they were not all included in the regression models to predict post-propulsion quantitative ultrasound. Age was significantly correlated to duration of wheelchair use ($p<0.001$, $r=0.428$), biceps tendinopathy ($p=0.005$, $\rho=0.344$), and supraspinatus tendinopathy ($p=0.005$, $\rho=0.343$). Since age was correlated to many other independent variables of interest, it was excluded from the regression analysis. Body weight was significantly correlated with maximum resultant force ($p<0.001$, $r=0.604$) and was also excluded from analysis. The final set of independent variables included: pre-propulsion QUS value, biceps or supraspinatus tendinopathy score, stroke frequency, resultant force, and years of wheelchair use. The repeated measures ANOVA included all post-propulsion QUS values as dependent values, but parameter estimates were computed for each time point: 0, 5, 10, 15, 20, 25, and 30 minutes post-propulsion. Data from 58 subjects was used for this analysis since biomechanical data was not collected for 8 participants. The two primary reasons biomechanical data was not collected was if an individual did not have a standard wheel size, or if his wheels could not be removed due to excessive equipment wear.

Pre-propulsion QUS values were always the strongest predictors of post-propulsion QUS values (most $p<0.001$). In addition to baseline QUS, risk factors for pathology predicted biceps QUS values immediately following propulsion (0 minutes post-propulsion). Table 8 lists the beta coefficients derived for each biceps tendon QUS variable at 0 minutes post-propulsion. The beta coefficients are computed with a regression model that includes all specified independent variables. None of the covariates significantly impacted tendon width immediately post-propulsion. For all other quantitative ultrasound measures, chronic tendinopathy and a longer

duration of wheelchair use had the opposite directional effect on post-propulsion QUS compared to a faster stroke frequency or larger resultant force. Baseline QUS was the only consistent predictor of post-propulsion supraspinatus tendon appearance.

Table 8. Chronic risk factors for pathology predict biceps QUS measures immediately post-propulsion

	Quantitative Ultrasound Measures						
	Width	Echogenicity	Variance	Entropy	Contrast	Energy	Homogeneity
Intercept	β= 0.35	β= -23.36	β= -186.5	B= 2.12*	β=-0.22	β= 0.73*	β= 1.46*
Baseline QUS	β= 0.99*	β= 0.72*	β= 0.57*	B= 0.64*	β= 0.63*	β= 0.56*	β= 0.69*
Biceps Tendinopathy	β= -0.08	β= -5.88†	β=-252.8*	B= -0.14*	β=-0.58*	β= 0.12*	β= 0.74†
Stroke Frequency	β= -0.12	β= 33.18*	β= 698.6*	B= 0.16	β= 1.90*	β= -0.25*	β= -0.26*
Resultant Force	β=-0.001	β= 0.20*	β= 3.73	B= 0.003*	β= 0.001	β= -0.002†	β= -0.001
Duration WC use	β= 0.001	β= -0.44*	β=-10.80†	B=-0.005†	β=-0.021	β= 0.006*	β= 0.004†

*indicates significant β values ($p \leq 0.05$); † indicates trended relationship ($0.05 < p \leq 0.10$)

Although biceps tendon width at 0 minutes post-propulsion was not significantly predicted by the specified covariates, a longer duration of wheelchair use showed a trended relationship with a smaller tendon ($p=0.09$, $\beta=-0.009$) at 5 minutes post-propulsion. A larger resultant force ($p=0.09$, $\beta=0.004$) and clinically graded tendinopathy ($p=0.06$, $\beta=0.21$) showed trended relationships that were indicative of an increase in tendon size. Increased stroke frequency contributed to a increased tendon echogenicity at 5, 10, 25, and 30 minutes post-propulsion although the effect was less than at 0 minutes as evidenced by smaller beta coefficients ($p<0.10$, $13.17<\beta<18.49$). Resultant force showed a negative relationship with biceps tendon contrast at 5, 15, 20, 25, and 30 minutes post-propulsion ($p<0.10$, $-0.014 \leq \beta \leq -0.010$). Resultant force had the opposite effect on biceps tendon homogeneity at 15, 25, and 30 minutes post-propulsion ($p<0.10$, $0.001 \leq \beta \leq 0.002$).

In general, supraspinatus tendon appearance at any time point after propulsion was only significantly predicted by the baseline QUS value however, resultant force showed significant relationships to post-propulsion supraspinatus tendon QUS. A larger resultant force predicted a lower supraspinatus tendon variance and entropy at 20 and 25 minutes post-propulsion ($p<0.05$).

4.4 DISCUSSION

This study was novel in that we computed quantitative ultrasound (QUS) descriptors of tendon appearance before and after an intense wheelchair propulsion task. We hypothesized that risk factors for chronic pathology and biomechanical variables significantly impact QUS descriptors of biceps and supraspinatus tendon appearance after propulsion. Since manual wheelchair users often develop shoulder injuries due to repeated loading from propulsion and transfers, we believed that these acute changes may accumulate over time and lead to chronic pathology. In accordance with our hypothesis, chronic biceps tendinopathy, duration of wheelchair use, stroke frequency, and resultant force significantly impacted biceps tendon QUS measures immediately post-propulsion. The effect of these variables was lessened or absent as the time after propulsion increased. Supraspinatus tendon appearance post-propulsion was significantly predicted by baseline QUS measures. At 20 and 25 minutes post-propulsion, a larger resultant force was indicative of lower supraspinatus variance and entropy.

Regression models, as part of a repeated measures ANOVA, were computed to determine if known risk factors for pathology contributed to post-propulsion QUS measures when controlling for baseline tendon appearance. The covariates had the greatest influence on tendon appearance at 0 minutes post-propulsion. A higher stroke frequency resulted in a brighter, less homogenous biceps tendon appearance at 0 minutes post-propulsion as evidenced by the direction of the beta coefficients in Table 2. A larger resultant force had the same effect, although the relationship was not significant for every QUS measure. The direction of the greyscale-based QUS changes caused by a faster stroke frequency or larger resultant force is consistent with a more aligned and prominent collagen pattern. Increasing tendinopathy, measured by the USPRS, or a longer duration of wheelchair use had the opposite directional

effect. Subjects with more tendinopathy, or those who had been using a wheelchair for a longer period of time, exhibited a darker, more homogenous tendon appearance after propulsion which may be an indicator of acute metabolic changes or inflammation.

We expected that subjects would experience a movement of fluid into the tendon as a result of the intense wheelchair propulsion task which would result in an overall darker, more homogeneous tendon appearance. Instead, from visual examination of the data, it appears that some subjects experienced an influx of fluid into the tendon, while others showed a more organized collagen pattern after loading, and some experienced no measurable change. Averaging data from all subjects obscures individual responses and results minimal changes from baseline among the entire group. This was confirmed by the repeated measures analysis, which in general found no change in QUS over time when covariates were not considered. However, when risk factors for pathology were entered as covariates, it became clear that these factors affect the biceps tendon in different ways. There is evidence from other investigators to support opposing acute tendon responses to loading. Langberg et al. measured an increased concentration of inflammatory factors in the peritendinous space of the Achilles tendon following isometric contractions [37]. Some have argued that inflammation is part of the normal response to excessive mechanical loading, however excessive production of inflammatory factors may increase the risk of tendinopathy [78]. Conversely, others have reported that mechanical loading of tendons results in a straightening and alignment of the collagen fibers, until loading increases to a point where microfailures begin to occur [36,79]. Tendon stretch may also result in fluid flow out of the tendon and a disruption of the extracellular matrix [79]. Fluid moving in to the tendon and collagen alignment would have the opposite directional effect on each of the QUS measures in this study.

As time after propulsion increased, chronic pathology risk factors appeared to have less influence on post-propulsion tendon appearance. There are a few exceptions worth noting. Subjects who used a higher stroke frequency tended to have a brighter biceps tendon appearance even at 30 minutes after propulsion. It is not clear, why other QUS variables were no longer affected by push frequency. Histological studies would be needed to confirm whether changes in the collagen microstructure occurred or if a change in fluid level had the largest influence on the greyscale ultrasound image. A larger resultant force predicted less contrast, and increased homogeneity from approximately 15-30 minutes after the propulsion task. This is indicative of a more homogeneous tendon appearance. This may indicate that the collagen fibers initially pulled into alignment during the propulsion task may no longer be as visible on the ultrasound image because of the presence of inflammatory factors or other fluid within the tendon. We can only speculate as to the physiological nature of these changes. It may be that alignment of collagen fibers is part of the normal response to loading, but if the forces exceed a certain limit, inflammatory factors move into the tendon. This mechanism can only be determined with histological study.

In general, supraspinatus post-propulsion tendon appearance was not significantly influenced by demographics, tendinopathy score, or biomechanics. The supraspinatus was imaged transversely to provide the most uniform view of the tendon while avoiding anisotropic artifact that results in the longitudinal view due to the tendons curved appearance. While this protocol leads to repeatable quantitative ultrasound measures, it may not be as sensitive to change as the biceps tendon which is imaged longitudinally. Collagen fiber organization is less visible in the transverse view. Future studies should image the supraspinatus longitudinally and transversely if anisotropy can be avoided to obtain a more comprehensive assessment of tendon

health. The biceps tendon may be a good indicator of overall musculoskeletal integrity as the shoulder since rotator cuff pathology is often accompanied by a symptomatic biceps tendon with degenerative changes visible on ultrasound [45].

The propulsion task was designed to be a self-determined maximal propulsion activity so that all subjects experienced intense loading of the upper limb. As a result some subjects propelled further and faster than others. However, a paced task may have challenged some participants, while it may have been very easy for others. We chose to control the duration of propulsion time and encouraged participants to complete as many laps as possible. We believe that this task design stressed all participants relative to their abilities, which allowed us to identify biomechanical risk factors for acute biceps tendon changes.

Since subject characteristics and propulsion biomechanics impact the direction of change in biceps tendon QUS, this may help us identify opportunities to intervene. Pre-existing chronic tendinopathy and a longer duration of wheelchair use result in a darker, more homogenous biceps tendon appearance after propulsion. This may indicate that they are more sensitive to the loading experienced during wheelchair propulsion than someone with healthy tendons. Longitudinal studies would help establish whether individuals who experience these same directional changes acutely will eventually develop chronic pathology. However, we believe that it is important to intervene before pathology develops. Previous research suggests that subjects who use a higher stroke frequency and larger propulsion force are more at risk for developing chronic pathology [13]. By altering an individual's wheelchair setup or propulsion technique, it may be possible to reduce the load experienced at the shoulder [13]. Future research should determine if QUS measures are sensitive to variable loading conditions within an individual.

Since tendinopathy and duration of wheelchair use will remain inherently constant, one may be able to isolate the effect of biomechanical loading on musculoskeletal structures of the shoulder.

4.5 CONCLUSIONS

Pre-existing tendinopathy of the biceps tendon and a longer duration of wheelchair use resulted in a darker more, homogenous tendon appearance post-propulsion. Subjects who used a higher stroke frequency or larger resultant force exhibited a brighter, more aligned fibrillar pattern within the tendon. We have shown that these measures are repeatable and that they relate to clinical measures of chronic pathology (Chapters 2 and 3). We believe that greyscale based ultrasound may be beneficial for studying the development of repetitive strain injury, particularly on an individual basis. Acutely, quantitative ultrasound could be applied to measure musculoskeletal responses to interventions designed to reduce the risk of developing chronic pathology. Longitudinal studies could take advantage of greyscale-based quantitative ultrasound to track objective measurements of tendon health that are not based on clinical judgments. This may help identify which individuals are developing tendinopathy before it becomes symptomatic, or before more serious pathology develops.

5.0 SHOULDER FORCES AND MOMENTS DURING WHEELCHAIR PROPULSION CORRELATE TO QUANTITATIVE ULTRASOUND MEASURES OF TENDINOPATHY

5.1 INTRODUCTION

Quantitative ultrasound (QUS) features based on first order statistics and co-occurrence matrices describe the greyscale texture within a region of interest. These features have proven to be reliable and valid descriptors of biceps and supraspinatus tendon health that correlate to clinical measures of pathology (Chapters 2 and 3). Traditionally tendinopathy has been judged qualitatively based on the ultrasonographer's interpretation of the scan. Greyscale-based QUS, however, provides a more objective measurement. Using these QUS features, one can measure structural changes within a tendon over time, or acutely in response to loading. One potential application is investigating the development and prevention of repetitive strain injuries.

Manual wheelchair users may benefit from this type of research since unavoidable loading on their upper limbs often results in shoulder pain and pathology [7,13]. Research has shown that changes in wheelchair setup or propulsion technique can reduce the amount of loading imparted to the upper limb [13]. However, it is not clear how these interventions impact musculoskeletal structures of the shoulder acutely or longitudinally. Before it is possible to evaluate the effectiveness of interventions, one must investigate whether QUS measures are

sensitive to loading and, in particular, to the forces generated during manual wheelchair propulsion.

A recent study derived QUS measures from images collected before and after an intense wheelchair propulsion task completed at a self-selected maximum speed (Chapter 4). When controlling for baseline differences in QUS measures, clinically rated tendinopathy at baseline or a longer duration of wheelchair use predicted a darker, less organized biceps tendon appearance following propulsion. This may indicate that inflammatory factors or other fluid moved into the tendon after loading [37,78]. Contrarily, subjects who used a faster stroke frequency or larger resultant force during the propulsion task tended to have a brighter, more contrasted tendon appearance post-propulsion. It is likely that the increased mechanical strain on the biceps tendon pulled the collagen fibers into alignment as has been previously reported [36,79]. QUS measures appear to be sensitive to propulsion technique during an intense propulsion task, but further research is needed to determine if an individual's typical propulsion biomechanics impact tendon integrity.

In this study, we investigate whether shoulder forces and moments experienced during wheelchair propulsion influence baseline QUS measures, or the amount of change experienced after an intense propulsion task. We believe that larger loads experienced at the shoulder will translate to poor tendon health at baseline and larger microstructure changes measured using greyscale-based QUS. Shoulder kinetics will be measured during constant velocity propulsion since velocity impacts propulsion forces [18]. This provides a standardized way to compare the effect of propulsion technique on shoulder tendon structure. Also, compared to maximal speed propulsion, it is likely more representative of the typical propulsion style utilized during normal activities of daily living.

5.2 METHODS

5.2.1 Subjects

Individuals who used a manual wheelchair, were between the ages of 18 and 65, and were at least one year post inpatient rehabilitation were recruited to participate in this study. Subjects were primarily recruited from local rehabilitation facilities as well as through IRB approved registries of individuals who use assistive technologies. Subjects were excluded if they had a history of traumatic injury to the non-dominant shoulder or a history of cardiopulmonary disease. Individuals with progressive or degenerative disabilities were not eligible for this study. All subjects provided informed consent prior to participation.

5.2.2 Data Collection

This study consisted of three primary phases: ultrasound examinations (before and after propulsion), propulsion at a constant velocity on a dynamometer, and an intense overground wheelchair propulsion task. All subjects were asked to refrain from strenuous physical activity for 24 hours prior to testing. Additionally, all subjects rested for one hour prior to the baseline ultrasound examination in order to allow the musculoskeletal structures of the shoulder to return to a resting state. Most testing sessions began in the late morning.

Ultrasound: A single ultrasonographer performed all examinations to improve the reliability of the exam, which has been previously described in detail (Chapter 2). During the baseline ultrasound exam, images of the long head of the biceps and supraspinatus tendons of the non-dominant shoulder were captured. Care was taken to orient the region of interest

perpendicular to the ultrasound waves to minimize anisotropy artifacts. Machine settings were kept constant across all individuals. Subjects sat in a standardized posture to optimize viewing of each tendon. Additionally, prior to capturing the first image, a specially designed reference marker was taped to the skin. This marker provides a landmark to define a region of interest during image analysis, and have been shown provide good reliability with repeated measurements (Chapter 2). The reference markers remained in place for the duration of the study. The ultrasound examination was repeated immediately after subjects completed the intense wheelchair propulsion task to identify acute musculoskeletal responses related to propulsion. All images were saved for later analysis.

Constant Velocity Propulsion: Each subject's wheelchair was fitted with SMARTWheels (Three Rivers Holdings, LLC, Mesa, AZ) which recorded the three-dimensional forces and moments applied to the push rim. A four-point tie down setup was used to secure the wheelchair to a dual-roller dynamometer system positioned between two Optotrak (Northern Digital, Inc., Ontario, Canada) kinematic analysis cameras. Infrared kinematic markers were placed on bony landmarks of the upper extremity and trunk including the third metacarpophalangeal joint, radial styloid, ulnar styloid, lateral epicondyle, acromion, and greater trochanter. After acclimating to the dynamometer, subjects propelled for 20 seconds at 0.9 m/s and 1.8 m/s (2 and 4 mph, respectively). Continuous speed feedback was provided on a computer screen positioned in front of the participants. During propulsion, kinetic data were collected at 240 Hz and kinematic data were collected at 60 Hz. Kinetic data was later downsampled to 60 Hz for inverse dynamics calculations. The constant velocity task was implemented solely to characterize shoulder kinetics during wheelchair propulsion which was not possible during the overground propulsion stress task.

Overground Propulsion Task: The overground propulsion task was designed to stress the upper limbs and included turning, stopping, and starting (Chapter 4). Subjects completed three 4-minute propulsion periods at a self-selected maximal speed, separated by 90 seconds of rest (Figure 11). The propulsion course was shaped like an elongated figure-8 with two cones set 30 meters apart. Subjects began in the center, then pushed to the first cone and made a left turn. Then they returned to center and braked to a completed stop before pushing to the second cone where they made a right turn and returned back to the center. Participants were instructed to complete as many laps as possible.

5.2.3 Data Analysis

Ultrasound images were processed using custom Matlab scripts (Appendix B) which allowed the investigator to identify a region of interest within the tendon relative to an interference pattern created by the external reference marker (Chapter 2). From this region of interest, 7 quantitative descriptors of tendon health were derived including: tendon width, echogenicity, variance, entropy, contrast, energy, and homogeneity. These methods have proven to be reliable (Chapter 2) and valid measures of tendinopathy (Chapter 3). Tendons with more severe degeneration or tendinosis as graded by an expert tend to be larger and less echogenic (darker). They also exhibit reduced variance, entropy, and contrast and greater energy and homogeneity (Chapter 3). Greater tendinopathy is characterized by a darker tendon appearance with the loss of the highly organized collagen fiber structure that is present in a healthy tendon. The ultrasound measures computed in this study describe the greyscale distribution of pixels within the tendon region of interest and quantify the amount of tendon degeneration that has occurred.

Shoulder kinetics were computed from the kinetic and kinematic data collected during the constant velocity propulsion trials. The inverse dynamics model has been previously described in detail (Appendices C and D)[21]. We have since modified the trunk coordinate system which is now defined using the right and left acromion (ACR_R and ACR_L) and greater trochanter (GT_R and GT_L) markers. The midpoint of the acromion (ACR_{mid}) and greater trochanter (GT_{mid}) markers were computed to define the long axis of the trunk (Equation 5.2). All shoulder forces are referenced to the trunk anatomical coordinate system where:

$$\vec{z}_{trunk} = \frac{A\vec{C}R_R - A\vec{C}R_L}{\left\| A\vec{C}R_R - A\vec{C}R_L \right\|} \quad [5.1]$$

$$\vec{x}_{trunk} = \vec{z}_{trunk} \times \frac{\vec{G}T_{mid} - A\vec{C}R_{mid}}{\left\| \vec{G}T_{mid} - A\vec{C}R_{mid} \right\|} \quad [5.2]$$

$$\vec{y}_{trunk} = \vec{z}_{trunk} \times \vec{x}_{trunk} \quad [5.3].$$

Positive $\vec{x}$ points anteriorly, positive $\vec{y}$ points superiorly, and positive $\vec{z}$ points medially for the left shoulder. Shoulder joints moments were calculated relative to the humeral local coordinate system described in previous work [17]. The humeral and trunk local coordinate systems are coincident when the arm is in a neutral posture. Abduction (+) and adduction (–) moments occurred about the *x* axis, external (+) and internal (–) rotation produced moments about the *y* axis and extension (+) and flexion (–) moments occurred about the *z* axis. Since non-dominant sided data was analyzed for each subject, all shoulder kinetics were transformed to the left shoulder convention as necessary.

Propulsive strokes were identified using a search algorithm that determines when pushrim forces deviate from and return to zero. Peak shoulder kinetics were computed during the contact phase of propulsion when the subject was applying force to the pushrim. During this active phase, subjects experience peak shoulder loading in the posterior, superior, and lateral directions. Also, abduction, internal rotation, and extension moments are experienced at the glenohumeral joint [21]. The maximum force or moment in each of these directions was computed for each stroke and averaged for all strokes collected during the 20-second trial. Additionally, the magnitude of the resultant force was computed as the vector sum of F_x, F_y, and F_z and maximum resultant force during each push phase was computed and averaged.

5.2.4 Data Reduction and Statistical Analysis

Pearson's correlations revealed that all shoulder kinetic variables were highly correlated ($p < 0.001$, $0.738 \leq r \leq 0.971$) between the two speed conditions (0.9 m/s and 1.8 m/s). Therefore, average shoulder kinetics were computed for each individual.

Quantitative ultrasound (QUS) variables were computed for images of the biceps and supraspinatus tendons collected at baseline and immediately post-propulsion. A paired t-test was performed to determine if significant changes in QUS variables occurred after the intense overground propulsion task. The percent change from baseline was computed for each quantitative ultrasound measure calculated from images collected post-propulsion. Pearson's correlations were computed to test for significant relationships between shoulder kinetics and QUS measures, including baseline values and percent change from baseline. Shoulder kinetic variables included: peak posterior force, superior force, lateral force, resultant force, abduction moment, internal rotation moment, and extension moment computed during the push phase of

propulsion. A secondary partial correlation analysis was conducted to determine the effect of body mass on the relationship between shoulder kinetics and quantitative ultrasound measures.

5.3 RESULTS

21 individuals who were 40.6±12.8 years old and had been using a wheelchair for 16.1±9.9 years participated in this study. On average, study participants were 1.77±0.10 m tall and weighed 82.4±27.5 kg.

5.3.1 Quantitative Ultrasound

Seven QUS measures of biceps and supraspinatus tendon appearance were measured before and after the intense overground propulsion task (Table 9). A significant decrease in supraspinatus tendon width was observed. A few other relationships that showed a trend ($0.05 \leq p < 0.10$) towards a significant difference after propulsion included biceps tendon mean, contrast, and homogeneity, as well as supraspinatus tendon variance.

5.3.2 Shoulder Kinetics

Mean (±standard deviation) shoulder kinetics averaged between the 0.9 and 1.8 m/s propulsion trials are shown in Figure 12. All forces are in reference to the trunk local coordinate system and moments were calculated relative to the humerus local coordinate system.

Table 9. Quantitative ultrasound (QUS) measures at baseline and immediately post-propulsion

QUS Measures	Biceps Tendon		Supraspinatus Tendon	
	Baseline	Post-Propulsion	Baseline	Post-Propulsion
Width (mm)	4.81 (1.21)	4.76 (1.20)	5.47 (1.16)	5.16 (1.04) *
Echogenicity	119.1 (24.8)	112.2 (23.7) †	106.8 (26.2)	101.5 (32.6)
Variance	1874.3 (742.7)	1967.7 (828.8)	1528.1 (748.3)	1369.1 (684.0) †
Entropy	7.09 (0.31)	7.06 (0.33)	6.91 (0.44)	6.83 (0.47)
Contrast	5.97 (2.43)	5.41 (2.32) †	4.35 (1.87)	4.09 (2.05)
Energy	0.59 (0.28)	0.65 (0.32)	0.77 (0.43)	0.84 (0.52)
Homogeneity	3.47 (0.28)	3.55 (0.30) †	3.67 (0.32)	3.72 (0.38)

Data presented as mean (standard deviation)
*indicates significant change from baseline ($p<0.05$)
†indicates trend towards significant change from baseline ($0.05 \leq p < 0.10$)

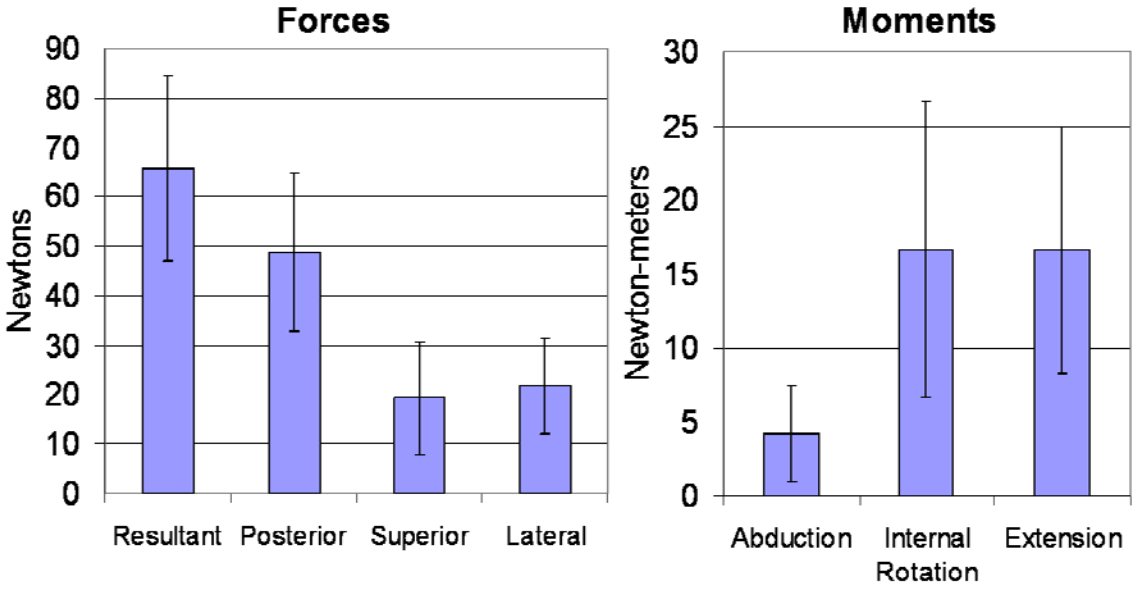

Figure 12. Mean shoulder kinetics during propulsion on a dynamometer

5.3.3 Shoulder Kinetics and Baseline Quantitative Ultrasound

Posterior force, internal rotation moment, and the extension moment correlated to supraspinatus tendon health at baseline, but not biceps tendon appearance. For the biceps tendon, the only statistically significant correlation was between the extension moment experienced at the

shoulder and tendon width (p=0.022, r=0.498). Significant correlations between shoulder kinetics and quantitative descriptors of supraspinatus tendon health at baseline are summarized in Table 10. In all cases, larger forces or moments predicted QUS changes indicative of more severe tendinopathy. Scatterplots of data from all subjects are shown in Figures 13 and 14.

Table 10. Correlations between shoulder kinetics and supraspinatus quantitative ultrasound (QUS) at baseline

	Supraspinatus QUS Measures				
	Echogenicity	Entropy	Contrast	Energy	Homogeneity
Posterior Force	-.597	-.450	-.583	.526	.600
Internal Rotation Moment	-.449	-.389†	-.420†	.397†	.438
Extension Moment	-.500	-.554	-.488	.555	.476

†indicates trended relationship ($0.05 \leq p < 0.10$), all other correlation coefficients significant at $p < 0.05$

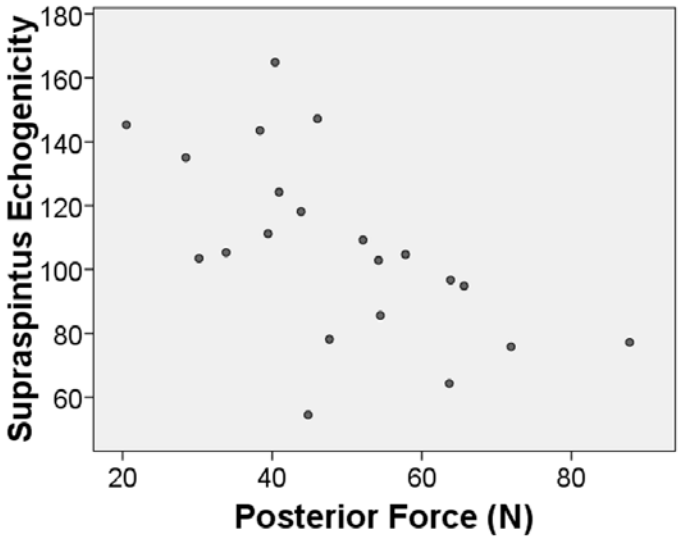

Figure 13. Supraspinatus echogenicity vs. posterior force experienced at the shoulder during manual wheelchair propulsion

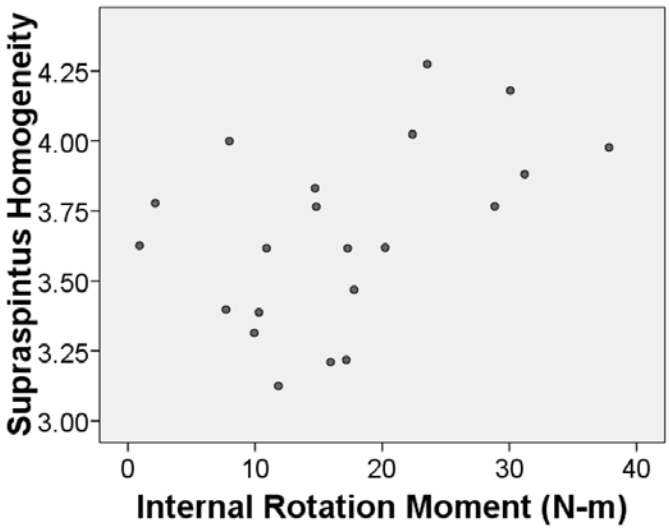

Figure 14. Supraspinatus homogeneity vs. internal rotation moment experienced at the shoulder during manual wheelchair propulsion

5.3.4 Shoulder Kinetics and Acute Quantitative Ultrasound Changes

Shoulder kinetics during continuous velocity propulsion correlated to QUS changes of the supraspinatus tendon after an intense overground wheelchair propulsion activity. Biceps tendon changes were not predicted by the loading experienced at the shoulder during propulsion. Changes in supraspinatus tendon width were correlated to resultant force ($p=0.039$, $r=-0.453$), posterior force ($p=0.017$, $r=-0.516$), and the extension moment ($p=0.012$, $r=-0.535$). Changes in supraspinatus tendon variance were correlated to posterior force ($p=0.029$, $r=-0.476$) and superior force ($p=0.039$, $r=-0.453$). Posterior force at the shoulder also correlated to the change in supraspinatus tendon entropy ($p=0.048$, $r=-0.436$). As an example, Figure 15 depicts the relationship between posterior force and percent change in supraspinatus tendon variance for all subjects.

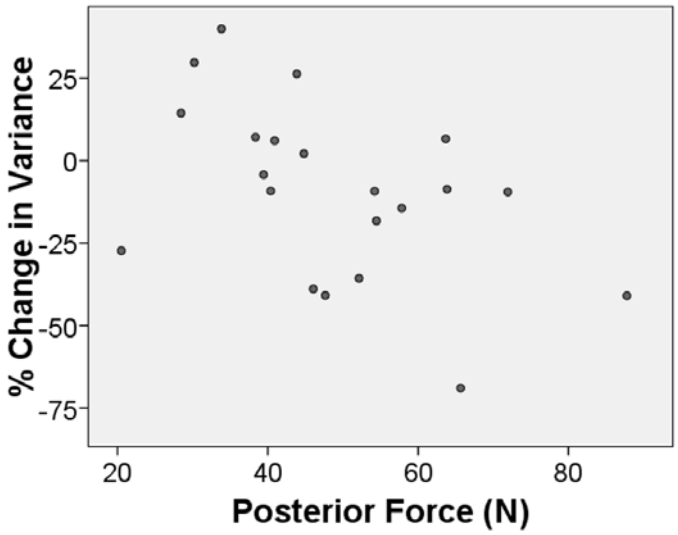

Figure 15. Percent change in supraspinatus tendon variance vs. posterior force experienced at the shoulder during manual wheelchair propulsion

5.3.5 Effect of Body Mass

Since body mass is known to be strongly correlated to propulsion forces, we computed partial correlations between shoulder kinetics and supraspinatus QUS variables while controlling for body mass. When controlling for body mass, extension moment was correlated to supraspinatus tendon entropy ($p=0.067$, $\rho=-0.418$) at baseline. All other previously identified relationships between shoulder kinetics and baseline QUS measures (Table 10) were no longer significant. However, when controlling for body mass, changes in supraspinatus tendon width and variance were still correlated to shoulder kinetics. Specifically, changes in tendon width were correlated to resultant force ($p=0.085$, $\rho=-0.395$), posterior force ($p=0.054$, $\rho=-0.437$), and extension moment ($p=0.045$, $\rho=-0.452$). Posterior force was also correlated to the percent change in tendon variance ($p=0.091$, $\rho=-0.388$).

5.4 DISCUSSION

This is the first study to relate constant velocity propulsion biomechanics to quantitative ultrasound (QUS) measures of tendon health. Higher forces and moments experienced at the shoulder were correlated to a darker, more diffuse supraspinatus tendon appearance consistent with tendinopathy. Participants that typically experience more shoulder loading saw greater decreases in supraspinatus tendon width and greyscale variance and entropy after completing an intense overground propulsion task.

Posterior force, internal rotation moment, and the extension moment were all correlated to QUS measures of supraspinatus tendon health. We previously reported that posterior force and the internal rotation moment were linked to a higher incidence of coracoacromial ligament pathology, a risk factor for rotator cuff tears [21,22]. In particular, coracoacromial ligament thickening is associated with narrowing of the supraspinatus outlet. This may partially explain why posterior force and internal rotation moment were correlated to supraspinatus tendon health, but not biceps tendon health. Additionally, an imbalance of internal and external rotators at the shoulder can lead to impingement syndrome which affects the supraspinatus tendon [34]. Reducing the peak loading, particularly in these directions, may reduce the risk of chronic supraspinatus tendinopathy.

Supraspinatus tendon changes after an intense propulsion task were influenced by typical propulsion biomechanics, measured during constant velocity propulsion. Posterior force showed the strongest relationship to QUS changes in supraspinatus tendon appearance. Subjects who typically use a larger posterior force tended to experience a decrease in tendon width, variance, and entropy. We can only speculate as to the physiological cause for these quantitative ultrasound changes. Tendon width may decrease acutely due to mechanical stretching along the

long axis of the tendon [36,79]. Animal models have shown that chronically, impingement is associated with a larger tendon size [38]. A reduction in variance and entropy corresponds to a more uniformly distributed greyscale histogram within the region of interest. Since it is unlikely that the collagen fiber structure became less organized with mechanical loading, a more plausible explanation is that inflammatory factors, or other fluid, moved into the tendon [37,78]. Additionally, since decreased tendon width was also observed, this may have led to other microstructure changes.

Our previous study reported that subjects with clinically graded biceps tendinopathy or a longer duration of wheelchair use tended to experience a decrease in biceps tendon width, variance, and entropy (among other changes) after the intense wheelchair propulsion task (Chapter 4). Subjects who used a higher stroke frequency or resultant force tended to experience tendon changes in the opposite direction, indicating a more organized, brighter tendon appearance after the intense propulsion task. Clearly, chronic pathology and loading conditions impact the acute biceps tendon response. The current study of a subsample of these subjects did not reveal a relationship between shoulder kinetics and biceps tendon health at baseline, or to the amount of change experienced after propulsion. It is possible that participants may have modified their propulsion technique in order to complete the overground propulsion task as fast as possible. Often the biceps tendon compensates for altered joint kinematics secondary to rotator cuff pathology, and this can lead to the development of biceps tendon pathology. While calculating shoulder kinetics adds information not provided by pushrim kinetics alone, additional noise is also introduced. With the small number of subjects in the current subsample, this may have limited our ability to relate kinetics to quantitative ultrasound changes within the biceps tendon. The combined results of these two studies suggest that the biceps tendon response is

related to the specific loading conditions of the task, while supraspinatus tendon changes are more influenced by individual's shoulder loading history. The physiological basis for these differences is not understood, and warrants future investigation.

Many risk factors for the development of chronic shoulder pathology among manual wheelchair users have been identified including increased body mass [29,73]. When controlling for body mass, shoulder kinetics were no longer significantly correlated to quantitative ultrasound measures at baseline. However, it should be noted that acute supraspinatus tendon changes were correlated to shoulder kinetics even when controlling for body weight. Clearly, body mass is the largest predictor of the amount of force required to propel a wheelchair and maintaining an appropriate body weight should be advised for all manual wheelchair users. Our sample size was not large enough to reveal other, more subtle, factors that contribute to propulsion forces. Age, years of wheelchair use, body mass, gender and loading experienced from other activities of daily living are just a few factors that can also influence shoulder integrity [29]. While weight loss may be desirable for some manual wheelchair users, other interventions related to wheelchair setup and propulsion technique may also help reduce shoulder loading. Even small load reductions could prove to be beneficial since manual wheelchair users actively propel for approximately 45 minutes per day [16]. With an estimated stroke cycle time of l second, this translates to 2700 propulsive strokes per day.

We know that optimizing wheelchair setup, particularly axle position, can reduce the amount of force that is required and increase the contact angle over which the force is applied [80,81]. Also, teaching manual wheelchair users to maximize their contact angle and to use a semicircular recovery pattern can reduce peak loading by distributing the load over a longer period of time [13,82]. These alternative interventions may help reduce the amount of acute

change observed in the supraspinatus tendon if shoulder kinetics can be reduced. Over time, this may reduce the risk of chronic pathology, although this remains to be investigated. Future research needs to use individuals as their own controls to isolate the effect of specific interventions. Conducting pre- and post-activity ultrasounds during repeated propulsion sessions under various conditions may help identify the best propulsion technique and wheelchair setup for an individual. This work could be extended to other groups who are also at risk for repetitive strain injuries.

5.5 CONCLUSIONS

Shoulder kinetics during constant velocity propulsion impact quantitative measures of supraspinatus tendinopathy, as well as the amount of change experienced after an intense propulsion task. Larger forces and moments at the shoulder were correlated to a more degenerated supraspinatus tendon appearance as measured by quantitative ultrasound measures. Body mass seems to be the most significant predictor of baseline tendon health. However, even when controlling for body mass, subjects who experienced larger forces and moments at the shoulder tended to have a larger decrease in supraspinatus tendon width and variance after an intense propulsion task. Because many factors contribute to the development of pathology, it seems logical to study musculoskeletal responses within an individual over various loading conditions to provide them with the best possible equipment and training. We have described quantitative measures of tendinopathy that are related to risk factors for chronic pathology and are sensitive to loading.

6.0 CONCLUSIONS

In this work, we have described a new method to objectively quantify tendon health and to evaluate acute musculoskeletal responses. Manual wheelchair users are an important group in which to evaluate this technique. Since independent mobility depends on preserving upper limb integrity, it is important to prevent pathology from developing. We believe that ultrasound provides a convenient and inexpensive way to monitor musculoskeletal integrity and identify degenerative changes in the early stages. Quantitative ultrasound also appears to be sensitive to upper limb loading. This provides a platform to evaluate assistive technology and propulsion techniques to create an individualized plan of upper limb preservation.

The quantitative ultrasound measures described in this work were selected to capture degenerative tendon changes as have been described clinically. Tendinopathy is often described as a hypoechoic tendon appearance with the absence of a strong collagen fiber structure parallel to the long axis of the tendon. Also, the tendon is often enlarged due to chronic inflammation. First, we completed a repeatability study to determine if these measures were reliable enough to characterize chronic pathology and to capture small acute changes. Ultrasound is known to be an operator-dependent imaging modality and image quality is also affected by many other parameters. One problem is localizing the same region of interest between subjects and within a subject during repeated imaging sessions. We worked with a musculoskeletal radiologist to develop a standardized positioning and scanning protocol. At the shoulder, there are no bony

landmarks visible in the same plane as the tendons of interest that can serve as reference points for repeated scanning. In a longitudinal view of the biceps, the humerus appears as a flat line beneath the tendon. When imaging the supraspinatus transversely, the curved humeral head appears below the tendon with no identifiable landmarks. Instead, we used bony landmarks near the structures to guide placement of the ultrasound transducer. The peak of the lesser tuberosity marked the proximal border for transducer placement when imaging the biceps tendon. Moving the transducer laterally brings the tendon midsubstance into view. We developed a reference marker that is taped to the skin at the distal end of the transducer. This marker not only provides a landmark in the image to define a region of interest, but it also ensures that the long axis of the transducer remains in the same plane for all imaging sessions. Tilting the probe alters the interference pattern which signals the operator that an adjustment should be made. A similar procedure is used at the supraspinatus where we use the transverse view of the biceps tendon to localize transducer placement. A reference marker is taped to define the medial border of the transducer.

The reference marker creates an interference pattern in the image which allows the region of interest to be defined in multiple images relative to a stationary landmark. The superficial and deep borders of the tendon are outlined manually using a graphical interface in Matlab. A standardized analysis procedure was developed for each tendon. Since biceps tendon inflammation often occurs within the paratendon, the tendon sheath was included within the superficial border of the tendon. The bright reflection from the humerus served as the deep border of the long head of the biceps tendon. The cortical surface was not included in the region of interest. The supraspinatus tendon is bordered superficially by the subacromial bursa. The interface between the tendon and bursa defined the superficial border of the region of interest.

The inferior border of the tendon was clearly visible above the cartilage on the humeral head surface. The tendon sheath often appears bright due to the transition from the superficial muscle to the tendon midsubstance and can vary in thickness. Including or excluding the tendon sheath can impact the magnitude of the quantitative ultrasound measures presented in this study. In order to make comparisons between individuals, one must standardize the region of interest definition in addition to following a reliable scanning protocol.

The reliability study confirmed that differences in quantitative ultrasound measurements existed between examiners. For the remainder of testing, one individual captured all ultrasound images. Increasing the number of images collected, or the number of readings performed, only provided marginal improvements in reliability. Therefore, the most time efficient protocol in which one image is captured at each time point and processed a single time was implemented for the remainder of testing. The quantitative ultrasound measures showed moderate to good reliability using the most conservative estimates.

Once reliability was established, the next step was to determine if these measures did in fact objectively describe tendon health. Unfortunately, there is no gold standard for evaluating tendinopathy to use for comparison. Our laboratory recently developed a grading scale for tendinopathy and other shoulder pathology. This represents the first attempt at quantifying tendon health. Our quantitative ultrasound measures correlated well with tendinopathy measured using this scale. This relationship was true even when controlling for the distance between the skin and the top of tendon. A larger distance between the skin and the top of the tendon means that the ultrasound amplitude is attenuated as the waves propagate through the biological tissue. Equation 6.1 approximates the attenuation through common biological material. These approximations are limited because, in practice, biological tissue is not homogenous and scatter

must be accounted for. Also, modern ultrasound technology employs image processing algorithms to reduce the effect of ultrasound wave attenuation on the resulting image. Manual adjustments to machine settings such as "gain" can amplify the ultrasound waves that are reflected back to the transducer. For this reason, the ultrasound machine and its settings were kept constant for all imaging sessions related to this dissertation. The same consistency needs to be maintained for future longitudinal studies or to make comparisons between subjects.

$$Attenuation[dB] = \alpha[dB/(MHz * cm)] * l[cm] * f[MHz] \qquad \text{Equation 6.1}$$

where:

α = attenutation coefficient (for reference, α=20 for bone and α=3.3 for muscle)

l = length of the medium that ultrasound wave travels though

f = ultrasound wave frequency

Our laboratory has also developed a physical examination scale focused on signs of shoulder pathology that has been performed on well over 100 manual wheelchair users. Quantitative ultrasound measures discriminated between subjects with and without pain on some maneuvers included in the physical exam. Quantitative ultrasound appears to be an objective measure of tendinosis has many potential applications including tracking degenerative changes over time and evaluating the effectiveness of treatments for tendinitis.

Very few studies have examined acute tendon changes in response to loading, and most have focused on animal models. Traditional imaging techniques, such as MRI, are expensive and may not capture acute responses occurring immediately after a task because the scan time is much longer than ultrasound. Ultrasound lends itself to this type of research because it is a

portable and inexpensive imaging modality that allows for real-time imaging of musculoskeletal structures. We used an overground wheelchair propulsion task to evaluate the sensitivity of quantitative ultrasound to acute musculoskeletal changes. This task was designed to incorporate starts, stops, and turning which manual wheelchair users encounter everyday. Subjects were asked to propel as fast as they could for the specified time interval so that everyone was stressed relative to their ability level. We narrowed the focus from nine quantitative ultrasound measures to seven since skewness and kurtosis showed relatively low reliability and the other measures all correlated to clinical pathology. When controlling for quantitative ultrasound measurements made at baseline, chronic tendinopathy and a longer duration of wheelchair use contributed to a darker, less organized biceps tendon microstructure after propulsion. This may mean that microfailures occurred and that inflammatory factors moved in to promote healing. However, a faster stroke frequency or a larger resultant force induced the opposite change. Increased loading predicted a brighter, more aligned fibrillar pattern after the propulsion task. In someone with a healthy tendon, the load may still be in a normal physiologic range so no acute healing takes place. Without histological studies, we can only speculate as to the physiological processes causing the changes in tendon microstructure. This study found that well-established risk factors for chronic pathology produced opposing directional changes after physical activity. Since pre-existing tendinopathy and duration of wheelchair use cannot be changed, developing interventions to reduce upper limb loading may limit the amount of acute change observed after an intense propulsion task.

Finally in a sub-sample of subjects, we investigated whether typical propulsion biomechanics, measured during constant velocity propulsion, influenced baseline tendon health or the amount of acute change observed after an intense propulsion task. Larger posterior force,

internal rotation moment, and extension moment at the shoulder correlated to more severe supraspinatus tendinopathy measured using quantitative ultrasound. These directional forces and moments have previously been related to chronic shoulder pathology measured on MRI. Posterior force also predicted larger changes in supraspinatus tendon width, variance, and entropy after the intense overground propulsion task. Body mass was the largest predictor of baseline quantitative ultrasound values, but it was not the most significant contributor to the acute changes observed in the supraspinatus tendon. Still, maintaining an ideal body weight is an effective way to reduce the amount of loading at the shoulder. However, other interventions, such as optimizing wheelchair setup and learning to take long, smooth propulsive strokes can also reduce the amount of force required to propel a wheelchair. We believe that any reduction in force is beneficial since the average manual wheelchair user takes over 2500 strokes per day. Quantitative ultrasound provides a new method to evaluate the effectiveness of interventions on an individual basis.

In the subsample of subjects tested at the Human Engineering Research Laboratories (HERL), we found significant, or trended, changes in 5 quantitative ultrasound measures following the intense propulsion task. Specifically, the mean biceps tendon echogenicity and contrast decreased, while on average, the biceps tendon appeared more homogenous after the propulsion task. The supraspinatus showed a significant decreased in tendon width, as well as reduced greyscale variance. In the entire sample of 66 subjects recruited at HERL and the National Veterans Wheelchair Games (NVWG), none of the quantitative ultrasound variables were significantly different immediately after the propulsion task as compared to baseline when covariates were not considered. One reason for this discrepancy is likely because testing at HERL was much more controlled. All subjects were asked to refrain from strenuous physical

activity for 24 hours prior to the study and also rested for 1 hour prior to the baseline ultrasound examination. At the NVWG, participants often propel long distances while traveling between events. Also, depending on the events they compete in, subjects may have experienced strenuous loading prior to the study. Since it is unknown how long a tendon takes to recover from this type of loading, varying activity level may have affected the results from the NVWG. All subjects did rest for approximately 30 minutes prior to the baseline ultrasound exam to reduce this potential confounder. Data collected from the entire pool of subject did reveal significant relationships between quantitative ultrasound measures, biomechanical loading, chronic tendinopathy, and duration of wheelchair use.

Due to correlations with other biomechanical variables, we did not include the total number of laps completed during the intense propulsion task as a predictor of acute tendon changes. The total number of laps completed was correlated to stroke frequency ($p=0.004$, $r=0.368$) and resultant force ($p<0.001$, $r=0.455$). Stroke frequency and resultant force were not correlated. However, during data analysis, trends between quantitative ultrasound variables and the total number of laps completed were noted. Specifically, the subset tested at HERL showed strong correlations between the number of laps completed and changes in the biceps tendon. This relationship was much weaker in the total sample of subjects. Only the percent change in echogenicity was significantly correlated to the total number of laps completed ($p=0.042$, $r=0.254$) in the entire sample of subjects. Pearson's correlations coefficients describing these relationships for the subjects tested at HERL are presented in Table 11. The direction of the changes indicates that a greater number of laps completed resulted in a brighter, less homogeneous tendon appearance after propulsion. This is the same direction of change predicted by increasing stroke frequency and resultant force (Table 8).

Table 11. Correlations between changes in quantitative ultrasound measures of the biceps tendon and the total number of laps completed

	Percent Change in QUS at 0 Minutes After Propulsion						
	Width	Echogenicity	Variance	Entropy	Contrast	Energy	Homogeneity
Total Number of Laps Completed	NS	r=0.712	r=0.621	r=0.692	r=0.523	r=-0.600	r=-0.485

All Pearson's correlation coefficients significant at $p<0.05$; NS= not significant

The discrepancies between subjects tested at HERL and those tested at the NVWG could be explained by differences in activity level prior to testing, but the subject groups also varied in terms of chronic tendinopathy. Table 12 summarizes number of subjects in both subject groups who presented with each tendinopathy grade. The group tested at the NVWG showed a higher percentage of subjects with mild and severe biceps tendinosis. Also, only two subjects at the NVWG presented with healthy supraspinatus tendons. A much larger percentage of subjects at the NVWG showed intrasubstance abnormalities or supraspinatus tendon tears as compared to the group tested at HERL.

Table 12. Biceps and supraspinatus tendinopathy for subjects tested at HERL and the NVWG

	Biceps Tendinopathy Score				Supraspinatus Tendinopathy Score						
	0	1	2	3	0	1	2	3	4	5	6
HERL (n=22)	n=13	n=7	n=1	n=1	n=6	n=7	n=0	n=2	n=6	n=1	n=0
NVWG (n=44)	n=13	n=25	n=5	n=1	n=2	n=12	n=2	n=8	n=13	n=6	n=1

Tendinopathy Scores: 0=normal; 1=mild tendinosis; 2=severe tendinosis; 3=intrasubstance abnormality; 4=partial thickness tear; 5=focal full-thickness tear; 6=massive full-thickness tear

In this study, we found that shoulder kinetics recorded during dynamometer propulsion significantly correlated to acute supraspinatus tendon changes experienced by the subjects tested at HERL. However, when the group was examined as a whole, biceps tendon changes were significantly predicted by stroke frequency and resultant force measured during the intense propulsion task. Animal models have found that rotator cuff tears often result in increased loading of the biceps tendon due to altered biomechanics [39]. In our sample, many of the subjects tested at the NVWG had partial or full thickness supraspinatus tendon tears. They may

have altered their biomechanics when asked to propel as fast as they could, thus increasing the load on the biceps tendon. However, since the majority of subjects tested at HERL had healthy tendons or only showed mild supraspinatus tendinosis, this likely did not affect their propulsion biomechanics on the dynamometer. Similarly, they may have used unaltered biomechanics during the propulsion course resulting in loading of the supraspinatus tendon rather than excess loading of the biceps tendon. We recommend that future research in this area enforces limited activity 24 hours prior to testing to avoid potential confounding factors. Additionally, if more subjects can be recruited, it would be interesting to compare the tendon response of subjects with normal tendons, tendinosis, and those with tendon tears.

Minimal detectable change (MDC) can be computed from the standard error of measurement presented in Chapter 2. The MDC describes the smallest magnitude of change at a 90% confidence interval needed to detect a true tendon change that significantly exceeds the measurement error. We did not use MDC to identify subjects with significant acute changes, yet in the subsample of subjects tested at HERL, significant changes in quantitative ultrasound variables were measured following propulsion. MDC may be too conservative when examining changes among a group. For example, only 5 subjects experienced a decrease in supraspinatus tendon width that was greater than the MDC (7.32%), yet a statistically significant decrease was observed among the entire group. The scatterplots in Chapter 5 indicate that these subjects do not appear to be outliers. For within-individual studies, the MDC can serve as a guideline for determining whether an observed change was significant, or possibly due to measurement error. However, since the MDC is based on data from a sample of individuals, this estimate has pitfalls as well. A better method may be to take repeated measurements at baseline to estimate the error

variance for a particular subject. Comparing the measured change to this estimate of variance may provide a better guideline on an individual basis.

It is worth noting that throughout this work, we consistently found relationships between most, or all, of the quantitative ultrasound variables and the chosen variable of interest (e.g. demographic information, clinical scores, or kinetics). Since all of these measures were chosen to describe tendon health and greyscale texture, it is expected that they would also be related to each other. However, it may be possible to select a subset of these features for analysis. Table 13 and 14 show the correlations between the 9 quantitative ultrasound measures of the biceps and supraspinatus tendon respectively. It is clear that most of the variables are correlated to each other, so each does not necessarily provide additional information. Depending out the outcome variable of interest, principal component analysis may reveal which set of quantitative ultrasound measures provide the most information. For example, the features that best describe the degree of tendinosis may not necessary be the same features that are the most sensitive to shoulder kinetics.

Table 13. Correlations between quantitative ultrasound measures of the biceps tendon

	Width	Echogenicity	Variance	Skewness	Kurtosis	Entropy	Contrast	Energy	Homogeneity
Width	--	-.503	-.456	.343	.327	-.433	-.572	.483	.595
Echogenicity	-.503	--	.725	-.751	-.686	.778	.857	-.823	-.911
Variance	-.456	.725	--	-.229	-.756	.814	.788	-.722	-.722
Skewness	.343	-.751	-.229	--	.520	-.428	-.580	.611	.688
Kurtosis	.327	-.686	-.756	.520	--	-.836	-.723	.842	.741
Entropy	-.433	.778	.814	-.428	-.836	--	.828	-.930	-.861
Contrast	-.572	.857	.788	-.580	-.723	.828	--	-.825	-.942
Energy	.483	-.823	-.722	.611	.842	-.930	-.825	--	.914
Homogeneity	.595	-.911	-.722	.688	.741	-.861	-.942	.914	--

All Pearson's correlation coefficients significant at $p<0.05$

Table 14. Correlations between quantitative ultrasound measures of the supraspinatus tendon

	Width	Echogenicity	Variance	Skewness	Kurtosis	Entropy	Contrast	Energy	Homogeneity
Width	--	-.358	NS	.327	NS	-.245	-.310	.351	.402
Echogenicity	-.358	--	.829	-.552	-.533	.804	.955	-.845	-.970
Variance	NS	.829	--	NS	-.606	.893	.866	-.772	-.822
Skewness	.327	-.552	NS	--	.406	NS	-.478	.356	.524
Kurtosis	NS	-.533	-.606	.406	--	-.605	-.552	.601	.548
Entropy	-.245	.804	.893	NS	-.605	--	.805	-.924	-.854
Contrast	-.310	.955	.866	-.478	-.552	.805	--	-.802	-.964
Energy	.351	-.845	-.772	.356	.601	-.924	-.802	--	.902
Homogeneity	.402	-.970	-.822	.524	.548	-.854	-.964	.902	--

NS= Not significant; All Pearson's correlation coefficients significant at $p<0.05$

It is apparent that tendon health measured on ultrasound is influenced by many factors including age, duration of wheelchair use, body mass, chronic pathology, and biomechanics. With sixty-seven subjects, this work would be considered a large study of manual wheelchair users. However, this sample size was not large enough to define multiple groups for comparison. For example, how would subjects with healthy tendons who use large forces compare to subjects with healthy tendons who use smaller forces? The same comparison could be made in subjects with varying degrees of tendinopathy. We do not know how tendon responses would differ between new manual wheelchair users and individuals with many more years of experience. In this study quantitative ultrasound measures appeared to be sensitive to many of these factors, but moving forward, an invidualized approach could help isolate subject-specific risk factors. Since chronic tendinopathy, duration of wheelchair use, age, and weight would all remain constant, we may be able to identify which other factors contribute most to acute tendon changes. Specifically, a single change, such as optimizing axle position, could be implemented to see if shoulder loading is reduced and if that translated to a smaller acute response. Due to equipment limitations, we were unable to record kinematics during the intense propulsion task. Instead, kinematics were recorded on a dynamometer, along with pushrim kinetics, in order to calculate

shoulder kinetics during constant velocity propulsion. In the future, efforts should be made to collect kinetic and kinematic data during the stress protocol so that shoulder joint kinetics can be computed.

Future research is planned to evaluate how interventions designed to reduce upper limb loading during manual wheelchair propulsion impact acute musculoskeletal changes. For this reason, the relationships between quantitative ultrasound changes and shoulder biomechanics may be the most significant finding of this work. While it is valuable to be able to quantify tendinosis, in order to intervene and prevent future injury, we must be able to detect these acute changes and identify ways to reduce them. Based on the results of this work, we could immediately begin to evaluate acute tendon responses to varying loading conditions. This work could have a broader impact if it is expanded to include other groups at risk for repetitive strain injuries. Additionally, similar quantitative ultrasound techniques could be extended to other joints commonly affected by overuse injuries. In this work, we have established a framework for developing a reliable and objective imaging protocol to measure musculoskeletal integrity. We hope that the techniques described in this work facilitate early intervention and the preservation of independent mobility for manual wheelchair users.

APPENDIX A

FORMULAS FOR QUANTITATIVE ULTRASOUND MEASURES

Nine quantitative ultrasound measures are discussed in this dissertation to describe tendon health. A custom Matlab program (Appendix B) was developed to identify a region of interest within the biceps and supraspinatus tendons relative to an externally placed reference marker. The operator is blinded to the time of image capture (baseline or post-propulsion). The user manually defines the top and bottom border of tendon. This region of interest is rotated so that the long axis of the tendon is oriented horizontally.

A function P(I) can be defined (Equation A.1) that represents the fraction of pixels with gray level I. This is essentially a histogram of the grey levels within the ROI. Mean is simply the average greyscale value of all of the pixels inside the ROI and can be calculated using Equation A.2. As fluid in the tendon increases, the image will become darker, and the mean echogenicity will decrease. Other first-order statistics are often calculated as central moments which are translationally invariant with respect to the mean greyscale value. Variance is a measure of the spread of the pixel values within the ROI and can be calculated using Equation A.3. One might expect variance of the tendon ROI to be higher for a healthy tendon with a highly oriented collagen fiber pattern, represented on ultrasound as alternating dark and light

stripes. Skewness describes the symmetry of a sample about its mean and is calculated using Equation A.4. Kurtosis measures the peakedness or flatness of a distribution relative to a normal distribution and is calculated using Equation A.5. Finally, entropy, which measures histogram uniformity, can be calculated using Equation A.6. As P(I) approaches a constant value for all greyscale values, the entropy approaches zero.

$$P(I) = \frac{number\ of\ \ pixels\ with\ gray\ level\ I}{total\ number\ of\ \ pixels\ in\ the\ region} \qquad \text{Histogram} \qquad [A.1]$$

$$m_1 = \sum_{I=0}^{N_g} I * P(I) \qquad \text{Mean} \qquad [A.2]$$

where N_g is number of possible greyscale values

$$\mu_2 = \sigma^2 = \sum_{I=0}^{N_g} (I - m_1)^2 P(I) \qquad \text{Variance} \qquad [A.3]$$

$$\mu_3 = \frac{1}{\sigma^3}\left[\sum_{I=0}^{N_g} (I - m_1)^3 P(I)\right] \qquad \text{Skewness} \qquad [A.4]$$

$$\mu_4 = \frac{1}{\sigma^4}\left[\sum_{I=0}^{N_g} (I - m_1)^4 P(I)\right] - 3 \qquad \text{Kurtosis} \qquad [A.5]$$

$$H = -\sum_{I=0}^{N_g - 1} P(I) \log_2 P(I) \qquad \text{Entropy} \qquad [A.6]$$

Second-order statistics provide additional information about the texture of a ROI. This analysis considers the pixels of an image in pairs. Therefore, the distance (d) between and orientation (φ) of a pixel pair enters into the analysis. The distance, d, is defined as the relative distance between a pixel pair measured in number of pixels. We included a range of d=1:5 pixels to capture small micro-texture patterns. Four orientations can be considered in a second-order statistical analysis (φ=0°, 45°, 90°, 135°). We focus only on φ=0° since we expect a collagen fiber pattern oriented in the horizontal direction. A two-dimensional histogram, $P(I_1,I_2)$, is defined for every combination of d and φ. The range of greyscale intensities (0-255) was divided into 8 bins rather than examining each greyscale value individually. Equations A.7-A.10 describe the two-dimensional histogram for the four orientation values. For each histogram, a co-occurrence matrix of size (N_gxN_g), where N_g equals the total number of grayscale values in an image, can be defined. Texture-related information (i.e. texture coefficients) can be derived from this co-occurrence matrix which describes the spatial dependence of the pixels in a ROI. Contrast (CON) measures local gray level variations (Equation A.11). Images with more greyscale texture variations have higher CON values. Energy (ENG) measures the smoothness of an image. CON differs from ENG in that it is looking for differences in greyscale values of the pixel pairs rather than the absolute greyscale values. Larger differences in greyscale are weighted higher than small differences. Homogeneity (HOM) measures the closes of the co-occurrence matrix to a diagonal matrix. HOM equals 1 for a diagonal matrix.

Two Dimensional Histogram (Equations A.7-A.10)

$$0°: P(I(m,n) = I_1, I(m \pm d, n) = I_2) \qquad \text{[A.7]}$$

$$= \frac{number\ of\ \ pairs\ of\ \ pixels\ at\ distance\ d\ \ with\ values\ (I_1, I_2)}{total\ number\ of\ \ possible\ \ pairs}$$

$$45°: P(I(m,n) = I_1, I(m \pm d, n \mp d) = I_2) \qquad \text{[A.8]}$$

$$90°: P(I(m,n) = I_1, I(m, n \mp d) = I_2) \qquad \text{[A.9]}$$

$$135°: P(I(m,n) = I_1, I(m \pm d, n \pm d) = I_2) \qquad \text{[A.10]}$$

$$CON = \sum_{i=0}^{N_g - 1} \sum_{j=0}^{N_g - 1} |i - j|^2 P(i, j) \qquad \text{Contrast} \qquad \text{[A.11]}$$

$$ENG = \sum_{i=0}^{N_g - 1} \sum_{j=0}^{N_g - 1} (P(i, j))^2 \qquad \text{Energy} \qquad \text{[A.12]}$$

$$HOM = \sum_{i=0}^{N_g - 1} \sum_{j=0}^{N_g - 1} \frac{(P(i, j))}{1 + |i - j|} \qquad \text{Homogeneity} \qquad \text{[A.13]}$$

APPENDIX B

ULTRASOUND IMAGE ANALYSIS: MATLAB CODE

```
function shoulder
%This program is designed to load a greyscale ultrasound image

%variable declaration/initialization
repeat=1;
first_time=1;
area=0;
length=0;
known_length=0;
loop_again=1;
conversion=0;
i=1;
one_time = 0;

%cell array declarations
store={};
coordinates={};
pixel_width={};
actual_width={};

%--------------------------------------------------------------------------
%Begin main body of program
%--------------------------------------------------------------------------

%allow for repeated iterations
while repeat==1
    quit=1;

    %Ask how many images will be analyzed
    %whos
    image_num_str=input('How many images do you want to analyze?: ','s');
    image_num=str2num(image_num_str);
    image_num_vector(1:image_num,1)=1:1:image_num;

    %generate random number to select which image is displayed first
    random_nums = randperm(image_num);
```

```
    for filenumber=1:image_num
        file_count=num2str(filenumber);
        message=['Select image number ', file_count, ': '];
        disp(message);
        [filename,pathname]= uigetfile('*.*');
        file_list(filenumber,:)=filename; %stores filenames of all images
    end


    for b = 1:image_num %count through number of images

        %define counter variable that loads images in a random order
        random = random_nums(b); %need to add one at the end of the loop

        filename_size = size(file_list(random,:));
        for j = 1:(filename_size(2)-4)
            shortname(random,j) = file_list(random,j);
            j=j+1;
        end

        %define values from filename
        ID=[shortname(random,1:4)];
        investigator=['JM'];
            if investigator == 'JM' %Jen
                invest_code=num2str(1);
            elseif investigator == 'BI' %Brad
                invest_code=num2str(2);
            else
                invest_code=num2str(-99);
            end

        structure=[shortname(random,5)];
            if structure == 'b' %Biceps
                struct_code=num2str(1);
            elseif structure== 's' %Supraspinatus
                struct_code=num2str(2);
            else
                struct_code=num2str(-99);
            end

        depth=[shortname(random,7)]; %already a number (3,4, or 5 cm)

        gain=[shortname(random,8:9)];
            if gain =='00'
                gain=['100']; %convert two digit code (00) to actual gain
(100)
            end

       image_time=[shortname(random,10:12)]; %usually 1, unless repeated
measurements were taken
       if image_time=='pre'
           image_number = 0;
       elseif image_time=='pr2'
           image_number = -1;
```

```
        elseif image_time=='pr3'
            image_number = -2;
        elseif image_time=='a00'
            image_number = 1;
        elseif image_time=='a05'
            image_number = 2;
        elseif image_time=='a10'
            image_number = 3;
        elseif image_time=='a15'
            image_number = 4;
        elseif image_time=='a20'
            image_number = 5;
        elseif image_time=='a25'
            image_number = 6;
        elseif image_time=='a30'
            image_number = 7;
        elseif image_time=='a35'
            image_number = 8;
        elseif image_time=='a40'
            image_number = 9;
        elseif image_time=='a45'
            image_number = 10;
        elseif image_time=='a50'
            image_number = 11;
        elseif image_time=='a55'
            image_number = 12;
        elseif image_time=='a60'
            image_number = 13;
        else
            image_number = '-99'
        end

        image_number=num2str(image_number);


         %reads image and stores as unsigned integer values from 0-255 in
%matrix 'image'
         image=imread(shortname(random,:),'bmp');
         image=image(:,:,1);
         if depth == '3'
             header_pix=80;
         else %depth = 4 or 5
             header_pix=55; %default number of pixels to start of skin
         end

         [size_check_x size_check_y] = size(image);
         if size_check_x > 570 %see if borrowed machine was used
             image=image(37:600,:); %resize to match HERL image size (564x800)
             if depth == '3'
                 header_pix=60;
             else %depth= 4 or 5
                 header_pix=35; %pixels to start of skin
             end
         end

         %calculates size of image matrix
```

```
        [size_x size_y] = size(image);

        %gets the conversion factor from pixels to area

[first_time,length,known_length,conversion,cm_convert,hconversion,hcm_convert
] = get_convert(first_time,image,length,known_length,loop_again,depth);

        %allows user to make polyline selections

[average_width,corners,distances,refleft,refright,skin_roi,muscle_roi] =
get_lines(image,size_x,size_y,hcm_convert,header_pix);

        %converts the pixel lengths to mm
        actual_width = average_width/conversion;
        actual_dist = distances./conversion;

        %function allows user to encircle selection using series of mouse
clicks
        %hit enter after zooming appropriately - (shift / double click to end
selection)
        %selects point right above tendon
        [cord_values,cords,out_y] = select_after_lines(size_x,size_y,image);

        %rotates image so that long axis of tendon is horizontal
        [rotated_cord_values]=rotate(cord_values,corners);

        %calculate imaging parameters for tendon ROI
        [t_counts, t_bins, t_meangrey, t_variance, t_std, t_skew, t_kurt,
t_entro, ...
            t_contrast, t_correlation, t_energy, t_homogeneity, t_imagefft,
t_logfft,...
            t_image_crop,t_imagefft100, t_logfft100, t_imagefftr, t_logfftr]
= imaging(rotated_cord_values);


        %calculate first order statistics for rectangular regions of interest

            %tendon (5 segments)

[t_region1,t_region2,t_region3,t_region4,t_region5,t_d,t_g_mean,t_g_var,t_g_s
kew,t_g_kurt,t_g_entro] = roi_segment(t_image_crop);

            %convert distances to mm
            t_d=t_d./conversion;

        %store segmented region of interest variables for saving;
        segment_stats=[t_d t_g_mean' t_g_var' t_g_skew' t_g_kurt'
t_g_entro'];

        %%%%%% begin output section of program %%%%%%

        %loops to remove .bmp file extension from path
        filename_size = size(file_list(random,:));
        for j = 1:(filename_size(2)-4)
```

```
            temp_id(j) = file_list(random,j);
            j=j+1;
        end

        %defines file label
        file_2_open = [temp_id];

        opening_name=['shoulder_tendon.txt'];

        j = b+2;
        k = b+1;
        %stores several global variables in single array for printing to file

shoulder_data=[actual_width,t_meangrey,(actual_dist'),t_variance,t_std,...
            t_skew,t_kurt,t_entro,t_contrast,t_energy,t_homogeneity];

        % prepares writing to a new file name using the original path,
appends data to end of file
        fid=fopen(opening_name,'a');

        if one_time == 0
            %writes headers to file
            fprintf(fid,'\n %8s\t %8s\t %8s\t %8s\t %8s\t %8s\t %8s\t %8s\t
%8s\t %8s\t %8s\t %8s\t  %8s\t %8s\t %8s\t %8s\t %8s\t %8s\t %8s\t %8s\t
%8s\t %8s\t %8s\t %8s\t %8s\t %8s\t %8s\t %8s\t %8s\t %8s\t %8s\t %8s\t %8s\t
%8s\t %8s\t %8s\t %8s\t %8s\t %8s\t %8s\t %8s\t %8s\t %8s\t %8s\t %8s\t %8s\t
%8s\t %8s\t %8s\t %8s\t %8s\t %8s\t %8s\t %8s\t %8s\t %8s\t %8s\t %8s\t %8s\t
%8s\t %8s\t %8s\t %8s\t %8s\t %8s\t %8s\t %8s\t %8s\t %8s\t %8s\t %8s\t %8s\t
%8s\t %8s\t %8s\t %8s\t %8s\t %8s\t %8s\t %8s\t %8s\t %8s\t %8s\t %8s\t %8s\t
%8s\t %8s\t %8s\t %8s\t %8s\t %8s\t %8s\t %8s\t %8s\t %8s\t %8s\t %8s\t %8s\t
%8s\t %8s\t %8s\t %8s\t %8s\t %8s\t %8s\t %8s\t %8s\t %8s\t %8s\t %8s\t %8s\t
%8s\t %8s\t %8s\t %8s\t %8s\t %8s\t %8s\t %8s\t %8s\t %8s\t %8s\t %8s\t %8s\t
%8s\t %8s\t %8s\t %8s\t %8s\t %8s\t %8s\t %8s\t %8s\t %8s\t %8s\t %8s\t %8s\t
%8s\t %8s\t %8s\t %8s\t %8s\t %8s\t %8s\t %8s\t %8s\t %8s\t %8s\t %8s\t %8s\t
%8s\t %8s\t %8s\n',...
                'Filename','ID', 'Investigator', 'Structure', 'Depth',
'Gain','Image_num','TendonWidth','T_Mean','Skin_dist','TenTop_dist','TenBot_d
ist','Bone_dist','T_Var','T_StD','T_Skew','T_Kurt','T_Entro', ...
'T_Con01','T_Con02','T_Con03','T_Con04','T_Con05','T_Con06','T_Con07','T_Con0
8','T_Con09','T_Con010','T_Con-11','T_Con-22','T_Con-33','T_Con-44','T_Con-
55','T_Con-66','T_Con-77','T_Con-88','T_Con-99','T_Con-1010','T_Con-
10','T_Con-20','T_Con-30','T_Con-40','T_Con-50','T_Con-60','T_Con-70','T_Con-
80','T_Con-90','T_Con-100','T_Con-1-1','T_Con-2-2','T_Con-3-3','T_Con-4-
4','T_Con-5-5','T_Con-6-6','T_Con-7-7','T_Con-8-8','T_Con-9-9','T_Con-10-10',
'T_Energy01','T_Energy02','T_Energy03','T_Energy04','T_Energy05','T_Energy06'
,'T_Energy07','T_Energy08','T_Energy09','T_Energy010'
'T_Energy-11','T_Energy-22','T_Energy-33','T_Energy-44','T_Energy-
55','T_Energy-66','T_Energy-77','T_Energy-88','T_Energy-99','T_Energy-1010',
'T_Energy-10','T_Energy-20','T_Energy-30','T_Energy-40','T_Energy-
50','T_Energy-60','T_Energy-70','T_Energy-80','T_Energy-90','T_Energy-100',
'T_Energy-1-1','T_Energy-2-2','T_Energy-3-3','T_Energy-4-4','T_Energy-5-
5','T_Energy-6-6','T_Energy-7-7','T_Energy-8-8','T_Energy-9-9','T_Energy-10-
10','T_Homogen01','T_Homogen02','T_Homogen03','T_Homogen04','T_Homogen05','T_
Homogen06','T_Homogen07','T_Homogen08','T_Homogen09','T_Homogen010',
'T_Homogen-11','T_Homogen-22','T_Homogen-33','T_Homogen-44','T_Homogen-
55','T_Homogen-66','T_Homogen-77','T_Homogen-88','T_Homogen-99','T_Homogen-
```

```
1010','T_Homogen-10','T_Homogen-20','T_Homogen-30','T_Homogen-40','T_Homogen-
50','T_Homogen-60','T_Homogen-70','T_Homogen-80','T_Homogen-90','T_Homogen-
100','T_Homogen-1-1','T_Homogen-2-2','T_Homogen-3-3','T_Homogen-4-
4','T_Homogen-5-5','T_Homogen-6-6','T_Homogen-7-7','T_Homogen-8-
8','T_Homogen-9-9','T_Homogen-10-10');
        end

        %reformats vectors to accommodate output
        [shoulder_data]=shoulder_data';

        %writes filename to file
        fprintf(fid,'\n %10s\t %10s\t %10s\t %10s\t %10s\t %10s\t %10s\t
',file_2_open,ID,invest_code,struct_code,depth,gain,image_number);

        %writes data to file
        fprintf(fid,'%10.4f\t %10.4f\t %10.4f\t %10.4f\t %10.4f\t %10.4f\t
%10.4f\t %10.4f\t %10.4f\t %10.4f\t %10.4f\t %10.4f\t %10.4f\t %10.4f\t
%10.4f\t %10.4f\t %10.4f\t %10.4f\t %10.4f\t %10.4f\t %10.4f\t %10.4f\t
%10.4f\t %10.4f\t %10.4f\t %10.4f\t %10.4f\t %10.4f\t %10.4f\t %10.4f\t
%10.4f\t %10.4f\t %10.4f\t %10.4f\t %10.4f\t %10.4f\t %10.4f\t %10.4f\t
%10.4f\t %10.4f\t %10.4f\t %10.4f\t %10.4f\t %10.4f\t %10.4f\t %10.4f\t
%10.4f\t %10.4f\t %10.4f\t %10.4f\t %10.4f\t %10.4f\t %10.4f\t %10.4f\t
%10.4f\t %10.4f\t %10.4f\t %10.4f\t %10.4f\t %10.4f\t %10.4f\t %10.4f\t
%10.4f\t %10.4f\t %10.4f\t %10.4f\t %10.4f\t %10.4f\t %10.4f\t %10.4f\t
%10.4f\t %10.4f\t %10.4f\t %10.4f\t %10.4f\t %10.4f\t %10.4f\t %10.4f\t
%10.4f\t %10.4f\t %10.4f\t %10.4f\t %10.4f\t %10.4f\t %10.4f\t %10.4f\t
%10.4f\t %10.4f\t %10.4f\t %10.4f\t %10.4f\t %10.4f\t %10.4f\t %10.4f\t
%10.4f\t %10.4f\t %10.4f\t %10.4f\t %10.4f\t %10.4f\t %10.4f\t %10.4f\t
%10.4f\t %10.4f\t %10.4f\t %10.4f\t %10.4f\t %10.4f\t %10.4f\t %10.4f\t
%10.4f\t %10.4f\t %10.4f\t %10.4f\t %10.4f\t %10.4f\t %10.4f\t %10.4f\t
%10.4f\t %10.4f\t %10.4f\t %10.4f\t %10.4f\t %10.4f\t %10.4f\t %10.4f\t
%10.4f\t %10.4f\t %10.4f\t %10.4f\t %10.4f\t %10.4f\t %10.4f\t %10.4f\t
%10.4f\t %10.4f\t %10.4f\t %10.4f\t %10.4f\t %10.4f\t %10.4f\t %10.4f\t
%10.4f\t %10.4f\t %10.4f\t %10.4f\t %10.4f\t %10.4f\t %10.4f\t %10.4f\t
%10.4f\t %10.4f\t %10.4f\t %10.4f\t %10.4f\t %10.4f\t %10.4f\t %10.4f\t
%10.4f\t %10.4f\t %10.4f\t %10.4f\t %10.4f\t %10.4f\t %10.4f\t %10.4f\t
%10.4f\t %10.4f', shoulder_data);


     % prepares writing to a new file name using the original path, appends
data to end of file
        fid4=fopen('Depth_Correction_Vars.txt','a');

        if one_time == 0
            %writes headers to file
            fprintf(fid4,'\n %8s\t %8s\t %8s\t %8s\t %8s\t %8s\t %8s\t %8s\t
%8s\t %8s\t %8s\t %8s\t %8s\t %8s\t %8s\t %8s\t %8s\t %8s\t %8s\t %8s\t %8s\t
%8s\t %8s\t %8s\t%8s\t %8s\t %8s\t %8s\t %8s\t %8s\t %8s\t %8s\t %8s\t%8s\t
%8s\t %8s\t %8s\t %8s\t %8s\t %8s\t %8s\t %8s\t%8s\t %8s\t %8s\t %8s\t %8s\t
%8s\t %8s\t %8s\t %8s\t%8s\t %8s\t %8s\t %8s\t %8s\t %8s\t %8s\t %8s\t
%8s\t%8s\t %8s\t %8s\t %8s\t %8s\t %8s\t %8s\t %8s\t %8s\t%8s\t %8s\t %8s\t
%8s\t %8s\t %8s\t %8s\t %8s\t %8s',...
                'Filename', 'ID', 'Investigator', 'Structure', 'Depth',
'Gain','Image_num',...
                    'Skin_dist','TenTop_dist','TenBot_dist','Bone_dist',...
```

```
'Skin_mid','Skin_mean','Skin_var','Skin_skew','Skin_kurt','Skin_entro',...

'Musc1_mid','Musc2_mid','Musc3_mid','Musc4_mid','Musc5_mid',...

'Musc1_mean','Musc2_mean','Musc3_mean','Musc4_mean','Musc5_mean',...

'Musc1_var','Musc2_var','Musc3_var','Musc4_var','Musc5_var',...

'Musc1_skew','Musc2_skew','Musc3_skew','Musc4_skew','Musc5_skew',...

'Musc1_kurt','Musc2_kurt','Musc3_kurt','Musc4_kurt','Musc5_kurt',...

'Musc1_entro','Musc2_entro','Musc3_entro','Musc4_entro','Musc5_entro',...

'Ten1_mid','Ten2_mid','Ten3_mid','Ten4_mid','Ten5_mid',...

'Ten1_mean','Ten2_mean','Ten3_mean','Ten4_mean','Ten5_mean',...

'Ten1_var','Ten2_var','Ten3_var','Ten4_var','Ten5_var',...

'Ten1_skew','Ten2_skew','Ten3_skew','Ten4_skew','Ten5_skew',...

'Ten1_kurt','Ten2_kurt','Ten3_kurt','Ten4_kurt','Ten5_kurt',...

'Ten1_entro','Ten2_entro','Ten3_entro','Ten4_entro','Ten5_entro');
        end


        %saves ROIs to file loadable by matlab
        save_image_1 = ['ROIs_',temp_id];

save(save_image_1,'rotated_cord_values','t_image_crop','ref','skin_roi','m_re
gion1',...

'm_region2','m_region3','m_region4','m_region5','t_region1','t_region2',...
            't_region3','t_region4','t_region5');

        %save histogram data
        save_hist = ['hist_',temp_id];
        save(save_hist,'r_bins','t_bins','r_counts','t_counts');

        %-----------------------------------------------------------------
------

        %increments counter to only display header once
        one_time = one_time + 1;
    end

    %close output files
    fclose(fid);
    fclose(fid2);
    fclose(fid3);
    fclose(fid4);
```

```
    %prompts user to repeat program
    repeat=menu('Would you like to analyze a new set of images?','Yes','No');

    %if analyzing new image, close all current figures
    if repeat == 1
        close all
    end

end %end external while loop

fclose('all');


%-------------------------Subfunctions-------------------------------------%


function[first_time,length,known_length,conversion,cm_convert,hconversion,hcm
_convert] =
get_convert(first_time,image,length,known_length,loop_again,depth)

%Program has been updated with default conversion values for 3, 4, and 5 cm
%depths

depth=str2num(depth);

%Default values
if depth==3
    conversion = 400/30; %vertical conversion
    hconversion=680/50; %horizontal conversion
elseif depth==4
    conversion = 453/40; %vertical conversion
    hconversion=576/50; %horizontal conversion
elseif depth==5
    conversion = 453/50; %vertical conversion
    hconversion=462/50; %horizontal conversion
else
    conversion=input('Enter vertical conversion factor: ');
    hconversion=input('Enter horizontal conversion factor: ');
end

cm_convert = (conversion*10); %convert to pixels/cm
hcm_convert = (hconversion*10); %convert horizontal factor to pixels/cm



%-------------------------------------------------------------------------%
function
[average_width,corners,distances,refleft,refright,skin_roi,muscle_roi] =
get_lines(image,x,y,hcm_convert,header_pix);

        a = 1;
run_total = 0;
```

```
coordinates={};

%displays image and allows user to zoom in before selection
imshow(image,'InitialMagnification',100);

%cover subject ID and label
text(90,15,['censoredcensored'],...
    'HorizontalAlignment','center',...
    'BackgroundColor',[0 0 0],...
    'Margin',8);
text(570,520,['censoredcensoredcensoredcensored'],...
    'HorizontalAlignment','center',...
    'BackgroundColor',[0 0 0],...
    'Margin',8);

hold on;

title('Click center of left and right interference patterns');
%allows user to click-input starting coordinates for rectangle
[x1,y1] = ginput(2); %click center of each interference pattern
x=mean(x1); %use average to place reference blocks
y=mean(y1); %use average to place reference blocks

rect_length = (0.5*hcm_convert);
 h = 1000;

 rectangle('Position',[x,y,3*rect_length,h],'edgecolor','r') %0 to 1.5 cm
 rectangle('Position',[(x+3*rect_length),y,4*rect_length,h],'edgecolor','r')
%1.5 to 3.5cm
 rectangle('Position',[(x-3*rect_length),y,3*rect_length,h],'edgecolor','r')
%0 to -1.5 cm
 rectangle('Position',[(x-7*rect_length),y,4*rect_length,h],'edgecolor','r')
%-1.5 to -3.5cm

%select reference points to control for pressure
     title('Click two points at the bottom of the skin surface');
     zoom on;
     pause
    %allows user to click-input bottom edge of skin surface
    [x2,y2] = ginput(2); %click center of each interference pattern
    skiny=mean(y2);

    %select region of skin
    title('Select largest rectangle within skin region');
    rect_skin=getrect;
    skin_roi=imcrop(image,[rect_skin]);

zoom out;
hold on;

    %select region of muscle
    title('Select largest rectangle within muscle region');
    rect_muscle=getrect;
    muscle_roi=imcrop(image,[rect_muscle]);
```

```
    title('Click two points on the bone underneath the tendon');
    zoom on;
    pause
    %allows user to click-input bottom edge of skin surface
    [x4,y4] = ginput(2); %click center of each interference pattern
    boney=mean(y4);

    %save x coordinates of reference area border
    refleft=x2(1);
    refright=x2(2);

text(400,500,['Select Two Lines, First Above, then Below, Hit Enter to
Continue'],...
    'HorizontalAlignment','center',...
    'BackgroundColor',[1 1 0],...
    'Margin',6);

title('Select Two Lines, First Above, then Below, Hit Enter to Continue');

%allows user to select 2 lines
for a = 1:2
    [get_x get_y] = getline;
    line(get_x,get_y,'color','g');

    temp_line = [get_x,get_y];
    num_elements = size(get_x);
    this = num_elements(2);

    if a == 1


        %the following code generates an approximation of the line connecting
the topmost points
        %it allows the line to be divided into segments
        %-------------------------------------------------------------

        %generates 200 x points between starting x and end x
        x_spl_top = linspace(get_x(1),get_x(num_elements(1)),200);
        %calculates the cubic spline coefficients for y values
        spl_coeff = spline(get_x,get_y);
        %evaluates piecewise polynomial using spline coefficients
        y_spl_top = ppval(spl_coeff,x_spl_top);

        plot(x,y,'*',x_spl_top,y_spl_top,'color','b');
        title('Cubic Spline Approximation');

        %corners used to linearly approximate to the top/bottom border
        %based on the 4 corners of the tendon ROI
        corners(1,1:2)=[get_x(1),get_y(1)];
        corners(2,1:2)=[get_x(length(get_x)),get_y(length(get_y))];
```

```
    end

    if a == 2
        %generates 200 x points between starting x and end x
        x_spl_bot = linspace(get_x(1),get_x(num_elements(1)),200);
        %calculates the cubic spline coefficients for y values
        spl_coeff = spline(get_x,get_y);
        %evaluates piecewise polynomial using spline coefficients
        y_spl_bot = ppval(spl_coeff,x_spl_bot);

        plot(x,y,'*',x_spl_bot,y_spl_bot,'color','g');


        %corners used to linearly approximate to the top/bottom border
        %based on the 4 corners of the tendon ROI
        corners(3,1:2)=[get_x(1),get_y(1)];
        corners(4,1:2)=[get_x(length(get_x)),get_y(length(get_y))];
     end
    %-------------------------------------------------------------

end

    %calculates average width
    plus = 20;
    n = 1;
    %size = size(x_spl_top);
    run_total = 0;

    for counter=1:10;

        x_cords_top = x_spl_top(n:plus);
        y_cords_top = y_spl_top(n:plus);
        x_cords_bot = x_spl_bot(n:plus);
        y_cords_bot = y_spl_bot(n:plus);

        cords_top = [x_cords_top;y_cords_top];
        cords_bottom = [x_cords_bot;y_cords_bot];

        cords_top = cords_top';
        cords_bottom = cords_bottom';

        run_total = run_total +
calculate_min_distance(cords_top,cords_bottom);

        n = n+20;
        plus = plus+20;
    end
    average_width = run_total / 10;

    %calculate distances of interest
    dist_skin=skiny-header_pix;%distance from bottom of skin to top of image
```

```
    dist_tentop=mean(y_spl_top-header_pix);%distance from top of tendon to
top of image
    dist_tenbot=mean(y_spl_bot-header_pix);%distance from bottom of tendon to
top of image
    dist_bone=boney-header_pix; %distance from bone underneath tendon to top
of image
    distances=[dist_skin;dist_tentop;dist_tenbot;dist_bone];

end


%-------------------------------------------------------------------------%

function [cord_values,cords,out_y] = select_after_lines(x,y,image)

m=1;
n=1;

title('Select Area inside lines')
text(400,500,['Select Area inside lines: Click to Zoom, Hit Enter to
Continue'],...
    'HorizontalAlignment','center',...
    'BackgroundColor',[1 1 0],...
    'Margin',6);

text(90,30,['censoredcensored'],...
    'HorizontalAlignment','center',...
    'BackgroundColor',[0 0 0],...
    'Margin',8);

hold on;
%zoom on;

%pause
delete(findobj('Margin',6));


%allows user to select an area of a figure for grayscale analysis and
%leaves lines drawn on figure
%roipoly stores data as 1 if point is inside, 0 if outside selection equal in
size to origional image
cords = roipoly;

%find indices of all non-zero values of cords
[r,c,vals] = find(cords);

%find min and max pixel coordinates (x and y) for tendon ROI
maxr=max(r);
minr=min(r);
maxc=max(c);
minc=min(c);

%loop to generate a matrix of grayscale values within selection
for n = 1:x
```

```
    for m = 1:y
        if cords(n,m) == 1
            cord_value(n,m) = image(n,m);
        end
    end
end

%store tendon ROI with minimal padding
cord_values=cord_value(minr:maxr,minc:maxc);

%releases current figure
hold off

title('Click above the sheath - topmost the tendon (outside)');
click_pts_1 = ginput(1);
out_y = round(click_pts_1(1,2));
delete(findobj('Margin',6));



%-------------------------------------------------------------------------%
function [rotated_cord_values]=rotate(cord_values, corners)

%calculate line through center of tendon
center_leftx=(corners(1,1)+corners(3,1))/2;
center_lefty=(corners(1,2)+corners(3,2))/2;
center_rightx=(corners(2,1)+corners(4,1))/2;
center_righty=(corners(2,2)+corners(4,2))/2;

%find angle from horizontal
ang=atan2((center_righty-center_lefty),(center_rightx-center_leftx));
angle=ang*(180/pi);

%save rotated tendon ROI
rotated_cord_values=imrotate(cord_values,angle,'bicubic','loose');



%-------------------------------------------------------------------------%
function [counts, bins, meangrey, variance, std, skew, kurt, entro, ...
    contrast2, correlation2, energy2, homogeneity2, imagefft, logfft, ...
    image_crop, imagefft100, logfft100, imagefftr, logfftr] = imaging(image)

%convert ROI to unsigned 8 bit integer
imagei=uint8(image);

%show image to identify part of tendon with no edge effects
   imshow(imagei,'InitialMagnification',100);

title('select largest rectangle that is entirely within the tendon border');

%save cropped image with no border effects
```

```
rect_tendon=getrect;
image_crop=imcrop(imagei,[rect_tendon]);

%blur edges of image for fft
    %define size of gaussian kernal
    %must be less than 1/2 of the smallest image dimension (# of rows)
       [r,c]=size(image_crop);
        if r>40
            hsize=20;
        else
            hsize=round(r/2)-1;
        end

    %define gaussian kernal
        PSF=fspecial('gaussian',hsize,3); %standard deviation of gaussian
kernal=3

    %blur edges of image
        image_blur=edgetaper(image_crop,PSF);

%convert ROI to double matrix
imaged=double(image);

%finds location and value of all non-zero entries in image
[rows,cols,vals] = find(image);

%find number of non-zero pixels in image
index=size(rows,1);

%store non-zero pixels in a one-dimensional vector
for k=1:index
    Id(k,1)=imaged(rows(k),cols(k)); %double precision
    I(k,1)=imagei(rows(k),cols(k)); %unsigned 8 bit integer
end



%figure
%imhist(I) %display histogram
[counts bins]=imhist(I); %store histogram

meangrey=mean(Id); %mean greyscale value
variance=var(Id); %variance, or second central moment
std=sqrt(variance); %standard deviation
skew=skewness(Id); %skewness, or third central moment
kurt=kurtosis(Id); %kurtosis, or fourth central moment
entro=entropy(image_crop); %entropy of image

offsets2=[0 1;0 2; 0 3; 0 4; 0 5;0 6;0 7;0 8;0 9;0 10;...
    -1 1;-2 2;-3 3;-4 4;-5 5;-6 6;-7 7;-8 8;-9 9;-10 10;...
    -1 0;-2 0;-3 0;-4 0;-5 0;-6 0;-7 0;-8 0;-9 0;-10 0;...
    -1 -1;-2 -2;-3 -3;-4 -4;-5 -5;-6 -6;-7 -7;-8 -8;-9 -9;-10 -10]; %offsets
(pixel relationship) for GLCM

for offset2=1:40
```

```
    glcm2(:,:,offset2)=graycomatrix(image_crop,'Offset',offsets2(offset2,:));
%Gray Level Co-Occurence Matrix
end

stats2 = graycoprops(glcm2,{'all'});
contrast2=stats2.Contrast; %image contrast
correlation2=stats2.Correlation; %image correlation
energy2=stats2.Energy; %image energy, or angular second moment(smoothness)
homogeneity2=stats2.Homogeneity; %image homogeneity

imagefft=fftshift(fft2(double(image_blur))); %2-D Fourier Transform
logfft=log(abs(imagefft)); %Log of Fourier Transform

%fourier transforms with zero padding (size rxr)
imagefftr=fftshift(fft2(double(image_blur),r,r)); %2-D Fourier Transform
logfftr=log(abs(imagefftr)); %Log of Fourier Transform

%fourier transform resized to 100x100
imagefft100=imresize(imagefft,[100 100],'bicubic');
logfft100=imresize(logfft,[100 100],'bicubic');



%-------------------------------------------------------------------------%
function
[region1,region2,region3,region4,region5,d,g_mean,g_var,g_skew,g_kurt,g_entro
] = roi_segment(roi)


%dimension variables
dimensions = size(roi);

num_rows = dimensions(1,1);

rows = floor(num_rows/5); %round to largest integer evenly divisible into
num_rows

%initialize variables to set row limits for each segment of the ROI
region_min=zeros(5,1);
region_max=zeros(5,1);

%define limits for first segment of the ROI
region_min(1) = 1;
region_max(1) = rows;

%define limits for other segments of the roi
for i=2:5
    region_min(i)=region_min(i-1)+rows;
    region_max(i)=region_max(i-1)+rows;
end

%isolate each segment of the roi
region1=roi(region_min(1):region_max(1),:);
region2=roi(region_min(2):region_max(2),:);
```

```
region3=roi(region_min(3):region_max(3),:);
region4=roi(region_min(4):region_max(4),:);
region5=roi(region_min(5):region_max(5),:);

%calculate distance to center of each region from top of ROI
for j=1:5
    %distance from top of ROI
    d(j)=(j-1)*rows+(rows/2);
end

%convert regions to double class
regiond1=double(region1);
regiond2=double(region2);
regiond3=double(region3);
regiond4=double(region4);
regiond5=double(region5);

%finds location and value of all non-zero entries in image
[row,col,val] = find(regiond1);

%find number of non-zero pixels in image
index=size(row,1);

%store non-zero pixels in a one-dimensional vector
for k=1:index
    regd1(k,1)=regiond1(row(k),col(k)); %double precision
    regd2(k,1)=regiond2(row(k),col(k)); %double precision
    regd3(k,1)=regiond3(row(k),col(k)); %double precision
    regd4(k,1)=regiond4(row(k),col(k)); %double precision
    regd5(k,1)=regiond5(row(k),col(k)); %double precision
end


%calculate first order statistics of greyscale of each region;
g_mean=[mean(regd1);mean(regd2);mean(regd3);mean(regd4);mean(regd5)]; %mean
g_var=[var(regd1);var(regd2);var(regd3);var(regd4);var(regd5)]; %variance
g_skew=[skewness(regd1);skewness(regd2);skewness(regd3);skewness(regd4);skewn
ess(regd5)]; %skewness
g_kurt=[kurtosis(regd1);kurtosis(regd2);kurtosis(regd3);kurtosis(regd4);kurto
sis(regd5)]; %kurtosis
g_entro=[entropy(region1);entropy(region2);entropy(region3);entropy(region4);
entropy(region5)]; %entropy
```

APPENDIX C

INVERSE DYANAMICS MODEL

Cooper et al previously described the anthropometric model used for this study [17]. Segment lengths and upper-extremity circumferences of all subjects were measured as input to Hanavan's mathematical model which calculates the inertial properties of each body segment [17,83]. Pushrim forces were transformed to the glenohumeral joint using a previously described inverse dynamics model [17]. Shoulder joint forces were transformed to the anatomic coordinate system of the proximal segment of the shoulder joint, the trunk, as follows: anterior (x), posterior ($-x$), superior (y), inferior ($-y$), medial (z), and lateral ($-z$) (Figure 16). Equations C.1-C.3 were applied to compute the trunk anatomical coordinate system during propulsion. This coordinate system approximates the local coordinate systems recommended by the International Society for Biomechanics [84].

Figure 16. Trunk anatomical coordinate system

$$\vec{z}_{trunk} = \frac{A\vec{C}R_R - A\vec{C}R_L}{\left\| A\vec{C}R_R - A\vec{C}R_L \right\|} \quad [C.1]$$

where ACR_R=right acromion and ACR_L=left acromion

$$\vec{x}_{trunk} = \vec{z}_{trunk} \times \frac{\vec{G}T_{mid} - A\vec{C}R_{mid}}{\left\| \vec{G}T_{mid} - A\vec{C}R_{mid} \right\|} \quad [C.2]$$

where ACR_{mid}=midpoint of right and left acromion markers and GT_{mid}= midpoint of right and left greater trochanter markers

$$\vec{y}_{trunk} = \vec{z}_{trunk} \times \vec{x}_{trunk} \quad [C.3]$$

Shoulder joints moments were calculated relative to the humeral local coordinate system described in Equations C.4-C.6. The humeral and trunk local coordinate systems are coincident when the arm is in a neutral posture. Abduction (+) and adduction (–) moments occurred about the *x* axis, external (+) and internal (–) rotation produced moments about the *y* axis and extension

(+) and flexion (–) moments occurred about the *z* axis.

$$\vec{y}_{humerus} = \frac{A\vec{C}R - L\vec{E}}{\left\| A\vec{C}R - L\vec{E} \right\|} \quad [C.4]$$

where ACR=acromion and LE=lateral epicondyle

$$\vec{z}_{humerus} = \frac{U\vec{S} - L\vec{E}}{\left\| U\vec{S} - L\vec{E} \right\|} \times \vec{y}_{humerus} \quad [C.5]$$

where US=ulnar styloid

$$\vec{x}_{humerus} = \vec{y}_{humerus} \times \vec{z}_{humerus} \quad [C.6]$$

A kinematic calibration trial was collected prior to testing. For this trial, subjects were instructed to sit in their wheelchair such that their trunk was perpendicular to the ground aligned with the global coordinate system. A corrective transformation matrix was calculated for each subject in order to satisfy this condition. This transformation matrix was then applied to the trunk local coordinate system as calculated in all other trials. Detailed Matlab code is provided in Appendix D.

APPENDIX D

INVERSE DYNAMICS MATLAB CODE

```
%References used in this program:

    %Hanavan, EP.  A Mathematical Model of the Human Body.  Wright-Patterson
Air Force Base. Pub:AMRL-TR-64-102, 1964.

    %Winter, DA. Biomechanics and Motor Control of Human Movement, Second
Edition. Wiley-Interscience, New York, 1990.

    %Cooper RA, Boninger ML, Shimada SD, Lawrence BM. (1999) Glenohumeral
Joint Kinematics and Kinetics for Three Coordinate System Representations
During Wheelchair Propulsion. Am J Phys Med Rehab. 78(5):435-446.

    %Wu G, van der Helm FCT, Veeger HEJ, Makhsous M, Van Roy P, Anglin C,
Nagels J, Karduna AR, McQuade K, Wang X, Werner FW, Bucholz B. (2005) ISB
recommendation on definitions of joint coordinate systems of various joints
for the reporting of human joint motion-PartII: shoulder, elbow,wrist, and
hand. Journal of Biomechanics. 38: 981-992.

% Based on BioCalc programs written by previous Biolab students

%Updated to calculate moments relative to the distal segment of joint
    %wrist moments given in hand coordinate system
    %elbow moments given in forearm coordinate system
    %shoulder moments given in upper arm coordinate system
%Forces are still in proximal segment coordinate system
    %wrist forces given in forearm coordinate system
    %elbow forces given in upper arm coordinate system
    %shoulder forces given in trunk coordinate system

%This version will work with the new marker set (4 digit subject IDs) and old
smartwheel data
%Uses average of hip marker (instead of hub marker) to compute trunk angle
clear all
```

```
%----------------Load subject data---------------------------------%
%User input
%ID = input('Enter the subject 3 digit (old) ID: ', 's');
newID= input('Enter the subject 4 digit ID: ', 's');
%condition = input('Enter wheelchair resistance condition: (usually 7) ',
's');
condition=7;
speed = input('Enter speed number: ', 's');

cd .. %change directory out of Inverse Dynamics folder

cd('clean mo') %change directory to clean mo folder

%Kinematic data
modata = [newID,'m7b',speed,'c.txt'];
kin=load(modata);

setpodata= [newID, 'msp1c.txt'];
setpo1=load(setpodata);
setpo=mean(setpo1);
setpo=setpo/1000; %converts to meters
setpo=setpo+1; %makes all values positive

cd .. %change directory out of clean mo folder

cd('fm files')
cd('dyno')

%Smartwheel data
swrdata= [newID, 'w7r', speed,'04fm.txt'];
FMr=load(swrdata);
swldata= [newID, 'w7l', speed,'06fm.txt'];
FMl=load(swldata);

cd .. %change directory out of dyno folder
cd .. %change directory out of fm files folder

%anthropometric data (first row= height(in), second row=weight(lbs), rest of
measurements are in meters)
%rows 3-8 are for the right side: axillary arm circ, elbow circ, wrist
%circ, fist circ, upper arm length, forearm length
%rows 9-14 are for the left side: axillary arm circ, elbow circ, wrist
%circ, fist circ, upper arm length, forearm length

anth=[newID, 'anthro.txt'];
anthro=load(anth);

cd('inverse dynamics') %change directory into Inverse Dynamics folder

%----------------define anthropometric variables (used for both sides) ------
-----------%
heightinch=anthro(1); %height in inches
heightm=heightinch*0.0254; %height in meters
weightlbs=anthro(2); %weight in pounds
```

```
weightN=weightlbs*4.448222; %weight in Newtons
pindex=heightinch/(weightlbs^(1/3)); %ponderal index (Winter pg. 53)
bodydenkgl=0.69 + (0.0297*pindex); %body density in kg/l
bodyden=bodydenkgl/.001; %body density in kg/m^3
swua=0.5*(0.08*weightlbs-2.9); %segment weight of upper arm in lbs (Hanavan)
swfa=0.5*(0.04*weightlbs-0.5); %segment weight of forearm in lbs (Hanavan)
swha=0.5*(0.01*weightlbs-0.7); %segment weight of hand in lbs (Hanavan)
handdens=1.16/.001; %hand density in kg/m^3 from Winter
fadens=1.13/.001; %forearm in kg/m^3 density
uadens=1.07/.001; %upper arm in kg/m^3 density

%----------------Filter kinematic data----------------------------%
[kinrows,kincolumns]=size(kin);
[b,a]=butter(2,7/30); %defines 4th order Butterworth filter with 7Hz cutoff
frequency
for i=1:kincolumns
    filteredkin(:,i)=filtfilt(b,a,kin(:,i)); %runs filter
end

kin=(filteredkin/1000); %convert from mm to meters
kin=kin+1; %shifts data by 1 meter so that all coordinates are positive

n=1;
for n=1:2

    %-------------Define variable names for right and left side--------------
-------%
    if n==1 %right side
        FM=FMr;
        [swrows,swcolumns]=size(FM);
        if swrows<4800 %makes sure SW data has 4800 rows to match kinematic
files
            FM(swrows:4800,:)=0; %set end of file=0 if data is short
        end
        forces=FM(1:4:4800, 1:6); %sampled force data
        step=FM(1:4:4800,7); %sampled step function
        encoder=FM(1:4:4800,8); %sampled encoder data
        thirdmp=kin(:,56:58); %third MP
        radsty=kin(:,53:55); %radial styloid
        ulnsty=kin(:,50:52); %ulnar styloid
        wristcen=0.5*(radsty+ulnsty); %wrist center
        olec=kin(:,47:49); %olecranon
        latep=kin(:,44:46); %lateral epicondyle
        acro=kin(:,41:43); %acromion
        axilc=anthro(3); %axillary arm circumference
        elbc=anthro(4); %elbow circumference
        wrc=anthro(5); %wrist circumference
        fistc=anthro(6); %fist circumference
        ualen=anthro(7); %upper arm length
        falen=anthro(8); %forearm length
    else %left side
        FM=FMl;
        [swrows,swcolumns]=size(FM);
        if swrows<4800
            FM(swrows:4800,:)=0;
        end
```

```
        forces=FM(1:4:4800, 1:6); %sampled force data
        step=FM(1:4:4800,7); %sampled step function
        encoder=FM(1:4:4800,8); %sampled encoder data
        thirdmp=kin(:,29:31); %third MP
        radsty=kin(:,26:28); %radial styloid
        ulnsty=kin(:,23:25);%ulnar styloid
        wristcen=0.5*(radsty+ulnsty); %wrist center
        olec=kin(:,20:22); %olecranon
        latep=kin(:,17:19); %lateral epicondyle
        acro=kin(:,14:16); %acromion
        axilc=anthro(9);%axillary arm circumference
        elbc=anthro(10); %elbow circumference
        wrc=anthro(11); %wrist circumference
        fistc=anthro(12); %fist circumference
        ualen=anthro(13); %upper arm length
        falen=anthro(14); %forearm length

    end %end of if loop to set FM file to FMr or FMl

    %---------------Calculate mass moment of inertia / center of mass--------
--------------------%

    g=9.81; %gravity m\s^2
    dt=1/60; %sampling interval

    %upper arm
    uapr=axilc/(2*pi); %upper arm proximal radius (shoulder)
    uadr=elbc/(2*pi); %upper arm distal radius (elbow)
    uavol=(pi*ualen/3*(uapr^2+uapr*uadr+uadr^2)); %segment volume in m^3
(modeled as elliptical cylinder (Hanavan))
    uamass=uadens*uavol;  %upper arm mass in kg (density in kg/m^3)
    uamu=uadr/uapr; %radius ratio constant "mu" defined by Hanavan
    uasigma=1+uamu+uamu^2; %constant "sigma" defined by Hanavan
    uaAA=(9/(20*pi))*((1+uamu+uamu^2+uamu^3+uamu^4)/(uasigma^2)); %constant
AA defined by Hanavan
    uaBB=(3/80)*((1+4*uamu+10*uamu^2+4*uamu^3+uamu^4)/(uasigma^2)); %constant
BB defined by Hanavan
    uaIxx=uamass*((uaAA*(uamass/(uadens*ualen)))+uaBB*(ualen^2)); %moment of
inertia perpendicular to longitudinal axis(kg*m^2)
    uaIzz=uaIxx; %moment of inertia perpendicular to longitudinal
axis(kg*m^2)
    uaIyy=(3/10)*uamass*((uapr^5-uadr^5)/(uapr^3-uadr^3));%moment of inertia
about the longitudinal axis of the upper arm (kg*m^2)
    uaIxy=0;
    uaIxz=0;
    uaIyz=0;
    uaI=[uaIxx uaIxy uaIxz; uaIxy uaIyy uaIyz; uaIxz uaIyz uaIzz]; %matrix of
upper arm mass moments of inertia
    uacmratio=((uapr^2+2*uapr*uadr+3*uadr^2))/(4*(uapr^2+uapr*uadr+uadr^2));
%upper arm center of mass ratio (center of mass/length)with respect to
proximal end (Hanavan)
    uacm=uacmratio*(latep-acro)+acro; %3-D coordinates of upper arm center of
mass

    %forearm
    fapr=elbc/(2*pi); %forearm proximal radius (elbow)
```

```
    fadr=wrc/(2*pi); %forearm distal radius (wrist)
    favol=(pi*falen/3*(fapr^2+fapr*fadr+fadr^2)); %segment volume in m^3
(modeled as elliptical cylinder (Hanavan))
    famass=fadens*favol;  %forearm mass in kg (density in kg/m^3)
    famu=uadr/uapr; %radius ratio constant "mu" defined by Hanavan
    fasigma=1+uamu+uamu^2; %constant "sigma" defined by Hanavan
    faAA=(9/(20*pi))*((1+famu+famu^2+famu^3+famu^4)/(fasigma^2)); %constant
AA defined by Hanavan
    faBB=(3/80)*((1+4*famu+10*famu^2+4*famu^3+famu^4)/(fasigma^2)); %constant
BB defined by Hanavan
    faIxx=famass*((faAA*(famass/(fadens*falen)))+faBB*(falen^2)); %moment of
inertia perpendicular to longitudinal axis(kg*m^2)
    faIzz=faIxx; %moment of inertia perpendicular to longitudinal
axis(kg*m^2)
    faIyy=(3/10)*famass*((fapr^5-fadr^5)/(fapr^3-fadr^3));%moment of inertia
about the longitudinal axis of the forearm (kg*m^2)
    faIxy=0;
    faIxz=0;
    faIyz=0;
    faI=[faIxx faIxy faIxz; faIxy faIyy faIyz; faIxz faIyz faIzz]; %matrix of
forearm mass moments of inertia
    facmratio=((fapr^2+2*fapr*fadr+3*fadr^2))/(4*(fapr^2+fapr*fadr+fadr^2));
%upper arm center of mass ratio (center of mass/length) with respect to
proximal end (Hanavan)
    facm=facmratio*(wristcen-latep)+latep; %3-D coordinates of forearm center
of mass

    %hand
    handrad=fistc/(2*pi); %hand radius
    handvol=(4/3)*pi*handrad^3; %hand volume in m^3
    handmass=handdens*handvol; %hand mass in kg
    handIany=(2/5)*handmass*handrad^2; %hand mass moment of inertia about any
axis (kg*m^2)
    handI=[handIany 0 0; 0 handIany 0; 0 0 handIany];
    handcmratio=0.5; %center of mass ratio for the hand (sphere) (Hanavan)
    handcm=handcmratio*(thirdmp-wristcen)+wristcen; %3-D coordinates of hand
center of mass

    %Save all segment masses into a matrix
    %1x3 matrix
    massall=[handmass famass uamass];

    %Save all center of mass locations in a matrix
    %kinrows(1200)x9 matrix
    cmall=[handcm facm uacm];

    %------------------------------Calculate absolute limb angular positions-
--------------------------%

    %Upper Arm
    upperarmvector=latep-acro; %vector along the long axis of the upper arm
    uazyangle=atan2(upperarmvector(:,2),upperarmvector(:,3)); %absolute upper
arm angle in ZY plane
    uaxzangle=atan2(upperarmvector(:,3),upperarmvector(:,1)); %absolute upper
arm angle in XZ plane
```

```
    uaxyangle=atan2(upperarmvector(:,2),upperarmvector(:,1)); %absolute upper
arm angle in XY plane

    %Forearm
    forearmvector=wristcen-latep; %vector along the long axis of the forearm
    fazyangle=atan2(forearmvector(:,2),forearmvector(:,3)); %absolute forearm
angle in ZY plane
    faxzangle=atan2(forearmvector(:,3),forearmvector(:,1)); %absolute forearm
angle in XZ plane
    faxyangle=atan2(forearmvector(:,2),forearmvector(:,1)); %absolute forearm
angle in XY plane

    %Hand
    handvector=thirdmp-wristcen; %vector along the long axis of the hand
    handzyangle=atan2(handvector(:,2),handvector(:,3)); %absolute hand angle
in ZY plane
    handxzangle=atan2(handvector(:,3),handvector(:,1)); %absolute hand angle
in XZ plane
    handxyangle=atan2(handvector(:,2),handvector(:,1)); %absolute hand angle
in XY plane

    %-------------------------Calculate angular velocities and
accelerations-------------------------------%
    %Velcities and accelerations calculated according to 3 point centered
different method (Winter)

    %store absolute angles in a single matrix
    %kinrows(1200)x9 matrix
    angles=[uazyangle uaxzangle uaxyangle fazyangle faxzangle faxyangle
handzyangle handxzangle handxyangle];

    %check to make sure all angles are in proper quadrant
    for row=1:kinrows
        for col=1:9
            if angles(row,col) <= -pi
                angles(row,col)=(angles(row,col)+2*pi);
            elseif angles(row,col) > pi
                angles(row,col)=(angles(row,col)-2*pi);
            end
        end
    end



    %calculate velocities
    count1=2;
    for count1=2:(kinrows-1)
        velocities(count1,1:9)=(angles(count1+1,:)-angles(count1-
1,:))/(2*dt);
        count1=count1+1;
    end
    %correct # of rows
    velocities(1,1:9)=velocities(2,1:9);
    velocities(kinrows,1:9)=velocities((kinrows-1),1:9);
```

```
    %calculate accelerations
    index1=2;
    for index1=2:(kinrows-2)
        accelerations(index1,1:9)=(velocities(index1+1,:)-velocities(index1-
1,:))/(2*dt);
        index1=index1+1;
    end
    %correct # of rows
    accelerations(1,1:9)= accelerations(2,1:9);
    accelerations((kinrows-1),1:9)= accelerations((kinrows-2),1:9);
    accelerations(kinrows,1:9)= accelerations((kinrows-2),1:9);

    %-------------------------Calculate linear velocities and accelerations-
------------------------------%
    %Velcities and accelerations calculated according to 3 point centered
different method (Winter)

    %Calculate linear velocities and accelerations for center of mass of each
segment

    %linear velocities of center of mass
    count2=2;
    for count2=2:(kinrows-1)
        cmvel(count2,1:9)=(cmall(count2+1,:)-cmall(count2-1,:))/(2*dt);
        count2=count2+1;
    end
    %correct # of rows
    cmvel(1,1:9)=cmvel(2,1:9);
    cmvel(kinrows,1:9)=cmvel((kinrows-1),1:9);

    %linear accelerations of center of mass;
    index2=2;
    for index2=2:(kinrows-2)
        cmaccel(index2,1:9)=(cmvel(index2+1,:)-cmvel(index2-1,:))/(2*dt);
        index2=index2+1;
    end
    %correct # of rows
    cmaccel(1,1:9)=cmaccel(2,1:9);
    cmaccel((kinrows-1),1:9)=cmaccel((kinrows-2),1:9);
    cmaccel(kinrows,1:9)=cmaccel((kinrows-2),1:9);

    %---------------------Calculate Net Joint Reaction Forces and Moments----
--------------------------%
    %Reference is Cooper et al. Glenohumeral Joint Kinematics and
Kinetics.....Am J Phys Med Rehab 1999.
    %All variable names in reference to Cooper et al.

    %Define blank arrays to be filled (defined) later

    %Hand matrices
    PHI_rD_hand=zeros(6,1,kinrows); %kinrows=#data points in kinematic file
    M_hand=zeros(6,1,kinrows);
    Mg_hand=zeros(6,1,kinrows);
    omega_hand=zeros(6,6,kinrows);
    T_hand=zeros(3,3,kinrows);
```

```
    Ip_hand=zeros(3,3,kinrows);
    I_hand=zeros(6,6,kinrows);
    w_hand=zeros(6,1,kinrows);
    omegaIw_hand=zeros(6,1,kinrows);
    a_hand=zeros(6,1,kinrows);
    Ia_hand=zeros(6,1,kinrows);
    rP_hand=zeros(6,1,kinrows);

    %Forearm matrices
    PHI_rD_fa=zeros(6,1,kinrows); %kinrows=#data points in kinematic file
    M_fa=zeros(6,1,kinrows);
    Mg_fa=zeros(6,1,kinrows);
    omega_fa=zeros(6,6,kinrows);
    T_fa=zeros(3,3,kinrows);
    Ip_fa=zeros(3,3,kinrows);
    I_fa=zeros(6,6,kinrows);
    w_fa=zeros(6,1,kinrows);
    omegaIw_fa=zeros(6,1,kinrows);
    a_fa=zeros(6,1,kinrows);
    Ia_fa=zeros(6,1,kinrows);
    rP_fa=zeros(6,1,kinrows);

    %Upper arm matrices
    PHI_rD_ua=zeros(6,1,kinrows); %kinrows=#data points in kinematic file
    M_ua=zeros(6,1,kinrows);
    Mg_ua=zeros(6,1,kinrows);
    omega_ua=zeros(6,6,kinrows);
    T_ua=zeros(3,3,kinrows);
    Ip_ua=zeros(3,3,kinrows);
    I_ua=zeros(6,6,kinrows);
    w_ua=zeros(6,1,kinrows);
    omegaIw_ua=zeros(6,1,kinrows);
    a_ua=zeros(6,1,kinrows);
    Ia_ua=zeros(6,1,kinrows);
    rP_ua=zeros(6,1,kinrows);

    %Phi Matrix (distances between proximal and distal landmarks with -1 on
diagonals) EQN. 20
    PHI_hand=zeros(6,6,kinrows);
    PHI_fa=zeros(6,6,kinrows);
    PHI_ua=zeros(6,6,kinrows);
    for i=1:6
        PHI_hand(i,i,1:kinrows)=-1; %put -1 along diagonal
        PHI_fa(i,i,1:kinrows)=-1; %put -1 along diagonal
        PHI_ua(i,i,1:kinrows)=-1; %put -1 along diagonal
    end

    %Hand segment
    rD_hand=zeros(kinrows,6);
    %Assume hand has a point contact with the pushrim at the third mp
    %Therefore SW forces are input to the third mp, but there is no moment
arm between the pushrim and the thirdmp, so the input moments are zero
    for t=1:kinrows
        if step(t,1) > 0, %will only input SW forces when hand is on the rim,
determined by step function
```

```
            rD_hand(t,1:3)=(-forces(t,1:3)); %reaction forces at hand are the
negative of the forces applied to the pushrim
        end
    end

    rD_hand=rD_hand';

    for t=1:kinrows
        %fill in Phi_hand matrix with distances between third mp and wrist
center
        %Signs in PHI matrix are different from Cooper et al. because his
        %paper assumes distances rather than directional vectors
        PHI_hand(4,2,t)=-(thirdmp(t,3)-wristcen(t,3)); %negative of vector
from prox to dist. in z direction EQN.20 (-Zdp)
        PHI_hand(5,1,t)=(thirdmp(t,3)-wristcen(t,3)); %vector from prox to
dist. in z direction EQN.20 (Zdp)
        PHI_hand(4,3,t)=-((thirdmp(t,2)-wristcen(t,2))); %negative of vector
from prox to dist. in y direction EQN.20 (-Ydp)
        PHI_hand(6,1,t)=((thirdmp(t,2)-wristcen(t,2))); %vector from prox to
dist. in y direction EQN.20 (Ydp)
        PHI_hand(6,2,t)=-(thirdmp(t,1)-wristcen(t,1)); %negative of vector
from prox to dist. in x direction EQN.20 (-Xdp)
        PHI_hand(5,3,t)=(thirdmp(t,1)-wristcen(t,1)); %vector from prox to
dist. in x direction EQN.20 (Xdp)


        %EQN. 21 PHI matrix times the reaction forces and moments at the
distal end of the segment
        PHI_rD_hand(:,:,t)=PHI_hand(:,:,t)*rD_hand(1:6,t);

        %EQN. 20 Define M matrix for hand (mass and moment arm vector)
        M_hand(2,1,t)=handmass;
        M_hand(4,1,t)=handmass*-1*(handcm(t,3)-wristcen(t,3));%hand mass
times distance in z direction b/w wrist center and hand center of mass
        %negative corrects for direction of moment
        M_hand(6,1,t)=handmass*(handcm(t,1)-wristcen(t,1));%hand mass times
distance in x direction b/w wrist center and hand center of mass

        %EQN. 21 Calculate M*g matrix
        Mg_hand(:,1,t)=M_hand(:,1,t)*g; %M matrix times gravity

        %EQN. 20 Calculate Capital Omega matrix
        omega_hand(4,5,t)=-(velocities(t,9)); %negative angular velocity @ z
axis
        omega_hand(5,4,t)=(velocities(t,9)); %angular velocity @ z axis
        omega_hand(4,6,t)=(velocities(t,8)); %angular velocity @ y axis
        omega_hand(6,4,t)=-(velocities(t,8)); %negative angular velocity @ y
axis
        omega_hand(5,6,t)=-(velocities(t,7)); %negative angular velocity @ x
axis
        omega_hand(6,5,t)=(velocities(t,7)); %angular velocity @ x axis

        %EQN.18 Set up transformation matrix to convert inertias about
        %segment axes to inertias about global x,y,z axes
        %angles(7)=psi_hand; angles(8)=theta_hand; angles(9)=phi_hand
```

```
        T_hand(1,1,t)=cos(angles(t,9))*cos(angles(t,8));
        T_hand(1,2,t)=sin(angles(t,9))*cos(angles(t,8));
        T_hand(1,3,t)=-sin(angles(t,8));
        T_hand(2,1,t)=-
sin(angles(t,9))*cos(angles(t,7))+cos(angles(t,9))*sin(angles(t,8))*sin(angle
s(t,7));

T_hand(2,2,t)=cos(angles(t,9))*cos(angles(t,7))+sin(angles(t,9))*sin(angles(t
,8))*sin(angles(t,7));
        T_hand(2,3,t)=cos(angles(t,8))*sin(angles(t,7));

T_hand(3,1,t)=sin(angles(t,9))*sin(angles(t,7))+cos(angles(t,9))*sin(angles(t
,8))*cos(angles(t,7));
        T_hand(3,2,t)=-
cos(angles(t,9))*sin(angles(t,7))+cos(angles(t,7))*sin(angles(t,8))*cos(angle
s(t,9));
        T_hand(3,3,t)=cos(angles(t,8))*cos(angles(t,7));

        %EQN.18 Calculate inertias about global x,y,z
        Ip_hand(:,:,t)=T_hand(:,:,t)*handI*T_hand(:,:,t)';

        %All inertia characteristics of the hand (angular velocity and
        %acceleration) will not be included in the calculated because they
        %have a very small contribution and are susceptible to noise)

        %EQN. 20 Set up angular velocity vector(lowercase omega-- will call
"w")

%w_hand(:,:,t)=[0;0;0;velocities(t,7);velocities(t,8);velocities(t,9)];

        %EQN. 21 Calculate product of angular velocity matrices (omega*I*w)
        %omegaIw_hand(:,:,t)=omega_hand(:,:,t)*I_hand(:,:,t)*w_hand(:,:,t);

        %EQN. 20 Define acceleration vector(linear [of center of mass] and
angular accelerations)

%a_hand(:,:,t)=[cmaccel(t,1);cmaccel(t,2);cmaccel(t,3);accelerations(t,7);acc
elerations(t,8);accelerations(t,9)];

        %EQN. 21 Calculate matrix that combines inertial properties and
linear accelerations
        %Ia_hand(:,:,t)=I_hand(:,:,t)*a_hand(:,:,t);

        %EQN. 21 Calculate reaction force at wrist center in global
coordinate system
        rP_hand(:,:,t)=PHI_rD_hand(:,:,t)+Mg_hand(:,:,t);

    end

    %Forearm segment
    rD_fa=-rP_hand; %reaction forces at hand are the negative of the forces
applied to the wrist (negative applied in PHI matrix below)

    for t=1:kinrows
```

```
        %fill in Phi_fa matrix with distances between wrist center and
lateral epicondyle
        %Signs in PHI matrix are different from Cooper et al. because his
        %paper assumes distances rather than directional vectors
        PHI_fa(4,2,t)=-(wristcen(t,3)-latep(t,3)); %negative of vector from
prox to dist. in z direction EQN.20 (-Zdp)
        PHI_fa(5,1,t)=(wristcen(t,3)-latep(t,3)); %vector from prox to dist.
in z direction EQN.20 (Zdp)
        PHI_fa(4,3,t)=-((wristcen(t,2)-latep(t,2))); %negative of vector from
prox to dist. in y direction EQN.20 (-Ydp)
        PHI_fa(6,1,t)=((wristcen(t,2)-latep(t,2))); %vector from prox to
dist. in y direction EQN.20 (Ydp)
        PHI_fa(6,2,t)=-(wristcen(t,1)-latep(t,1)); %negative of vector from
prox to dist. in x direction EQN.20 (-Xdp)
        PHI_fa(5,3,t)=(wristcen(t,1)-latep(t,1)); %vector from prox to dist.
in x direction EQN.20 (Xdp)

        %EQN. 21 PHI matrix times the reaction forces and moments at the
distal end of the segment
        PHI_rD_fa(:,:,t)=PHI_fa(:,:,t)*rD_fa(1:6,t);

        %EQN. 20 Define M matrix for forearm (mass and moment arm vector)
        M_fa(2,1,t)=famass;
        M_fa(4,1,t)=famass*-1*(facm(t,3)-latep(t,3));%forearm mass times
distance in z direction b/w latep and forearm center of mass
        %negative corrects for direction of moment
        M_fa(6,1,t)=famass*(facm(t,1)-latep(t,1));%forearm mass times
distance in x direction b/w latep and forearm center of mass

        %EQN. 21 Calculate M*g matrix
        Mg_fa(:,1,t)=M_fa(:,1,t)*g; %M matrix times gravity

        %EQN. 20 Calculate Capital Omega matrix
        omega_fa(4,5,t)=-(velocities(t,6)); %negative angular velocity @ z
axis
        omega_fa(5,4,t)=(velocities(t,6)); %angular velocity @ z axis
        omega_fa(4,6,t)=(velocities(t,5)); %angular velocity @ y axis
        omega_fa(6,4,t)=-(velocities(t,5)); %negative angular velocity @ y
axis
        omega_fa(5,6,t)=-(velocities(t,4)); %negative angular velocity @ x
axis
        omega_fa(6,5,t)=(velocities(t,4)); %angular velocity @ x axis

        %EQN.18 Set up transformation matrix to convert inertias about
        %segment axes to inertias about global x,y,z axes
        %angles(4)=psi_fa; angles(5)=theta_fa; angles(6)=phi_fa
        T_fa(1,1,t)=cos(angles(t,6))*cos(angles(t,5));
        T_fa(1,2,t)=sin(angles(t,6))*cos(angles(t,5));
        T_fa(1,3,t)=-sin(angles(t,5));
        T_fa(2,1,t)=-
sin(angles(t,6))*cos(angles(t,4))+cos(angles(t,6))*sin(angles(t,5))*sin(angle
s(t,4));

T_fa(2,2,t)=cos(angles(t,6))*cos(angles(t,4))+sin(angles(t,6))*sin(angles(t,5
))*sin(angles(t,4));
        T_fa(2,3,t)=cos(angles(t,5))*sin(angles(t,4));
```

```
T_fa(3,1,t)=sin(angles(t,6))*sin(angles(t,4))+cos(angles(t,6))*sin(angles(t,5
))*cos(angles(t,4));
        T_fa(3,2,t)=-
cos(angles(t,6))*sin(angles(t,4))+cos(angles(t,4))*sin(angles(t,5))*cos(angle
s(t,6));
        T_fa(3,3,t)=cos(angles(t,5))*cos(angles(t,4));

        %EQN.18 Calculate inertias about global x,y,z
        Ip_fa(:,:,t)=T_fa(:,:,t)*faI*T_fa(:,:,t)';

        %EQN.20 Set up I matrix that contains mass and inertia information
        I_fa(1,1,t)=famass;
        I_fa(2,2,t)=famass;
        I_fa(3,3,t)=famass;
        I_fa(4:6,4:6,t)=Ip_fa(:,:,t);

        %EQN. 20 Set up angular velocity vector(lowercase omega-- will call
"w")
        w_fa(:,:,t)=[0;0;0;velocities(t,4);velocities(t,5);velocities(t,6)];

        %EQN. 21 Calculate product of angular velocity matrices (omega*I*w)
        omegaIw_fa(:,:,t)=omega_fa(:,:,t)*I_fa(:,:,t)*w_fa(:,:,t);

        %EQN. 20 Define acceleration vector(linear [of center of mass] and
angular accelerations)

%a_fa(:,:,t)=[cmaccel(t,4);cmaccel(t,5);cmaccel(t,6);accelerations(t,4);accel
erations(t,5);accelerations(t,6)];

a_fa(:,:,t)=[cmaccel(t,4);cmaccel(t,5);cmaccel(t,6);0;0;accelerations(t,6)];
        %xz and yz plane angular accelerations ignored because they are
        %prone to quadrant changes when the arm is vertical.  contributions
        %are negligable in these two planes

        %EQN. 21 Calculate matrix that combines inertial properties and
linear accelerations
        Ia_fa(:,:,t)=I_fa(:,:,t)*a_fa(:,:,t);

        %EQN. 21 Calculate reaction force at elbow center in global
coordinate system
        rP_fa(:,:,t)=PHI_rD_fa(:,:,t)-Ia_fa(:,:,t)-
omegaIw_fa(:,:,t)+Mg_fa(:,:,t);

    end

    %Upper arm segment
    rD_ua=-rP_fa; %reaction forces at shoulder are the negative of the forces
applied to the elbow (negative applied in PHI matrix below)

    for t=1:kinrows
        %fill in Phi_ua matrix with distances between lateral epicondyle and
acromion
        %Signs in PHI matrix are different from Cooper et al. because his
        %paper assumes distances rather than directional vectors
```

```
        PHI_ua(4,2,t)=-(latep(t,3)-acro(t,3)); %negative of vector from prox
to dist. in z direction EQN.20 (-Zdp)
        PHI_ua(5,1,t)=(latep(t,3)-acro(t,3)); %vector from prox to dist. in z
direction EQN.20 (Zdp)
        PHI_ua(4,3,t)=-((latep(t,2)-acro(t,2))); %negative of vector from
prox to dist. in y direction EQN.20 (-Ydp)
        PHI_ua(6,1,t)=((latep(t,2)-acro(t,2))); %vector from prox to dist. in
y direction EQN.20 (Ydp)
        PHI_ua(6,2,t)=-(latep(t,1)-acro(t,1)); %negative of vector from prox
to dist. in x direction EQN.20 (-Xdp)
        PHI_ua(5,3,t)=(latep(t,1)-acro(t,1)); %vector from prox to dist. in x
direction EQN.20 (Xdp)

        %EQN. 21 PHI matrix times the reaction forces and moments at the
distal end of the segment
        PHI_rD_ua(:,:,t)=PHI_ua(:,:,t)*rD_ua(1:6,t);

        %EQN. 20 Define M matrix for upperarm (mass and moment arm vector)
        M_ua(2,1,t)=uamass;
        M_ua(4,1,t)=uamass*-1*(uacm(t,3)-acro(t,3));%upperarm mass times
distance in z direction b/w acromion and upperam center of mass
        %negative corrects for direction of moment
        M_ua(6,1,t)=uamass*(uacm(t,1)-acro(t,1));%upperarm mass times
distance in x direction b/w acromion and upperam center of mass


        %EQN. 21 Calculate M*g matrix
        Mg_ua(:,1,t)=M_ua(:,1,t)*g; %M matrix times gravity

        %EQN. 20 Calculate Capital Omega matrix
        omega_ua(4,5,t)=-(velocities(t,3)); %negative angular velocity @ z
axis
        omega_ua(5,4,t)=(velocities(t,3)); %angular velocity @ z axis
        omega_ua(4,6,t)=(velocities(t,2)); %angular velocity @ y axis
        omega_ua(6,4,t)=-(velocities(t,2)); %negative angular velocity @ y
axis
        omega_ua(5,6,t)=-(velocities(t,1)); %negative angular velocity @ x
axis
        omega_ua(6,5,t)=(velocities(t,1)); %angular velocity @ x axis

        %EQN.18 Set up transformation matrix to convert inertias about
        %segment axes to inertias about global x,y,z axes
        %angles(1)=psi_ua; angles(2)=theta_ua; angles(3)=phi_ua
        T_ua(1,1,t)=cos(angles(t,3))*cos(angles(t,2));
        T_ua(1,2,t)=sin(angles(t,3))*cos(angles(t,2));
        T_ua(1,3,t)=-sin(angles(t,2));
        T_ua(2,1,t)=-
sin(angles(t,3))*cos(angles(t,1))+cos(angles(t,3))*sin(angles(t,2))*sin(angle
s(t,1));

T_ua(2,2,t)=cos(angles(t,3))*cos(angles(t,1))+sin(angles(t,3))*sin(angles(t,2
))*sin(angles(t,1));
        T_ua(2,3,t)=cos(angles(t,2))*sin(angles(t,1));

T_ua(3,1,t)=sin(angles(t,3))*sin(angles(t,1))+cos(angles(t,3))*sin(angles(t,2
))*cos(angles(t,1));
```

```
        T_ua(3,2,t)=-
cos(angles(t,3))*sin(angles(t,1))+cos(angles(t,1))*sin(angles(t,2))*cos(angle
s(t,3));
        T_ua(3,3,t)=cos(angles(t,2))*cos(angles(t,1));

        %EQN.18 Calculate inertias about global x,y,z
        Ip_ua(:,:,t)=T_ua(:,:,t)*uaI*T_ua(:,:,t)';

        %EQN.20 Set up I matrix that contains mass and inertia information
        I_ua(1,1,t)=uamass;
        I_ua(2,2,t)=uamass;
        I_ua(3,3,t)=uamass;
        I_ua(4:6,4:6,t)=Ip_ua(:,:,t);

        %EQN. 20 Set up angular velocity vector(lowercase omega-- will call
"w")
        w_ua(:,:,t)=[0;0;0;velocities(t,1);velocities(t,2);velocities(t,3)];

        %EQN. 21 Calculate product of angular velocity matrices (omega*I*w)
        omegaIw_ua(:,:,t)=omega_ua(:,:,t)*I_ua(:,:,t)*w_ua(:,:,t);

        %EQN. 20 Define acceleration vector(linear [of center of mass] and
angular accelerations)

%a_ua(:,:,t)=[cmaccel(t,7);cmaccel(t,8);cmaccel(t,9);accelerations(t,1);accel
erations(t,2);accelerations(t,3)];

a_ua(:,:,t)=[cmaccel(t,7);cmaccel(t,8);cmaccel(t,9);0;0;accelerations(t,3)];
        %xz and yz plane angular accelerations ignored because they are
        %prone to quadrant changes when the arm is vertical.  contributions
        %are negligable in these two planes

        %EQN. 21 Calculate matrix that combines inertial properties and
linear accelerations
        Ia_ua(:,:,t)=I_ua(:,:,t)*a_ua(:,:,t);

        %EQN. 21 Calculate reaction force at shoulder center in global
coordinate system
        rP_ua(:,:,t)=PHI_rD_ua(:,:,t)-Ia_ua(:,:,t)-
omegaIw_ua(:,:,t)+Mg_ua(:,:,t);



        %----------------------- Calculate Local Coordinate Systems for
Segments--------------------%

        %-------------------------Hand local coordinate system--------------
------%

        %temporary k axis of hand (use to calculate i)
        if n==1 %vector points to right for both sides in standard anatomical
position
            v1_hand(t,1:3)=radsty(t,1:3)-ulnsty(t,1:3); %vector 1, not
normalized
            k_hand_temp(t,1:3)= v1_hand(t,1:3)/norm(v1_hand(t,1:3));
%normalized vector 1 (temporary k vector)
```

```
        else %vector points to right for both sides in standard anatomical
position
            v1_hand(t,1:3)=ulnsty(t,1:3)-radsty(t,1:3); %vector 1, not
normalized
            k_hand_temp(t,1:3)= v1_hand(t,1:3)/norm(v1_hand(t,1:3));
%normalized vector 1 (temporary k vector)
        end

        %j axis of the hand
        v2_hand(t,1:3)=wristcen(t,1:3)-thirdmp(t,1:3); %vector 2, not
normalized
        j_hand(t,1:3)= v2_hand(t,1:3)/norm(v2_hand(t,1:3)); %normalized
vector 2 (j vector)

        %i axis of the hand
        v3_hand(t,1:3)=cross(j_hand(t,1:3),k_hand_temp(t,1:3));%vector 3, not
normalized
        i_hand(t,1:3)=v3_hand(t,1:3)/norm(v3_hand(t,1:3)); %normalized vector
2 (k vector)

        %k axis of the hand
        v4_hand(t,1:3)=cross(i_hand(t,1:3),j_hand(t,1:3));%vector 4, not
normalized
        k_hand(t,1:3)=v4_hand(t,1:3)/norm(v4_hand(t,1:3)); %normalized vector
2 (i vector)

        %rotation matrix for hand
        rot_hand(1,1:3,t)=i_hand(t,1:3); %first row is i unit vector
        rot_hand(2,1:3,t)=j_hand(t,1:3); %second row is j unit vector
        rot_hand(3,1:3,t)=k_hand(t,1:3); %third row is k unit vector

        %-----------------Forearm local coordinate system--------------------
-----%

        %temporary k axis of forearm (use to calculate i)
        if n==1 %vector points to right for both sides in standard anatomical
position
            v1_fa(t,1:3)=radsty(t,1:3)-ulnsty(t,1:3); %vector 1, not
normalized
            k_fa_temp(t,1:3)= v1_fa(t,1:3)/norm(v1_fa(t,1:3)); %normalized
vector 1 (temporary k vector)
        else %vector points to right for both sides in standard anatomical
position
            v1_fa(t,1:3)=ulnsty(t,1:3)-radsty(t,1:3); %vector 1, not
normalized
            k_fa_temp(t,1:3)= v1_fa(t,1:3)/norm(v1_fa(t,1:3)); %normalized
vector 1 (temporary k vector)
        end

        %j axis of the forearm
        v2_fa(t,1:3)=latep(t,1:3)-ulnsty(t,1:3); %vector 2, not normalized
        j_fa(t,1:3)= v2_fa(t,1:3)/norm(v2_fa(t,1:3)); %normalized vector 2 (j
vector)

        %i axis of the forearm
```

```
        v3_fa(t,1:3)=cross(j_fa(t,1:3),k_fa_temp(t,1:3));%vector 3, not
normalized
        i_fa(t,1:3)=v3_fa(t,1:3)/norm(v3_fa(t,1:3)); %normalized vector 2 (i
vector)

        %k axis of the forearm
        v4_fa(t,1:3)=cross(i_fa(t,1:3),j_fa(t,1:3));%vector 4, not normalized
        k_fa(t,1:3)=v4_fa(t,1:3)/norm(v4_fa(t,1:3)); %normalized vector 2 (k
vector)

        %rotation matrix for forearm
        rot_fa(1,1:3,t)=i_fa(t,1:3); %first row is i unit vector
        rot_fa(2,1:3,t)=j_fa(t,1:3); %second row is j unit vector
        rot_fa(3,1:3,t)=k_fa(t,1:3); %third row is k unit vector


        %-------------------Humerus local coordinate system-----------------
----%
        %Reference is Cooper et al. Glenohumeral Joint Kinematics and
Kinetics.....Am J Phys Med Rehab 1999.
        %EQN. 1-2,5

        %temporary i axis of upper arm (use to calculate k)
        v1_ua(t,1:3)=ulnsty(t,1:3)-latep(t,1:3); %vector 1, not normalized
        i_ua_temp(t,1:3)= v1_ua(t,1:3)/norm(v1_ua(t,1:3)); %normalized vector
1 (temporary i vector)

        %j axis of the upper arm (called j_s in cooper's paper)
        v2_ua(t,1:3)=acro(t,1:3)-latep(t,1:3); %vector 2, not normalized
        j_ua(t,1:3)= v2_ua(t,1:3)/norm(v2_ua(t,1:3)); %normalized vector 2 (j
vector)

        %k axis of the upper arm (called k_s in cooper's paper)
        v3_ua(t,1:3)=cross(i_ua_temp(t,1:3),j_ua(t,1:3));%vector 3, not
normalized
        k_ua(t,1:3)=v3_ua(t,1:3)/norm(v3_ua(t,1:3)); %normalized vector 2 (k
vector)

        %i axis of the upper arm (called i_s in cooper's paper)
        v4_ua(t,1:3)=cross(j_ua(t,1:3),k_ua(t,1:3));%vector 4, not normalized
        i_ua(t,1:3)=v4_ua(t,1:3)/norm(v4_ua(t,1:3)); %normalized vector 2 (i
vector)

        %rotation matrix for upper arm
        rot_ua(1,1:3,t)=i_ua(t,1:3); %first row is i unit vector
        rot_ua(2,1:3,t)=j_ua(t,1:3); %second row is j unit vector
        rot_ua(3,1:3,t)=k_ua(t,1:3); %third row is k unit vector

        %-----------Trunk local coordinate system-----------------%
        %Cooper used a triad on the chest to create coordinate system
        %I updated the coordinate system to follow the same convention, but
        %avoided using the chest triad

        %k (z) axis points from the left acromion to the right acromion
```

```
        k_tr_nn(t,1:3)=kin(t,41:43)-kin(t,14:16); %k axis of trunk, not
normalized
        k_tr(t,1:3)=k_tr_nn(t,1:3)/norm(k_tr_nn(t,1:3)); %k unit vector

        %intermediate vector points from mid acromion to mid hip
        %this vector should be perpendicular to the direction of the trunk,
pointing anteriorly
        %will be crossed with z to create the y axis of the trunk

        %Midpoint of Acromions
        apmid(t,1)=(kin(t,14)+kin(t,41))/2;
        apmid(t,2)=(kin(t,15)+kin(t,42))/2;
        apmid(t,3)=(kin(t,16)+kin(t,43))/2;

        %Midpoint of Hip Markers
        hipmid(t,1)=mean((kin(:,35)+kin(:,62))/2);
        hipmid(t,2)=mean((kin(:,36)+kin(:,63))/2);
        hipmid(t,3)=mean((kin(:,37)+kin(:,64))/2);

        int_tr_nn(t,1:3)=hipmid(t,1:3)-apmid(t,1:3); %intermediate vector,
not normalized


        %i (x) is perpendicular to k (z) and the intermediate vector (points
anteriorly in setpo)
        i_tr_nn(t,1:3)=cross(k_tr(t,1:3),int_tr_nn(t,1:3)); %i axis of trunk,
not normalized
        i_tr(t,1:3)=i_tr_nn(t,1:3)/norm(i_tr_nn(t,1:3)); %i unit vector

        %j (y) is perpendicular to i (x) and k (z) (points superiorly in
setpo)
        j_tr_nn(t,1:3)=cross(k_tr(t,1:3),i_tr(t,1:3)); %j axis of trunk, not
normalized
        j_tr(t,1:3)=j_tr_nn(t,1:3)/norm(j_tr_nn(t,1:3)); %j unit vector

        %rotation matrix for trunk (not corrected for setpo)
        rot_tr1(1,1:3,t)=i_tr(t,1:3); %first row is i unit vector
        rot_tr1(2,1:3,t)=j_tr(t,1:3); %second row is j unit vector
        rot_tr1(3,1:3,t)=k_tr(t,1:3); %third row is k unit vector

        %-----------Trunk local coordinate system in SETPO-----------------%
        %Same coordinate system as above... Calculated in setpo as a
        %correction factor

        %k (z) axis points from the left acromion to the right acromion
        k_tr_nns(1,1:3)=setpo(1,41:43)-setpo(1,14:16); %k axis of trunk, not
normalized
        k_trs(1,1:3)=k_tr_nns(1,1:3)/norm(k_tr_nns(1,1:3)); %k unit vector

        %intermediate vector points from mid acromion to mid hip
        %this vector should be perpendicular to the direction of the trunk,
pointing anteriorly
        %will be crossed with z to create the y axis of the trunk
```

```
        %Midpoint of Acromions
        apmids(1,1)=(setpo(1,14)+setpo(1,41))/2;
        apmids(1,2)=(setpo(1,15)+setpo(1,42))/2;
        apmids(1,3)=(setpo(1,16)+setpo(1,43))/2;

        %Midpoint of Hip Markers
        hipmids(1,1)=(setpo(1,35)+setpo(1,62))/2;
        hipmids(1,2)=(setpo(1,36)+setpo(1,63))/2;
        hipmids(1,3)=(setpo(1,37)+setpo(1,64))/2;

        int_tr_nns(1,1:3)=hipmids(1,1:3)-apmids(1,1:3); %intermediate vector,
not normalized


        %i (x) is perpendicular to k (z) and the intermediate vector (points
anteriorly in setpo)
        i_tr_nns(1,1:3)=cross(k_trs(1,1:3),int_tr_nns(1,1:3)); %i axis of
trunk, not normalized
        i_trs(1,1:3)=i_tr_nns(1,1:3)/norm(i_tr_nns(1,1:3)); %i unit vector

        %j (y) is perpendicular to i (x) and k (z) (points superiorly in
setpo)
        j_tr_nns(1,1:3)=cross(k_trs(1,1:3),i_trs(1,1:3)); %j axis of trunk,
not normalized
        j_trs(1,1:3)=j_tr_nns(1,1:3)/norm(j_tr_nns(1,1:3)); %j unit vector

        %rotation matrix for trunk
        rot_trs(1,1:3)=i_trs(1,1:3); %first row is i unit vector
        rot_trs(2,1:3)=j_trs(1,1:3); %second row is j unit vector
        rot_trs(3,1:3)=k_trs(1,1:3); %third row is k unit vector

        %rotation matrix for trunk corrected for setpo
        rot_tr(:,:,t)=rot_tr1(:,:,t)*inv(rot_trs(:,:)); %rotation from trunk
local to trunk in setpo (like a local to global matrix)

        %----------Calculate reaction forces/moments in anatomical coordinate
systems---------%
        %forces at the wrist
        f_wrist(1:3,1,t)=rot_fa(:,:,t)*-rP_hand(1:3,1,t); %local
forces=T*global forces

        %moments at the wrist
        m_wrist(1:3,1,t)=rot_hand(:,:,t)*-rP_hand(4:6,1,t); %local
moments=T*global moments

        %reformat variables for plotting
        if n==1
            fm_rwrist(t,1)=f_wrist(1,1,t);
            fm_rwrist(t,2)=f_wrist(2,1,t);
            fm_rwrist(t,3)=f_wrist(3,1,t);
            fm_rwrist(t,4)=m_wrist(1,1,t);
            fm_rwrist(t,5)=m_wrist(2,1,t);
            fm_rwrist(t,6)=m_wrist(3,1,t);
        else
            fm_lwrist(t,1)=f_wrist(1,1,t);
```

```
            fm_lwrist(t,2)=f_wrist(2,1,t);
            fm_lwrist(t,3)=f_wrist(3,1,t);
            fm_lwrist(t,4)=m_wrist(1,1,t);
            fm_lwrist(t,5)=m_wrist(2,1,t);
            fm_lwrist(t,6)=m_wrist(3,1,t);
        end

        %forces at the elbow
        f_elbow(1:3,1,t)=rot_ua(:,:,t)*-rP_fa(1:3,1,t); %local
forces=T*global forces

        %moments at the elbow
        m_elbow(1:3,1,t)=rot_fa(:,:,t)*-rP_fa(4:6,1,t); %local
moments=T*global moments

        %reformat variables for plotting
        if n==1
            fm_relbow(t,1)=f_elbow(1,1,t);
            fm_relbow(t,2)=f_elbow(2,1,t);
            fm_relbow(t,3)=f_elbow(3,1,t);
            fm_relbow(t,4)=m_elbow(1,1,t);
            fm_relbow(t,5)=m_elbow(2,1,t);
            fm_relbow(t,6)=m_elbow(3,1,t);
        else
            fm_lelbow(t,1)=f_elbow(1,1,t);
            fm_lelbow(t,2)=f_elbow(2,1,t);
            fm_lelbow(t,3)=f_elbow(3,1,t);
            fm_lelbow(t,4)=m_elbow(1,1,t);
            fm_lelbow(t,5)=m_elbow(2,1,t);
            fm_lelbow(t,6)=m_elbow(3,1,t);
        end


        %forces at the shoulder
        %EQN. 27 from Cooper et al.
        f_shoulder(1:3,1,t)=rot_tr(:,:,t)*-rP_ua(1:3,1,t); %local
forces=T*global forces

        %moments at the shoulder
        %EQN. 28 from Cooper et al.
        m_shoulder(1:3,1,t)=rot_ua(:,:,t)*-rP_ua(4:6,1,t); %local
moments=T*global moments

        %reformat variables for plotting
        if n==1
            fm_rsho(t,1)=f_shoulder(1,1,t);
            fm_rsho(t,2)=f_shoulder(2,1,t);
            fm_rsho(t,3)=f_shoulder(3,1,t);
            fm_rsho(t,4)=m_shoulder(1,1,t);
            fm_rsho(t,5)=m_shoulder(2,1,t);
            fm_rsho(t,6)=m_shoulder(3,1,t);
            stepr=step; %save step function
        else
            fm_lsho(t,1)=f_shoulder(1,1,t);
            fm_lsho(t,2)=f_shoulder(2,1,t);
```

```
            fm_lsho(t,3)=f_shoulder(3,1,t);
            fm_lsho(t,4)=m_shoulder(1,1,t);
            fm_lsho(t,5)=m_shoulder(2,1,t);
            fm_lsho(t,6)=m_shoulder(3,1,t);
            stepl=step; %save step function
        end

        %--------------------------------Calculate Euler Angles--------------
----------------------------%

        %Reference for all Euler Angle calculations is Wu G. et al... ISG
        %recommendation on definitions of joint coordinate systems of
        %various joints (see top for complete citation)


        %--------------Relating trunk position to the global coordinate
system-----------------%

        %need to take transpose of rotation matrices so that LCS axes are in
columns instead of rows
        rot_tr(1:3,1:3,t)=rot_tr(1:3,1:3,t)';

        %Assume a yx'z'' rotation for Euler Angle Calculations
        %This is updated from 1996 standards
        %Code for Euler Angle calculations using 1996 standards was adapted
from rotyxz.m function on ISB webpage
        %alpha is the first rotation (about y)
            %+ alpha = torsion to the left
            %- alpha = torsion to the right
        %beta is the second rotation (about x)
            %+ beta = lateral bending to the right
            %- beta = lateral bending to the left
        %gamma is the third rotation (about z)
            %+ gamma = extension
            %- gamma = flexion


        beta1_tr(t)= asin(-rot_tr(2,3,t)); %calculate x' rotation first

        salpha_tr(t) = rot_tr(1,3,t)/cos(beta1_tr(t)); %sin alpha
        calpha_tr(t) = rot_tr(3,3,t)/cos(beta1_tr(t)); %cos alpha
        alpha1_tr(t) = atan2(salpha_tr(t),calpha_tr(t)); %alpha one

        sgamma_tr(t) = rot_tr(2,1,t)/cos(beta1_tr(t)); %sin gamma
        cgamma_tr(t) = rot_tr(2,2,t)/cos(beta1_tr(t)); %cos gamma
        gamma1_tr(t) = atan2(sgamma_tr(t),cgamma_tr(t)); %gamma one

        if beta1_tr(t)>=0
            beta2_tr(t)=pi-beta1_tr(t); %beta two
        else
            beta2_tr(t)=-pi-beta1_tr(t); %beta two
        end

        salpha2_tr(t) = rot_tr(1,3,t)/cos(beta2_tr(t)); %sin alpha two
```

```
        calpha2_tr(t) = rot_tr(3,3,t)/cos(beta2_tr(t)); %cos alpha two
        alpha2_tr(t) = atan2(salpha2_tr(t),calpha2_tr(t)); %alpha two

        sgamma2_tr(t) = rot_tr(2,1,t)/cos(beta2_tr(t)); %sin gamma two
        cgamma2_tr(t) = rot_tr(2,2,t)/cos(beta2_tr(t)); %cos gamma two
        gamma2_tr(t) = atan2(sgamma2_tr(t),cgamma2_tr(t)); %gamma two


        if -pi/2 <= beta1_tr(t) & beta1_tr(t) <= pi/2 %loop sets values of
all angles, based on the x rotation
            %convert to degrees
            alpha_tr(t)=alpha1_tr(t)*(180/pi);
            beta_tr(t)=beta1_tr(t)*(180/pi);
            gamma_tr(t)=gamma1_tr(t)*(180/pi);
        else
            %convert to degrees
            alpha_tr(t)=alpha2_tr(t)*(180/pi);
            beta_tr(t)=beta2_tr(t)*(180/pi);
            gamma_tr(t)=gamma2_tr(t)*(180/pi);
        end


        %------------Relating humeral motion to the trunk (shoulder angles)--
------%

        %need to take transpose of rotation matrices so that LCS axes are in
columns instead of rows
        %trunk rotation matrix already transposed
        rot_ua(1:3,1:3,t)=rot_ua(1:3,1:3,t)';

        %calculate the inverse of the trunk rotation matrix
        rot_tr_inv(1:3,1:3,t)=inv(rot_tr(1:3,1:3,t));

        %find rotation matrix from trunk to humerus
        rot_tr_ua(1:3,1:3,t)=rot_tr_inv(1:3,1:3,t)*rot_ua(1:3,1:3,t);

        %Assume a yx'y'' rotation for Euler Angle Calculations
        %This is updated from 1996 standards
        %Code for Euler Angle calculations using 1996 standards was adapted
from rotyzy.m function on ISB webpage
        %There is no code on the ISB webpage for yxy rotations, so these
changes were made by JLM
        %All output is relative to the defined local coordinate system
        %Before averaging, the sign of either the right or left side will
have to be flipped
        %alpha is the first rotation (about y)
            %Right side
                %+ alpha = plane of elevation in front of horizontal line
connecting the two acromions
                %- alpha = plane of elevation behind horizontal line
connecting the two acromions
            %Left side
                %+ alpha = plane of elevation behind horizontal line
connecting the two acromions
```

```
                %- alpha = plane of elevation in front of horizontal line
connecting the two acromions
        %beta is the second rotation (about x)
            %Right side
                %+ beta = negative elevation (or adduction)
                %- beta = positive elevation (or abduction)
            %Left side
                %+ beta = positive elevation (or abduction)
                %- beta = negative elevation (or adduction)
        %gamma is the third rotation (about y)
            %Right side
                %+ gamma = internal rotation
                %- gamma = external rotation
            %Left side
                %+ gamma = external rotation
                %- gamma = internal rotation

        beta1(t)= acos(rot_tr_ua(2,2,t)); %calculate x' rotation first
        if beta1(t)==0 %if there is no x rotation, then the first and third
rotations will be the same
            alpha(t)=acos(rot_tr_ua(1,1,t)); %assign all rotation to be about
the first y axis
            beta(t)=beta1(t); %x rotation is still zero
            gamma(t)=0.0; %assign y'' rotation equal to zero since all
rotation was about y
        end


        salpha(t) = rot_tr_ua(1,2,t)/sin(beta1(t)); %sin alpha
        calpha(t) = rot_tr_ua(3,2,t)/sin(beta1(t)); %cos alpha
        alpha1(t) = atan2(salpha(t),calpha(t)); %alpha one

        sgamma(t) = rot_tr_ua(2,1,t)/sin(beta1(t)); %sin gamma
        cgamma(t) = -rot_tr_ua(2,3,t)/sin(beta1(t)); %cos gamma
        gamma1(t) = atan2(sgamma(t),cgamma(t)); %gamma one

        beta2(t)=-beta1(t); %beta two

        salpha2(t) = rot_tr_ua(1,2,t)/sin(beta2(t)); %sin alpha two
        calpha2(t) = rot_tr_ua(3,2,t)/sin(beta2(t)); %cos alpha two
        alpha2(t) = atan2(salpha2(t),calpha2(t)); %alpha two

        sgamma2(t) = rot_tr_ua(2,1,t)/sin(beta2(t)); %sin gamma two
        cgamma2(t) = -rot_tr_ua(2,3,t)/sin(beta2(t)); %cos gamma two
        gamma2(t) = atan2(sgamma2(t),cgamma2(t)); %gamma two


        if n==1

            %beta should always be negative on the right side
            if beta1(t) <= 0 & beta1(t) >= -pi %loop sets values of all
angles, based on the x rotation
                alpha(t)=alpha1(t);
                beta(t)=beta1(t);
                gamma(t)=gamma1(t);
```

```
            else
                alpha(t)=alpha2(t);
                beta(t)=beta2(t);
                gamma(t)=gamma2(t);
            end

            %convert to degrees
            alpha_rsho=alpha*(180/pi);
            beta_rsho=beta*(180/pi);
            gamma_rsho=gamma*(180/pi);

        else

            %beta should always be positive on rightside
            if beta1(t) >= 0 & beta1(t) <= pi %loop sets values of all
angles, based on the x rotation
                alpha(t)=alpha1(t);
                beta(t)=beta1(t);
                gamma(t)=gamma1(t);
            else
                alpha(t)=alpha2(t);
                beta(t)=beta2(t);
                gamma(t)=gamma2(t);
            end

            %convert to degrees
            alpha_lsho=alpha*(180/pi);
            beta_lsho=beta*(180/pi);
            gamma_lsho=gamma*(180/pi);
        end

        %------------Relating forearm motion to the upper arm (elbow angles)-
-------%

        %need to take transpose of rotation matrices so that LCS axes are in
columns instead of rows
        %rot_ua already transposed
        rot_fa(1:3,1:3,t)=rot_fa(1:3,1:3,t)';

        %calculate the inverse of the upper arm rotation matrix
        rot_ua_inv(1:3,1:3,t)=inv(rot_ua(1:3,1:3,t));

        %find rotation matrix from upper arm to forearm on the
        rot_ua_fa(1:3,1:3,t)=rot_ua_inv(1:3,1:3,t)*rot_fa(1:3,1:3,t);

        %Assume a zx'y'' rotation for Euler Angle Calculations
        %This is updated from 1996 standards
        %Code for Euler Angle calculations uwas adapted from rotzxy.m
function on ISB webpage
        %All output is relative to the defined local coordinate system
        %Before averaging, the sign of either the right or left side will
have to be flipped
        %alpha is the first rotation (about z)
            %Right and left side are the same
                %+ alpha = flexion
```

```
            %- alpha = extension
        %beta is the second rotation (about x) (usually ~=0)
            %Right side
                %+ beta = adduction
                %- beta = abduction
            %Left side
                %+ beta = abduction
                %- beta = adduction
        %gamma is the third rotation (about y)
            %Right side
                %+ gamma = internal rotation
                %- gamma = external rotation
            %Left side
                %+ gamma = external rotation
                %- gamma = internal rotation

        beta1_elb(t)= asin(rot_ua_fa(3,2,t)); %calculate x' rotation first

        sgamma_elb(t) = -rot_ua_fa(3,1,t)/cos(beta1_elb(t)); %sin gamma
        cgamma_elb(t) = rot_ua_fa(3,3,t)/cos(beta1_elb(t)); %cos gamma
        gamma1_elb(t) = atan2(sgamma_elb(t),cgamma_elb(t)); %gamma one

        salpha_elb(t) = -rot_ua_fa(1,2,t)/cos(beta1_elb(t)); %sin alpha
        calpha_elb(t) = rot_ua_fa(2,2,t)/cos(beta1_elb(t)); %cos alpha
        alpha1_elb(t) = atan2(salpha_elb(t),calpha_elb(t)); %alpha one

        if beta1_elb(t)>=0
            beta2_elb(t) = pi-beta1_elb(t);
        else
            beta2_elb(t)= -pi-beta1_elb(t);
        end

        %the next 2 if loops check to see if beta is unstable at 180/-180
        %degrees and sets beta to zero if it is unstable
        %the elbow should have very little ROM about the x axis
        if beta2_elb(t) == pi
            beta2_elb(t)=0;
        end
        if beta2_elb(t)== -pi
            beta2_elb(t)=0;
        end

        sgamma2_elb(t) = -rot_ua_fa(3,1,t)/cos(beta2_elb(t)); %sin gamma two
        cgamma2_elb(t) = rot_ua_fa(3,3,t)/cos(beta2_elb(t)); %cos gamma two
        gamma2_elb(t) = atan2(sgamma2_elb(t),cgamma2_elb(t)); %gamma two

        salpha2_elb(t) = -rot_ua_fa(1,2,t)/cos(beta2_elb(t)); %sin alpha two
        calpha2_elb(t) = rot_ua_fa(2,2,t)/cos(beta2_elb(t)); %cos alpha two
        alpha2_elb(t) = atan2(salpha2_elb(t),calpha2_elb(t)); %alpha two


        if n==1

            if -pi/2 <= beta1_elb(t) & beta1_elb(t) <= pi/2 %loop sets values
of all angles, based on the x rotation
```

```
                alpha_elb(t)=alpha1_elb(t);
                beta_elb(t)=beta1_elb(t);
                gamma_elb(t)=gamma1_elb(t);
            else
                alpha_elb(t)=alpha2_elb(t);
                beta_elb(t)=beta2_elb(t);
                gamma_elb(t)=gamma2_elb(t);
            end

            if gamma_elb(t)<0 %correct for switch at 180 degrees due to atan2
                gamma_elb(t)=gamma_elb(t)+2*pi;
            end

            %convert to degrees
            alpha_relb=alpha_elb*(180/pi);
            beta_relb=beta_elb*(180/pi);
            gamma_relb=gamma_elb*(180/pi);


        else

            if -pi/2 <= beta1_elb(t) & beta1_elb(t) <= pi/2 %loop sets values
of all angles, based on the x rotation
                alpha_elb(t)=alpha1_elb(t);
                beta_elb(t)=beta1_elb(t);
                gamma_elb(t)=gamma1_elb(t);
            else
                alpha_elb(t)=alpha2_elb(t);
                beta_elb(t)=beta2_elb(t);
                gamma_elb(t)=gamma2_elb(t);
            end

            if gamma_elb(t)>0 %correct for switch at -180 degrees due to
atan2
                gamma_elb(t)=gamma_elb(t)-2*pi;
            end

            %convert to degrees
            alpha_lelb=alpha_elb*(180/pi);
            beta_lelb=beta_elb*(180/pi);
            gamma_lelb=gamma_elb*(180/pi);
        end

        %------------------Relating hand motion to the forearm (wrist
angles)--------%

        %need to take transpose of rotation matrices so that LCS axes are in
columns instead of rows
        %rot_fa already transposed
        rot_hand(1:3,1:3,t)=rot_hand(1:3,1:3,t)';

        %calculate the inverse of the forearm rotation matrix
        rot_fa_inv(1:3,1:3,t)=inv(rot_fa(1:3,1:3,t));

        %find rotation matrix from upper arm to forearm on the
```

```
        rot_fa_hand(1:3,1:3,t)=rot_fa_inv(1:3,1:3,t)*rot_hand(1:3,1:3,t);

        %Assume a zy'x'' rotation for Euler Angle Calculations
        %This is updated from 1996 standards
        %Code for Euler Angle calculations uwas adapted from rotzyx.m
function on ISB webpage
        %All output is relative to the defined local coordinate system
        %Before averaging, the sign of either the right or left side will
have to be flipped
        %alpha is the first rotation (about z)
            %Right and Left side are the same
                %+ alpha = flexion
                %- alpha = extension
        %beta is the second rotation (about y)
            %Right side
                %+ beta = internal rotation
                %- beta = external rotation
            %Left side
                %+ beta = external rotation
                %- beta = internal rotation
        %gamma is the third rotation (about x)
            %Right side
                %+ gamma = ulnar deviation
                %- gamma = radial deviation
            %Left side
                %+ gamma = radial deviation
                %- gamma = ulnar deviation

        beta1_wr(t)= asin(-rot_fa_hand(3,1,t)); %calculate y' rotation first

        sgamma_wr(t) = rot_fa_hand(3,2,t)/cos(beta1_wr(t)); %sin gamma
        cgamma_wr(t) = rot_fa_hand(3,3,t)/cos(beta1_wr(t)); %cos gamma
        gamma1_wr(t) = atan2(sgamma_wr(t),cgamma_wr(t)); %gamma one

        salpha_wr(t) = rot_fa_hand(2,1,t)/cos(beta1_wr(t)); %sin alpha
        calpha_wr(t) = rot_fa_hand(1,1,t)/cos(beta1_wr(t)); %cos alpha
        alpha1_wr(t) = atan2(salpha_wr(t),calpha_wr(t)); %alpha one

        if beta1_wr(t)>=0
            beta2_wr(t) = pi-beta1_wr(t);
        else
            beta2_wr(t)= -pi-beta1_wr(t);
        end

        sgamma2_wr(t) = rot_fa_hand(3,2,t)/cos(beta2_wr(t)); %sin gamma two
        cgamma2_wr(t) = rot_fa_hand(3,3,t)/cos(beta2_wr(t)); %cos gamma two
        gamma2_wr(t) = atan2(sgamma2_wr(t),cgamma2_wr(t)); %gamma two

        salpha2_wr(t) = rot_fa_hand(2,1,t)/cos(beta2_wr(t)); %sin alpha two
        calpha2_wr(t) = rot_fa_hand(1,1,t)/cos(beta2_wr(t)); %cos alpha two
        alpha2_wr(t) = atan2(salpha2_wr(t),calpha2_wr(t)); %alpha two


        if -pi/2 <= beta1_wr(t) & beta1_wr(t) <= pi/2 %loop sets values of
all angles, based on the x rotation
```

```
            alpha_wr(t)=alpha1_wr(t);
            beta_wr(t)=beta1_wr(t);
            gamma_wr(t)=gamma1_wr(t);
        else
            alpha_wr(t)=alpha2_wr(t);
            beta_wr(t)=beta2_wr(t);
            gamma_wr(t)=gamma2_wr(t);
        end

        if n==1 %convert to degrees
            alpha_rwr=alpha_wr*(180/pi);
            beta_rwr=beta_wr*(180/pi);
            gamma_rwr=gamma_wr*(180/pi);
        else
            alpha_lwr=alpha_wr*(180/pi);
            beta_lwr=beta_wr*(180/pi);
            gamma_lwr=gamma_wr*(180/pi);
        end


    end

    n=n+1; %analyze left side

end %end of for n=1:2 loop (right and left side)

%create plots to check data

x=1:1:kinrows;

figure(1)
subplot(3,2,1),
plot(x,fm_rsho(:,1),'r',x,FM(1:4:4800,7),'c',x,fm_lsho(:,1),'b:');
plottitle=['Right(red) and Left (blue) Shoulder Fx: ',newID];
title(plottitle)
subplot(3,2,3),
plot(x,fm_rsho(:,2),'r',x,FM(1:4:4800,7),'c',x,fm_lsho(:,2),'b:');
plottitle=['Right(red) and Left (blue) Shoulder Fy: ',newID];
title(plottitle)
subplot(3,2,5),
plot(x,fm_rsho(:,3),'r',x,FM(1:4:4800,7),'c',x,fm_lsho(:,3),'b:');
plottitle=['Right(red) and Left (blue) Shoulder Fz: ',newID];
title(plottitle)
subplot(3,2,2),
plot(x,fm_rsho(:,4),'r',x,FM(1:4:4800,7),'c',x,fm_lsho(:,4),'b:');
plottitle=['Right(red) and Left (blue) Shoulder Mx: ',newID];
title(plottitle)
subplot(3,2,4),
plot(x,fm_rsho(:,5),'r',x,FM(1:4:4800,7),'c',x,fm_lsho(:,5),'b:');
plottitle=['Right(red) and Left (blue) Shoulder My: ',newID];
title(plottitle)
subplot(3,2,6),
plot(x,fm_rsho(:,6),'r',x,FM(1:4:4800,7),'c',x,fm_lsho(:,6),'b:');
plottitle=['Right(red) and Left (blue) Shoulder Mz: ',newID];
title(plottitle)
```

```
graphname=[newID,'ShoulderFM',speed];
saveas(gcf, graphname, 'fig')

figure(2)
subplot(3,2,1),
plot(x,fm_relbow(:,1),'r',x,FM(1:4:4800,7),'c',x,fm_lelbow(:,1),'b:');
plottitle=['Right(red) and Left (blue) Elbow Fx: ',newID];
title(plottitle)
subplot(3,2,3),
plot(x,fm_relbow(:,2),'r',x,FM(1:4:4800,7),'c',x,fm_lelbow(:,2),'b:');
plottitle=['Right(red) and Left (blue) Elbow Fy: ',newID];
title(plottitle)
subplot(3,2,5),
plot(x,fm_relbow(:,3),'r',x,FM(1:4:4800,7),'c',x,fm_lelbow(:,3),'b:');
plottitle=['Right(red) and Left (blue) Elbow Fz: ',newID];
title(plottitle)
subplot(3,2,2),
plot(x,fm_relbow(:,4),'r',x,FM(1:4:4800,7),'c',x,fm_lelbow(:,4),'b:');
plottitle=['Right(red) and Left (blue) Elbow Mx: ',newID];
title(plottitle)
subplot(3,2,4),
plot(x,fm_relbow(:,5),'r',x,FM(1:4:4800,7),'c',x,fm_lelbow(:,5),'b:');
plottitle=['Right(red) and Left (blue) Elbow My: ',newID];
title(plottitle)
subplot(3,2,6),
plot(x,fm_relbow(:,6),'r',x,FM(1:4:4800,7),'c',x,fm_lelbow(:,6),'b:');
plottitle=['Right(red) and Left (blue) Elbow Mz: ',newID];
title(plottitle)
graphname=[newID,'ElbowFM',speed];
saveas(gcf, graphname, 'fig')

figure(3)
subplot(3,2,1),
plot(x,fm_rwrist(:,1),'r',x,FM(1:4:4800,7),'c',x,fm_lwrist(:,1),'b:');
plottitle=['Right(red) and Left (blue) Wrist Fx: ',newID];
title(plottitle)
subplot(3,2,3),
plot(x,fm_rwrist(:,2),'r',x,FM(1:4:4800,7),'c',x,fm_lwrist(:,2),'b:');
plottitle=['Right(red) and Left (blue) Wrist Fy: ',newID];
title(plottitle)
subplot(3,2,5),
plot(x,fm_rwrist(:,3),'r',x,FM(1:4:4800,7),'c',x,fm_lwrist(:,3),'b:');
plottitle=['Right(red) and Left (blue) Wrist Fz: ',newID];
title(plottitle)
subplot(3,2,2),
plot(x,fm_rwrist(:,4),'r',x,FM(1:4:4800,7),'c',x,fm_lwrist(:,4),'b:');
plottitle=['Right(red) and Left (blue) Wrist Mx: ',newID];
title(plottitle)
subplot(3,2,4),
plot(x,fm_rwrist(:,5),'r',x,FM(1:4:4800,7),'c',x,fm_lwrist(:,5),'b:');
plottitle=['Right(red) and Left (blue) Wrist My: ',newID];
title(plottitle)
subplot(3,2,6),
plot(x,fm_rwrist(:,6),'r',x,FM(1:4:4800,7),'c',x,fm_lwrist(:,6),'b:');
plottitle=['Right(red) and Left (blue) Wrist Mz: ',newID];
title(plottitle)
```

```
graphname=[newID,'WristFM',speed];
saveas(gcf, graphname, 'fig')

figure(7)
subplot(3,1,1), plot(x,alpha_tr(1,:),'r',x,FM(1:4:4800,7),'c');
plottitle=['Alpha angle of the Trunk ',newID];
title(plottitle)
subplot(3,1,2), plot(x,beta_tr(1,:),'r',x,FM(1:4:4800,7),'c');
plottitle=['Beta angle of the Trunk ',newID];
title(plottitle)
subplot(3,1,3), plot(x,gamma_tr(1,:),'r',x,FM(1:4:4800,7),'c');
plottitle=['Gamma angle of the Trunk ',newID];
title(plottitle)
graphname=[newID,'Trunk Euler Angles (Yxz)',speed];
saveas(gcf, graphname, 'fig')

figure(8)
subplot(3,1,1),
plot(x,alpha_rsho(1,:),'r',x,FM(1:4:4800,7),'c',x,alpha_lsho(1,:),'b:');
plottitle=['Alpha angles at Shoulder (Right(red) and Left (blue)) ',newID];
title(plottitle)
subplot(3,1,2),
plot(x,beta_rsho(1,:),'r',x,FM(1:4:4800,7),'c',x,beta_lsho(1,:),'b:');
plottitle=['Beta angles at Shoulder (Right(red) and Left (blue)) ',newID];
title(plottitle)
subplot(3,1,3),
plot(x,gamma_rsho(1,:),'r',x,FM(1:4:4800,7),'c',x,gamma_lsho(1,:),'b:');
plottitle=['Gamma angles at Shoulder (Right(red) and Left (blue)) ',newID];
title(plottitle)
graphname=[newID,'Shoulder Euler Angles (Yxy)',speed];
saveas(gcf, graphname, 'fig')

figure(9)
subplot(3,1,1),
plot(x,alpha_relb(1,:),'r',x,FM(1:4:4800,7),'c',x,alpha_lelb(1,:),'b:');
plottitle=['Alpha angles at Elbow (Right(red) and Left (blue)) ',newID];
title(plottitle)
subplot(3,1,2),
plot(x,beta_relb(1,:),'r',x,FM(1:4:4800,7),'c',x,beta_lelb(1,:),'b:');
plottitle=['Beta angles at Elbow(Right(red) and Left (blue)) ',newID];
title(plottitle)
subplot(3,1,3),
plot(x,gamma_relb(1,:),'r',x,FM(1:4:4800,7),'c',x,gamma_lelb(1,:),'b:');
plottitle=['Gamma angles at Elbow (Right(red) and Left (blue)) ',newID];
title(plottitle)
graphname=[newID,'Elbow Euler Angles (Zxy)',speed];
saveas(gcf, graphname, 'fig')

figure(10)
subplot(3,1,1),
plot(x,alpha_rwr(1,:),'r',x,FM(1:4:4800,7),'c',x,alpha_lwr(1,:),'b:');
plottitle=['Alpha angles at Wrist (Right(red) and Left (blue)) ',newID];
title(plottitle)
subplot(3,1,2),
plot(x,beta_rwr(1,:),'r',x,FM(1:4:4800,7),'c',x,beta_lwr(1,:),'b:');
plottitle=['Beta angles at Wrist(Right(red) and Left (blue)) ',newID];
```

```
title(plottitle)
subplot(3,1,3),
plot(x,gamma_rwr(1,:),'r',x,FM(1:4:4800,7),'c',x,gamma_lwr(1,:),'b:');
plottitle=['Gamma angles at Wrist(Right(red) and Left (blue)) ',newID];
title(plottitle)
graphname=[newID,'Wrist Euler Angles (Zyx)',speed];
saveas(gcf, graphname, 'fig')


     %-----------------------------------Save data--------------------------
-------%

     %Save right side data
     new_file_r=zeros(1,10);
     new_file_r(1,1)=newID(1,1);
     new_file_r(1,2)=newID(1,2);
     new_file_r(1,3)=newID(1,3);
     new_file_r(1,4)=newID(1,4);
     new_file_r(1,5:7)='dyn';
     new_file_r(1,8)='7';
     new_file_r(1,9)='r';
     new_file_r(1,10)=speed;
     new_file_r(1,11:14)='.txt';
     new_file_r=setstr(new_file_r);


angles_r=[alpha_tr;beta_tr;gamma_tr;alpha_rsho;beta_rsho;gamma_rsho;alpha_rel
b;beta_relb;gamma_relb;alpha_rwr;beta_rwr;gamma_rwr;]';

     finalr=[fm_rwrist,fm_relbow, fm_rsho, angles_r, stepr];
     finalr=finalr';

     fid=fopen(new_file_r,'w');
     fprintf(fid, '%f\t %f\t %f\t %f\t %f\t %f\t %f\t %f\t %f\t %f\t %f\t
%f\t %f\t %f\t %f\t %f\t %f\t %f\t %f\t %f\t %f\t %f\t %f\t %f\t %f\t %f\t
%f\t %f\t %f\t %f\t %f\n', finalr);
     fclose(fid);

     %Save left side data
     new_file_l=zeros(1,10);
     new_file_l(1,1)=newID(1,1);
     new_file_l(1,2)=newID(1,2);
     new_file_l(1,3)=newID(1,3);
     new_file_l(1,4)=newID(1,4);
     new_file_l(1,5:7)='dyn';
     new_file_l(1,8)='7';
     new_file_l(1,9)='l';
     new_file_l(1,10)=speed;
     new_file_l(1,11:14)='.txt';
     new_file_l=setstr(new_file_l);


angles_l=[alpha_tr;beta_tr;gamma_tr;alpha_lsho;beta_lsho;gamma_lsho;alpha_lel
b;beta_lelb;gamma_lelb;alpha_lwr;beta_lwr;gamma_lwr;]';
```

```
      finall=[fm_lwrist,fm_lelbow, fm_lsho, angles_l, stepl];
      finall=finall';

      fid=fopen(new_file_l,'w');
      fprintf(fid, '%f\t %f\t %f\t %f\t %f\t %f\t %f\t %f\t %f\t %f\t %f\t
%f\t %f\t %f\t %f\t %f\t %f\t %f\t %f\t %f\t %f\t %f\t %f\t %f\t %f\t %f\t
%f\t %f\t %f\t %f\n', finall);
      fclose(fid);
```

BIBLIOGRAPHY

[1] Curtis K, Drysdale G, Lanza R, Kolber M, Vitolo R, West R. Shoulder pain in wheelchair users with tetraplegia and paraplegia. *Arch Phys Med Rehabil*. Apr 1999; 80: 453-7.

[2] Ballinger DA, Rintala DH, Hart KA. The relation of shoulder pain and range of motion problems to functional limitations, disability, and perceived health of men with spinal cord injury: a multifaceted longitudinal study. *Arch Phys Med Rehabil*. Dec 2000; 81(12): 1575-81.

[3] Gellman H, Sie I, Waters RL. Late complications of the weight-bearing upper extremity in the paraplegic patient. *Clin Ortho Rel Res*. 1988; 233(Aug): 132-5.

[4] Pentland WE, Twomey LT. The weight-bearing upper extremity in women with long term paraplegia. *Paraplegia*. 1991; 29: 521-30.

[5] Lundqvist C, Siosteen A, Blomstrand C, Lind B, Sullivan M. Spinal cord injuries. Clinical, functional, and emotional status. *Spine*. 1991; 16(1): 78-83.

[6] Gerhart KA, Bergstrom E, Charlifue SW, Menter RR, Whiteneck GG. Long-term spinal cord injury: functional changes over time. *Arch Phys Med Rehabil*. Oct 1993; 74(10): 1030-4.

[7] Bayley JC, Cochran TP, Sledge CB. The weight-bearing shoulder. The impingement syndrome in paraplegics. *J Bone Joint Surg Am*. 1987; 69: 676-8.

[8] Subbarao JV, Klopfstein J, Turpin R. Prevalence and impact of wrist and shoulder pain in patients with spinal cord injury. *J Spinal Cord Med*. 1994; 18(1): 9-13.

[9] Nichols PJ, Norman PA, Ennis JR. Wheelchair user's shoulder? Shoulder pain in patients with spinal cord lesions. *Scand J Rehabil Med*. 1979; 11: 29-32.

[10] Sie IH, Waters RL, Adkins RH, Gellman H. Upper extremity pain in the postrehabilitation spinal cord injured patient. *Arch Phys Med Rehabil*. 1992; 73: 44-8.

[11] Pentland WE, Twomey LT. Upper limb function in persons with long term paraplegia and implications for independence: Part II. *Paraplegia*. 1994; 32(4): 219-24.

[12] Goldstein B, Young J, Escobedo EM. Rotator cuff repairs in individuals with paraplegia. *Am J Phys Med Rehabil*. 1997; 76(4): 316-22.

[13] Paralyzed Veterans of America Consortium for Spinal Cord Medicine. Preserving upper limb function in spinal cord injury: a clinical practice guideline for health-care professionals. *J Spinal Cord Med*. 2005; 28(5): 434-470.

[14] Escobedo EM, Hunter JC, Hollister MC, Patten RM, Goldstein B. MR imaging of rotator cuff tears in individuals with paraplegia. *Am J Roentology*. 1997; 168(4): 919-23.

[15] Boninger ML, Towers JD, Cooper R.A., Dicianno BE, Munin MC. Shoulder imaging abnormalities in individuals with paraplegia. *J Rehab Res Dev*. Jul 2001; 38(4): 401-8.

[16] Tolerico ML, Ding D, Cooper RA, Spaeth DM, Fitzgerald SG, Cooper R, Kelleher A, Boninger ML. Assessing mobility characteristics and activity levels of manual wheelchair users. *J Rehab Res Dev*. 2007; 44(4): 561-72.

[17] Cooper RA, Boninger ML, Shimada SD, Lawrence BM. Glenohumeral joint kinematics and kinetics for three coordinate system representations during wheelchair propulsion. *Am J Phys Med Rehabil*. Sept 1999; 78(5): 435-46.

[18] Kulig K, Rao SS, Mulroy SJ, Newsam CJ, Gronley JK, Bontrager EL, Perry J. Shoulder joint kinetics during the push phase of wheelchair propulsion. *Clin Ortho Rel Res*. Sept 1998; 354: 132-43.

[19] Finley M, Rasch E, Keyser R, Rodgers M. The biomechanics of wheelchair propulsion in individuals with and without upper-limb impairment. *J Rehab Res Dev*. 2004; 41(3B):395-402.

[20] Newsam CJ, Rao SS, Mulroy SJ, Gronley JK, Bontrager EL, Perry J. Three dimensional upper extremity motion during manual wheelchair propulsion in men with different levels of spinal cord injury. *Gait Posture*. Dec 1999; 10(3): 223-32.

[21] Mercer JL, Boninger ML, Koontz AM, Ren D, Dyson-Hudson TA, Cooper RA. Shoulder joint pathology and kinetics in manual wheelchair users. *Clin Biomech*. 2006; 21(8): 781-9.

[22] Farley T, Neumann CH, Steinbach LS, Petersen SA. The coracoacromial arch: MR evaluation and correlation with rotator cuff pathology. *Skeletal Radiol*. Nov 1994; 23(8): 641-5.

[23] Mulroy SJ, Gronley JK, Newsam CJ, Perry J. Electromyographic activity of shoulder muscles during wheelchair propulsion by paraplegic persons. *Arch Phys Med Rehab*. Feb 1996; 77: 187-193.

[24] Mulroy SJ, Farrokhi S, Newsaw CJ, Perry J. Effects of spinal cord injury level on the activity of shoulder muscles during wheelchair propulsion: an electromyographic study. *Arch Phys Med Rehab*. 2004; 85: 925-34.

[25] Rodger MM, Gayle GW, Gigoni SF, Kobayashi M, Lieh J, Glaser RM. Biomechanics of Wheelchair Propulsion During Fatigue. *Arch Phys Med Rehab*. Jan 1994; 75: 85-93.

[26] Brose SW, Boninger ML, Fullerton B, McCann T, Collinger JL, Impink BG, Dyson-Hudson TA. Shoulder ultrasound abnormalities, physical examination finding, and pain in manual wheelchair users with spinal cord injury. *Arch Phys Med Rehabil*. 2008; 89: 2086-93.

[27] Jenkins, D. Hollinshead's Functional Anatomy of the Limbs and Back. Seventh Edition. Philadelphia: W.B. Saunders Company, 1998.

[28] Collinger JL, Boninger ML, Koontz AM, Price R, Sisto SA, Tolerico ML, Cooper RA. Shoulder biomechanics during the push phase of propulsion: a multi-site study of persons with paraplegia. *Arch Phys Med Rehab*. Apr 2008; 89(4): 667-76.

[29] Dyson-Hudson T, Kirshblum S. Shoulder pain in chronic spinal cord injury, part I: epidemiology, etiology, and pathomechanics. *J Spinal Cord Med*. 2004; 27(1): 4-17.

[30] Jobe FW, Kvitne RS, Giangarra CE. Shoulder pain in the overhand or throwing athlete. The relationship of anterior instability and rotator cuff impingement. *Orthop Rev*. 1989; 18: 963-75.

[31] Kibler WB. The role of the scapula in athletic shoulder function. *Am J Sports Med*. Mar 1998; 26(2): 325-37.

[32] Reyes ML, Gronley JK, Newsam CJ, Mulroy SJ, Perry J. Electromyographic analysis of shoulder muscles of men with low-level paraplegia during a weight relief raise. *Arch Phys Med Rehabil*. May 1995; 76(5): 433-9.

[33] Hardy DC, Vogler JB, White RH. The shoulder impingement syndrome: Prevalence of radiographic findings. *Am J Roentgenol*. 1986; 147: 557-61.

[34] McMaster WC, Long SC, Caiozzo VJ. Isokinetic torque imbalances in the rotator cuff of the elite water polo player. *Am J Sports Med*. 1991; 19: 72-5.

[35] Burnham RS, May L, Nelson E, Steadward R, Reid DC. Shoulder pain in wheelchair athletes. The role of muscle imbalance. *Am J Sports Med*. 1993; 21: 238-42.

[36] Wang J-C. Mechanobiology of Tendon. *J Biomech*. 2006; 39: 1563-82.

[37] Langberg H, Skovgaard D, Karamouzis M, Bulow J, Kjaer M. Metabolism and inflammatory mediators in the peritendinous space measured by microdialysis during intermittent isometric exercise in humans. *J Physiology*. 1999; 515(3): 919-27.

[38] Soslowsky LJ, Thomopoulos S, Esmail A, Flanagan C, Iannotti JP, Williamson J, Carpenter J. Rotator cuff tendinosis in an animal model: role of extrinsic and overuse factors. *Ann Biomed Eng*. 2002; 30: 1057-63.

[39] Peltz CD, Perry SM, Getz CL, Soslowsky LJ. Mechanical properties of the long-head of the biceps tendon are altered in the presence of rotator cuff tears in a rat model. *J Orthop Res*. March 2009; 27(3): 416-20.

[40] Arslan G, Apaydin A, Kabaalioglu A, Sindel T, Luleci E. Sonographically detected subacromical/subdeltoid bursal effusion and biceps tendon sheath fluid: reliable signs of rotator cuff tear? *J Clin Ultrasound*. 1999; 27(6): 335-9.

[41] Hashimoto B, Kramer D, Wiitala L. Applications of musculoskeletal sonography. *J Clin Ultrasound*. 1999; 27(6): 293-318.

[42] Thain L, Adler R. Sonography of the rotator cuff and biceps tendon: Technique, normal anatomy, and pathology. *J Clin Ultrasound*. 1999; 27(8): 446-58.

[43] Zanetti M, Hodler J. Imaging of degenerative and posttraumatic disease in the shoulder joint with ultrasound. *Eur J Radiol*. 2000; 35: 119-25.

[44] Wallny T, Wagner U, Prange S, Schmitt O, Reich H. Evaluation of chronic tears of the rotator cuff by ultrasound: A NEW INDEX. *J Bone Joint Surg Br*. Jul 1999; 81(B4): 675-8.

[45] Teefey S, Middleton W, Yamaguchi K. Musculoskeletal ultrasound: shoulder sonography: state of the art. *Radiol Clin North Am*. Jul 1999; 37(4): 767-85.

[46] Leung JLY, Griffith JF. Sonography of Chronic Achilles Tendinopathy: A Case-Control Study. *J Clin Ultrasound*. Jan 2008; 36(1): 27-32.

[47] Sharma N, Ray AK, Sharma S, Shukla KK, Pradhan S, Aggarwal LM. Segmentation and classification of medical images using texture-primative features: Application of BAM-type artificial neural network. *J Med Phys*. 2008; 33(3): 119-26.

[48] Nielsen PK, Jensen BR, Darvann T, Jorgensen K, Bakke M. Quantitative ultrasound tissue characterization in shoulder and thigh muscles-a new approach. *BMC Musculoskelet Disord*. 2006; 7: 2.

[49] Alvarenga A, Pereira WCA, Infantosi AFC. Complexity curve and grey level co-occurrence matrix in the texture evaluation of breast tumor on ultrasound images. *Med Phys*. Feb 2007; 34(2): 379-387.

[50] Scholten RR, Pillen S, Verrips A, Zwarts MJ. Quantitative ultrasonography of skeletal muscles in children: normal values. *Muscle Nerve*. Jun 2003; 27(6): 693-8.

[51] Pillen S, Scholten RR, Zwarts MJ, Verrips A. Quantitative skeletal muscle ultrasonography in children with suspected neuromuscular disease. *Muscle Nerve*. Jun 2003; 27(6): 699-705.

[52] Tuthill T, Rubin J, Fowlkes J, Jamadar D, Bude R. Frequency analysis of echo texture in tendon. *Ultrasound Med Biol*. 1999; 25(6): 959-68.

[53] Bashford GR, Tomsen N, Arya S, Burnfield JM, Kulig K. Tendinopathy discrimination by use of spatial frequency parameters in ultrasound B-mode images. *IEEE Trans Med Imag*. May 2008; 27(5): 608-15.

[54] Massy-Westropp N, Grimmer K, Bain G. The Effect of a Standard Activity on the Size of the Median Nerve as Determined by Ultrasound Visualization. *J Hand Surg*. Jul 2001; 26A(4): 649-54.

[55] Altinok M, Baysal O, Karakas H, Firat A. Sonographic Evaluation of the Carpal Tunnel After Provocative Exercises. *J Ultrasound Med*. 2004; 23: 1301-6.

[56] van Drongelen S, Boninger ML, Impink BG, Khalaf TM. Acute bicep tendon changes after wheelchair sports. *Arch Phys Med Rehabil*. 2007; 88(3): 381-5.

[57] Rudzki JR, Adler RS, Warren RF, Kadrmas WR, Verma N, Pearle AD, Lyman S, Fealy S. Contrast-enhanced ultrasound characterization of the vascularity of the rotator cuff tendon: Age- and activity-related changes in the intact asymptomatic rotator cuff. *J Shoulder Elbow Surg*. 2008; 17(1S): 96S-100S.

[58] Boesen MI, Koenig MJ, Torp-Pedersen S, Bliddal H, Langberg H. Tendinopathy and Doppler activity: the vascular response of the achilles tendon to exercise. *Scan J Med Sci Sports*. 2006; 16: 463-9.

[59] Shalabi A, Kristoffersen-Wiberg M, Aspelin P, Movin T. Immediate achilles tendon response after strength training evaluated by MRI. *Med Sci Sports Exerc*. 2004; 36(11): 1841-6.

[60] Hendee WR, Ritenour ER. Ultrasound Waves. In: Medical Imaging Physics. Hoboken, NJ: Wiley-Liss, Inc., 2002; Fourth Edition, pp. 303-316.

[61] Maganaris C, Reeves N, Rittweger J, Sargeant A, Jones D, Gerrits K, De Haan A. Adaptive response of human tendon to paralysis. *Muscle Nerve*. 2005; 33: 85-92.

[62] Sipila S, Suominen H. Quantitative ultrasonography of muscle: detection of adaptations to training in elderly women. *Arch Phys Med Rehabil*. Nov 1996; 77(11): 1173-8.

[63] Brushoj C, Henriksen BM, Albrecht-Beste E, Holmich P, Larsen K, Bachmann Nielsen M. Reproducibility of ultrasound and magnetic resonance imaging measurements of tendon size. *Acta Radiologica*. 2006; 9: 954-9.

[64] O'Connor PJ, Grainger AJ, Morgan SR, Smith KL, Waterton JC, Nash AFP. Ultrasound assessment of tendons in asymptomatic volunteers: a study of reproducibility. *Eur Radiol*. 2004; 14: 1968-73.

[65] Ying M, Yeung E, Li B, Li W, Lui M, Tsoi C-W. Sonographic evaluation of the size of the achilles tendon: the effect of exercise and dominance of the ankle. Ultrasound Med Biol. 2003; 29(5): 637-42.

[66] Haralick R, Shanmugam K, Dinstein I. Textural features for image classification. IEEE Trans Syst Man Cybern. Nov 1993; SMC-3(6): 610-21.

[67] Nielsen PK, Jensen BR, Darvann T, Jorgensen K, Bakke M. Quantitative ultrasound image analysis of the supraspinatus muscle. Clin Biomech. 2000; 15(Supp 1): S13-S16.

[68] Shavelson RJ, Webb NM. Generalizability theory: A primer. Newbury Park, CA: Sage, 1991.

[69] Brennan R, Kane M. An index of dependability for mastery tests. J Education and Management. 1977; 14: 277-289.

[70] Portney LG, Watkins MP. *Foundations of clinical research: Application to practice*. Second ed. Stamford: Appleton & Lange, 2000.

[71] Churchill RS, Fehringer EV, DubinskyTJ, Matsen FA, III. Rotator cuff ultrasonography: diagnostic capabilities. *J Am Acad Orthop Surg*. Jan 2004; 12(1): 6-11.

[72] Gardin A, Bruno J, Movin T, Kristoffersen-Wiberg M, Shalabi A. Magnetic resonance signal, rather than tendon volume, correlates to pain and functional impairment in chronic achilles tendinopathy. *Acta Radiologica*. 2006; 7: 718-24.

[73] Boninger ML, Koontz AM, Sisto SA, Dyson-Hudson TA, Chang M, Price R, Cooper RA. Pushrim biomechanics and injury prevention in spinal cord injury: recommendations based on CULP-SCI investigations. *J Rehab Res Dev*. 2005; 42(3, Supp. 1): 9-20.

[74] Curtis KA, Roach KE, Applegate EB, Amar T, Benbow CS, Genecco TD, Gualano J. Reliability and Validity of the Wheelchair User's Shoulder Pain Index (WUSPI). *Paraplegia*. 1995; 33(10): 595-601.

[75] Allen GM. Shoulder ultrasound imaging-integrating anatomy, biomechanics and disease process. *Eur J Radiol*. 2008; 68: 137-46.

[76] Arts IMP, van Rooij FG, Overeem S, et al. Quantitative muscle ultrasonography in Amyotrophic Lateral Sclerosis. *Ultrasound Med Biol*. 2008; 34(3): 354-61.

[77] He X, An S, Shi P. Statistical Texture Analysis-Based Approach for Fake Iris Detection Using Support Vector Machines. *ICB07*. Seoul, Korea. 2007:540-6.

[78] Wang J H-C. Iosifidis MI, Fu FH. Biomechanical basic for tendinopathy. *Clin Orthop Rel Res*. 2006; 443: 320-32.

[79] Lanvagnino M, Arnoczky SP, Kepich E, Caballero O, Haut RC. A finite element model predicts the mechanotransduction response of tendon cells to cyclic tensile loading. *Biomechan Model Mechanobiol*. 2008; 7(5): 405-16.

[80] Hughes CJ, Weimar WH, Sheth PN, Brubaker CE. Biomechanics of wheelchair propulsion as a function of seat position and user-to-chair interface. *Arch Phys Med Rehabil*. 1992; 73: 263-9.

[81] Boninger ML, Baldwin MA, Cooper RA, Koontz AM, Chan L. Manual wheelchair pushrim biomechanics and axle position. *Arch Phys Med Rehabil*. 2000; 81: 608-13.

[82] Boninger ML, Souza AL, Cooper RA, Fitzgerald SG, Koontz AM, Fay BT. Propulsion patterns and pushrim biomechanics in manual wheelchair propulsion. *Arch Phys Med Rehabil*. May 2002; 83(5): 718-23.

[83] Hanavan E. *A mathematical model of the human body*. Wright-Patterson Air Force Base, Ohio: Aerospace Medical Research Laboratories; Oct 1964. Report AMRL-TR-64-102.

[84] Wu G, van der Helm F, Veeger HEJ, Makhsous M, Van Roy P, Anglin C, Nagels J, Karduna A, McQuade K, Wang X, Werner F, Bucholz B. ISB recommendation on definitions of joint coordinate systems of various joints for the reporting of human joint motion - Part II: shoulder, elbow, wrist and hand. *J Biomech*. 2005; 38: 981-92.